Asymmetries in Nucleon Transfer Reactions Induced by Polarized Protons

by

John Michael Nelson

Worcester College

BODLEIAN LIBRARY OXFORD
DEPOSITED
THESIS
13-2-69

A thesis submitted to the Board of the Faculty of Physical Sciences of the University of Oxford for the degree of Doctor of Philosophy.

October 1968

TABLE OF CONTENTS

Acknowledgements.

Abstract.

CHAPTER 1. The Two Nucleon Transfer Reaction. 1

i) The distorted wave Born approximation theory 3

ii) Application of two nucleon transfer theory to experiment 12

CHAPTER 2. Polarization and Pick-up Reactions. 19

i) The polarization-asymmetry theorem 20

ii) Pick-up reactions with polarised protons 23

iii) A general spin-dependent computer programme 26

CHAPTER 3. Experimental Apparatus. 29

i) The accelerator 29

ii) Beam transport system 31

iii) Scattering chamber, counters and targets 32

iv) The beam monitor 35

v) Electronics 36

CHAPTER 4. Experimental Measurements and Data Analysis. 42

A: Measurement of differential cross sections 43

i) $^{12}C(p,t)^{10}C$ Ground state and 3.34 MeV 43

ii) $^{16}O(p,t)^{14}O$ Ground state 44

iii) $^{16}O(p,^{3}He)^{14}N$ Ground state and 2.311 MeV 45

iv) $^{28}Si(p,t)^{26}Si$ Ground state 46

v) Calculation of the centre of mass differential cross section 47

B: Measurement of polarization analysing powers 48

i) Experimentation with polarised beams 48

ii) The polarimeter and the gold foil monitor 52

iii) $^{12}C(p,t)^{10}C$ Ground state and 3.34 MeV 56

iv) $^{16}O(p,t)^{14}O$ Ground state

$^{16}O(p,^{3}He)^{14}N$ Ground state and 2.311 MeV 57

v) $^{28}Si(p,t)^{26}Si$ Ground state 58

vi) Possible sources of systematic error 59

vii) Calculation of the polarisation analysing power 61

CHAPTER 5. The Predictions of Born Approximation Theory. 63

i) Optical model potentials 64

ii) The reaction $^{16}O(p,^{3}He)^{14}N$ (2.311 MeV) 69

iii) The reaction $^{16}O(p,t)^{14}O$ (Ground state) 85

iv) The reactions $^{12}C(p,t)^{10}C$ (Ground state, 3.34) 87

v) The reaction $^{28}Si(p,t)^{26}Si$ (Ground state) 94

vi) The reaction $^{16}O(p,^{3}He)^{14}N$ (Ground state) 97

vii) Summary and Conclusions 102

APPENDICES. 107

REFERENCES. 116

ACKNOWLEDGEMENTS.

At the close of this research programme, it is a pleasure to express my thanks to the many people who have helped me during the last three years. In particular, I would like to thank Professor D.H. Wilkinson F.R.S., for his kind assistance and for allowing me to join the Nuclear Physics Laboratory to carry out this research. My supervisor, Dr. P.S. Fisher, has been generous in his help in many ways, both inside and outside the laboratory, and this has been very much appreciated.

The experiments were carried out at the Rutherford High Energy Laboratory and I thank Dr. W.D. Allen for allowing me to use the Proton Linear Accelerator. The experiments could not possibly have been performed single handed, and I would like to thank Dr. D.K. Scott for his help, and especially Dr. N.S. Chant for his advice and willing assistance throughout this work. For his readiness to help at any hour of the day or night, and to perform any task no matter how much of a nuisance it may have been to him, Mr. R. Bustany deserves special thanks. Very little experimental time was lost because of machine faults, and all credit for this goes to the accelerator operators and the maintenance crew for their efficient handling of the machine. I would also like to thank Mr. J. Macken for his

patience and care in checking the components and alignment of our beam line as this contributed a great deal to the smooth running of the experiments.

I would also like to thank my colleagues in Oxford, notably Dr. I.S. Towner, for many helpful discussions, and also Dr. A.C. Shotter for his encouragement and advice. The analysis of the data required the extensive modification of a computer programme and I am indebted to Mr. B.E.F. Macefield not only for allowing me to alter his programme so radically, but also for his advice while I was doing so. The development of this programme would have been a very arduous task had it not been for the cheerful cooperation of the staff of the Atlas Computing Laboratory. It is a pleasure to thank them for their help and, in particular, the Director of the Laboratory for permitting me to use the excellent facilities.

I owe a special debt of gratitude to my wife for her constant support and encouragement during this research, as well as her patience and help with the preparation of this thesis. My parents have also given me considerable help over many years, and for this I am grateful.

I would like to thank the University of the Witwatersrand and, especially Professor J.P.F. Sellschop, the Director of

the Nuclear Physics Research Unit, for granting me extended leave to enable me to come to Oxford. While in Oxford, I have been supported by a Shell Postgraduate Scholarship awarded by Shell (South Africa) Limited, and I am glad to express my thanks to the Company for their help, and also to the Shell International Petroleum Company in London for their interest in my work and for their very generous hospitality.

Finally, I would like to thank Miss G. Hepworth for the loan of a typewriter and her advice on matters of typing.

ABSTRACT.

Nucleon transfer reactions play an important part in studies of nuclear spectroscopy, and it is necessary that the basic reaction theory should be thoroughly examined. In the case of two nucleon transfer reactions, this examination has been confined to the differential cross section since a proper study of polarization phenomena in these reactions has not been made. In this thesis, the results of a number of asymmetry measurements in double pick-up reactions will be reported. These measurements, based on (p,t) and (p,^{3}He) experiments, were performed at the Rutherford High Energy Laboratory using the 50 MeV polarised proton beam from the linear accelerator. During the course of this report, the techniques of experimentation with such a beam will be described. The differential cross sections of the reactions were measured with the more intense unpolarised beam, and these results will also be presented.

An analysis of the data in terms of the distorted wave Born Approximation theory will be given in Chapter 5. The theory, in its two most frequently used forms, is outlined in Chapter 1. Special attention is paid to the consequences of neglecting spin-orbit coupling in the

description of the optical model potentials. A summary is given in Chapter 2 of a general, spin-dependent distorted wave computer programme which was written as part of this research so that the DWBA analysis could be made. The programme is based on a code initially written specifically for deuteron stripping.

In the analysis, it will be shown that the usual zero-range spin-independent form of the nucleon transfer process is unable to account for the experimental observations. The two forms of double pick-up theory will be compared, and the possibility of avoiding the zero-range approximation will be investigated. In fact, it will be seen that finite-range corrections are essential to a proper analysis of the data. The importance of interference effects and spin-orbit coupling in two nucleon transfer reactions will be evaluated. The results of two optical model analyses of published cross section data are included in a discussion of the triton and ^{3}He optical potentials. Finally, a possible new method of examining the relative phases of nuclear wave function components will be described.

FIGURES.

The diagrams relevant to a particular chapter are to be found at the end of that chapter. The one exception to this rule is Figure 1.1 in Chapter 1 which is to be found after Page 4.

CHAPTER 1. THE TWO NUCLEON TRANSFER REACTION.

The interpretation of the structure of the nucleus is a problem which depends for its solution on detailed and accurate information about nuclear states. One of the most prolific sources of this spectroscopic information has been the study of direct reactions and and in particular the (d,p) stripping process. The advent of accelerated triton and ^{3}He ion beams has made possible the investigation of two nucleon transfer reactions which are used to advantage since the residual nucleus can be 2 mass units removed from the nearest stable target. In this way, final states can be examined which are inaccessible to the usual (d,p) techniques. Double pick-up reactions such as (p,t) and (p,^{3}He) have been studied with medium energy proton beams and in 1964 Cerny and Pehl showed that the simultaneous observation of these processes provides a powerful method of studying isobaric analogue states. The popularity of (t,p) and (^{3}He,p) reactions and their inverse processes in nuclear spectroscopy studies has increased because it is now abundantly clear that the analysis of the two nucleon transfer reaction can yield even more spectroscopic information than the analysis of the more simple (d,p) or (p,d) process.

These analyses have been made within the framework of the well-known distorted wave Born approximation (DWBA) theory which has been extensively tested in the study of (d,p) reactions by the comparison of theoretical predictions with experimental angular distributions (eg. Lee et al.,1964). In this way, new light has been thrown on

basic approximations made in the DWBA theory such as the neglect of spin-orbit forces in the entrance and exit channels and the assumption that the interaction potential responsible for the reaction process has zero range. The modifications to the theory have been a consequence of these investigations and have improved the reliability of spectroscopic information derived from the application of the DWBA theory to experimental data. In a recent conference on polarization phenomena Weidenmüller (1965) and others stressed the importance of measuring the polarization of the reaction products (or the azimuthal asymmetry in the angular distribution if the incident beam is polarised) in the course of these experimental investigations. Several papers have reported on this type of measurement for (d,p) and (p,d) reactions (Hjorth et al.,1965; Chant et al.,1967; Chant and Nelson,1968), but no polarization or asymmetry measurements have been reported for two nucleon transfer reactions at a bombarding energy sufficiently high that interference from compound nucleus processes can be ignored. If the DWBA theory as applied to two nucleon transfer reactions is to be as comprehensively tested as it has been for the single nucleon case, then these experiments must be undertaken.

In this thesis a report will be given of the results of asymmetry measurements which were made at the Rutherford High Energy Laboratory with the 50 MeV polarised proton beam. The high incident energy ensures that the reactions can confidently be assumed to proceed via the direct interaction mechanism only. For reasons that will be

elaborated presently, the reactions chosen for this study were, in the p-shell:

$^{12}C(p,t)^{10}C$: ground state (0^+) and 1st excited state (3.34 MeV 2^+)

$^{16}O(p,t)^{14}O$: ground state (0^+)

$^{16}O(p,^3He)^{14}N$: ground state (1^+) and 1st excited state (2.311 MeV 0^+)

and in the s-d shell,

$^{28}Si(p,t)^{26}Si$: ground state (0^+).

The differential cross sections and the polarisation analysing powers have been compared with the predictions of the simple DWBA theory. This has permitted the underlying assumptions of the theory to be examined and in the course of this report certain modifications will be discussed after the usual spin-independent zero-range DWBA theory has been shown to be quite inadequate to the task of the present analysis.

i) The distorted wave Born approximation theory.

The general formalism of the DWBA theory has been described in great detail by Satchler (1964) and others (Tobocman,1961; Glendenning,1963) and it would be tedious and unnecessary to reproduce this work here in full. However, if the problems that will be discussed in this thesis are to be presented concisely, it is necessary to consider in a brief outline some aspects of the theory. The computer programme used in the analysis will be described later but suffice it to say that as it is based on a deuteron stripping code, the theory will be considered from a stripping point of view.

The relation between the stripping and pick-up cross sections is simple and will be given when it is required. In the interests of clarity, the incident beam (and target) will be considered to be unpolarised and the case of a polarised incident beam will be deferred to the next chapter. The nomenclature that will be used follows that of Satchler. The reaction A(a,b)B in which a group x is transferred is shown diagrammatically in Figure 1.1.

The interaction potential V_I in the final state is $V_{bB} - U_{bB}$ (Tobocman,1961) where U_{bB} is the optical model potential in the channel and V_{bB} is the two-body potential between the nucleon b and the nucleons in B. If V_I is treated as a perturbation then the matrix element for the transition is given by

$$M_{ab} = \int \chi^*_{bB}(k_b, r_{bB})\ I^{eff}\ \chi_{aA}(k_a, r_{aA})\ dr_{aA}\ dr_{bB} \qquad 1.1$$

where I^{eff} appears as an effective interaction between the elastic scattering states χ_{aA} and χ_{bB}. The functions χ are solutions of the Schrodinger equation containing the optical model potential relevant to each channel. The factor I^{eff} is dependent only on the physics of the interaction and is given by

$$I^{eff} = P_1 P_2 \int \psi^*_{J_B}(r_{xA}, \xi_x, \xi_A)\ \sigma^*_{J_b}\ V_I\ \psi_{J_a}(r_{bx}, \xi_b, \xi_x)\ \psi_{J_A}(\xi_A)\ d\xi_x d\xi_A d\xi_b \qquad 1.2$$

The factors P_1 and P_2 arise from antisymmetrization of the full channel wave function (Towner and Hardy,1968), and are given in Appendix A1(i). The remaining symbols ψ_{J_a}, ψ_{J_A}, ψ_{J_B} refer to the wave functions of the projectile, target and residual nuclei respectively

SCHEMATIC DIAGRAM OF THE REACTION A(a,b)B

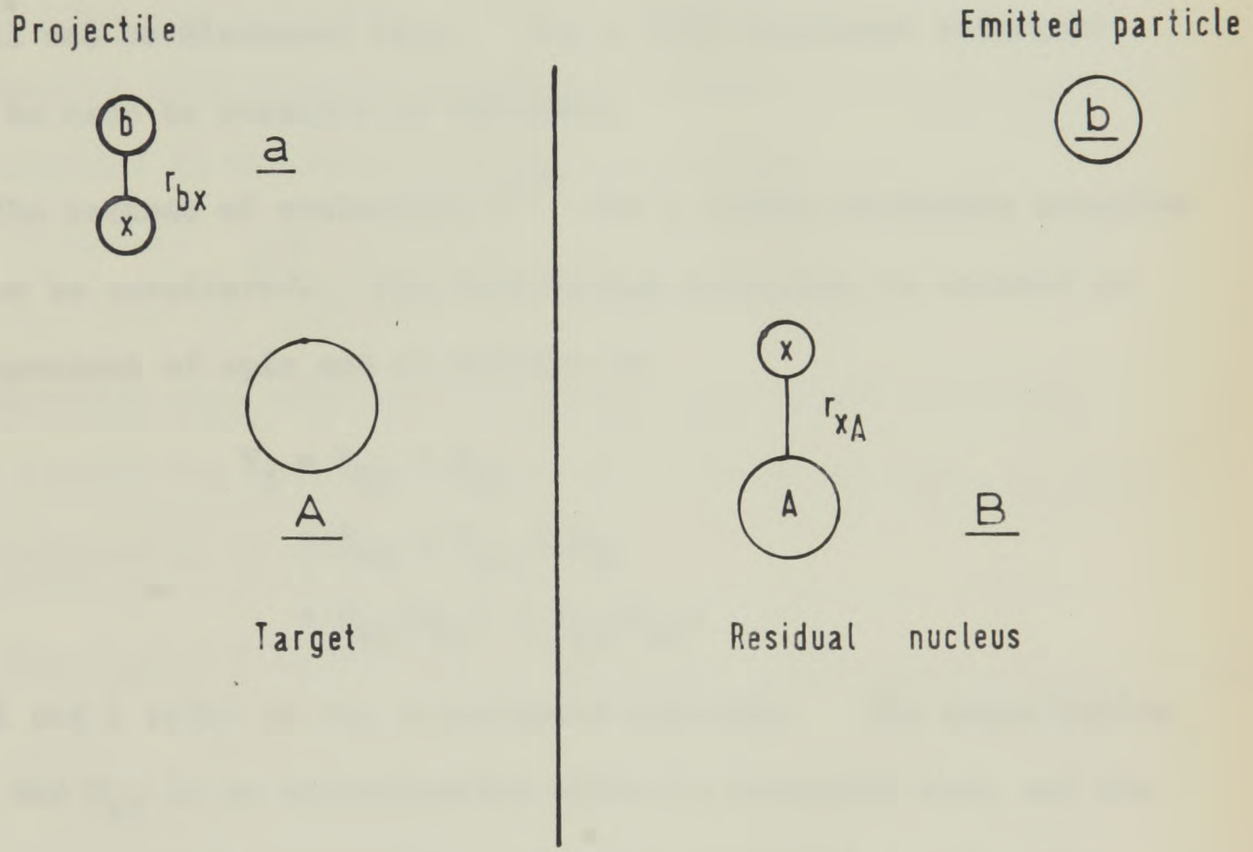


FIGURE 1.1

which have spins J_a, J_A and J_B. The spin function of the outgoing particle is given by σ_{J_b}. The symbol ξ_μ refers to the internal coordinates of the system μ. After the integral I^{eff} has been evaluated the remaining integration over r_{aA} and r_{bB} can be carried out by the usual method of writing χ_{aA} and χ_{bB} in a partial wave expansion. This is a mathematical rather than a physical problem and will not be discussed here. For a full treatment reference should be made to Satchler or Tobocman.

The methods of evaluating I^{eff} for a double stripping reaction will now be considered. The interaction potential is assumed to be independent of spin and is written as

$$\begin{aligned} V_I &= V_{bB} - U_{bB} \\ &= V_{bx} + V_{bA} - U_{bB} \\ &\approx V_{b1}(r_{b1}) + V_{b2}(r_{b2}) \end{aligned}$$

where 1 and 2 refer to the transferred nucleons. The cancellation of V_{bA} and U_{bB} is an approximation which is generally made and the disappearance of V_{bA} from the interaction potential implies that the core nucleus A is not excited in the reaction. The notation will be simplified wherever possible by using curly brackets with a subscript to indicate angular momentum coupling. The summations are to be understood to include the magnetic quantum numbers and only those quantum numbers which are of particular relevance to the discussion will be given explicitly.

The wave function ψ_B of the residual nucleus is expanded in terms of the two transferred nucleons which are in shell model orbits (nℓj), and the eigenstates of the target.

In j-j coupling:

$$P_1\ \psi_{J_B}(r_{xA},\xi_x,\xi_A) = P_1\ \Sigma_N\ G_{(j_1j_2)J}\ \{\psi_{J_A'}(\xi_A')\ \psi_{(j_1j_2)J}(r_{xA},\xi_x)\}_{J_B} \qquad 1.3$$

where $N = n_1\ell_1j_1;\ n_2\ell_2j_2$

The expansion coefficient G is given by the overlap $\langle\psi_A,\psi_x|\psi_B\rangle$ and is related to the spectroscopic factor SF by

$$SF^{\frac{1}{2}}_{(j_1j_2)J} = P_1\ G_{(j_1j_2)J}$$

An integration over spin functions will later become necessary, and to isolate the spin function of the transferred pair, ψ_J must be transformed to LS coupling. Thus:

$$P_1\ \psi_{J_B}(r_{xA},\xi_x,\xi_A) = \Sigma_N\ SF^{\frac{1}{2}}_J\ E_{LSJ}\ \{\{\psi_{(\ell_1\ell_2)L}(r_{xA},\xi_x)\sigma_S\}_J\ \psi_{J_A'}(\xi_A)\}_{J_B} \qquad 1.4$$

where the spin wave function of the transferred pair is σ_S and the symbol E_{LSJ} is related to the wigner 9-j symbol by

$$E_{LSJ} = ((2L+1)(2S+1)(2j_1+1)(2j_2+1))^{1/2}\begin{Bmatrix} \ell_1 & \ell_2 & L \\ \frac{1}{2} & \frac{1}{2} & S \\ j_1 & j_2 & J \end{Bmatrix}$$

The effective interaction can now be written after substitution of eqn.(1.4) into eqn.(1.2) and integration over the core coordinates ξ_A

$$I^{eff} = P_2 \Sigma_N C \times SF_J^{\frac{1}{2}} \times \int \sigma^*_{J_b} \sigma^*_S \psi^*_{(\ell_1 \ell_2)L}(r_{xA}, \xi_x) V_I \psi_{J_a}(r_{bx}, \xi_x, \xi_b) d\xi_x d\xi_b \qquad 1.5$$

The coupling coefficients are lumped into C. The wave function ψ_L for the bound state of the captured nucleons describes the motion of the two particles in terms of the motion of their centre of mass about A (coordinate r_{xA}) and their relative or "internal" motion (ξ_x). This function cannot in general be factorised into the two constituent components and thus some assumption must be made before the integration can be performed. The problem will be dealt with from the two approaches that are most commonly employed in practice.

a) Zero range point "tri-nucleon" approximation.

This treatment was first described by Rook and Mitra (1964) and has been used extensively in the analysis of (t,p) reactions (eg. Glover and Jones,1966) as well as (^{3}He,n) reactions (eg. McMurray et al.,1967). The Rook-Mitra approach ignores the relative motion and the two transferred particles are assumed to occupy the same point in space so that the dependence on ξ_x disappears. Each of the two nucleons is to be described by a single particle wave function $\phi_{n\ell j}(r_{xA})$ so that the effective interaction can be written:

$$I^{eff} = g P_2 \Sigma_N C \times SF_J^{\frac{1}{2}} \{\phi^*_{n_1 \ell_1 j_1}(r_{xA}) \phi^*_{n_2 \ell_2 j_2}(r_{xA})\}_L$$
$$\times \int \sigma^*_S \sigma^*_b V_{bx}(r_{bx}) \psi_{J_a}(r_{bx}, \xi_b) d\xi_b \qquad 1.6$$

where g is another antisymmetrization factor and is given by

$$g = 1 \text{ if } n_1\ell_1j_1 = n_2\ell_2j_2$$

$$\text{and} = \sqrt{2} \text{ otherwise.}$$

The wave function ψ_{J_a} is assumed to have zero range and this effectively replaces the integral by a delta function.

$$I^{eff} = g\, P_2\, L_N\, C \times SF_J^{\frac{1}{2}} (\phi^{\dagger}_{n_1\ell_1j_1}(r_{xA}) \phi^{\dagger}_{n_2\ell_2j_2}(r_{xA}))_L \times D_o\, \delta(r_{bx})\, b_s \quad 1.6a$$

where D_o is a constant which depends on the strength of the interaction and the structure of the projectile a, and b_s is a structure coefficient which depends on the spin S of the transferred pair and has the value

$$b_s^2 = \delta_{S,0} \quad \text{for (t,p)}$$

$$= \tfrac{1}{2}(\delta_{S,0} + \delta_{S,1}) \quad \text{for } {}^3\text{He,p.}$$

The final integration in eqn.(1.1) can now be performed and the cross section evaluated.

The physical significance of the use of the delta functions $\delta(r_{bx})$ and $\delta(\xi_x)$ is that the projectile (whether triton or ^{3}He ion) which is described by the wave function $\psi_{J_a}(r_{bx},\xi_b,\xi_x)$, is considered to be a point particle. Glover et al., (1966) have evaluated the integral in eqn.(1.6) using elementary forms for the interaction potential and the projectile wave function. A better value for D_o was determined by Mathur and Rook (1967) with a general, spin-dependent interaction potential and a realistic wave function for the projectile. Their result is

$$D_o^2 = 31.4 \times 10^6 \quad \text{MeV}^2\ \text{fm}^6$$

and with this value of D_o, the theoretical prediction for the absolute cross section of the $^{16}O(t,p)^{18}O$ ground state reaction was found to be in reasonable agreement with experiment.

The single particle wave functions ϕ are taken to be solutions of the Schrodinger equation in a Saxon-Woods well with a depth which is adjusted until the asymptotic behaviour of the wave function is consistent with the binding energy of the transferred nucleon.

b) Zero-range Gaussian "tri-nucleon" approximation.

The evaluation of I^{eff} as written in the form of eqn.(1.5) depends partly on the factorization of the wave function $\phi_L(\vec{r}_{xA},\xi_x)$ describing the transferred nucleons. If the bound state can be described in terms of harmonic oscillator functions then ϕ_L can be separated simply and exactly into the components of relative motion and centre of mass motion (de-Shalit,1963). Thus if $\phi_{n_1\ell_1}(\vec{r}_1)$ and $\phi_{n_2\ell_2}(\vec{r}_2)$ are oscillator wave functions then

$$\psi_{(\ell_1\ell_2)L}(r_{xA},\xi_x) = \{\phi_{n_1\ell_1}(\vec{r}_1)\ \phi_{n_2\ell_2}(\vec{r}_2)\}_L$$

$$= \sum_{(n\lambda N\Lambda)} \langle n\lambda N\Lambda;L|n_1\ell_1 n_2\ell_2;L\rangle_x \{\phi_{n\lambda}(\xi_x)\phi_{N\Lambda}(r_{xA})\}_L$$

where $\vec{r}_1 - \vec{r}_2 = \xi_x$ and $\vec{r}_1 + \vec{r}_2 = 2\,\vec{r}_{xA}$.

In this expansion, λ and Λ are the orbital angular momenta of the relative and centre of mass motions and n and N are the respective principal quantum numbers. The D-state component of relative motion of the triton or ^{3}He ion amounts to less then 5%, (Phillips,1966;

Mathur and Rook,1967). If this is ignored then

$$\psi_{(\ell_1\ell_2)L}(r_{xA},\xi_x) = \Sigma_{(nN)} \langle nONL;L|n_1\ell_1n_2\ell_2;L\rangle \phi_{no}(\xi_x)\ \phi_{NL}(r_{xA})$$

and the expansion coefficients are known and have been tabulated (Brody and Moshinsky,1960). The properties of the transformation restrict the summation to values of n and N which satisfy the relation

$$2(n + N) + L = 2(n_1 + n_2) + \ell_1 + \ell_2$$

If the space part of the triton or ^{3}He ion wave function is assumed to have a Gaussian form then Glendenning (1965) has shown that the effective interaction I^{eff} can be written as:

$$I^{eff} = U\ \tilde{g}\ b_s\ \Sigma_{N'}C\ SF_J^{\frac{1}{2}} \times\Sigma_{(nN)} \langle nONL;L|n_1\ell_1n_2\ell_2;L\rangle\ \Omega_n\ \phi_{NL}(r_{xA}) \qquad 1.7$$

where $N' = (n_1\ell_1j_1;\ n_2\ell_2j_2)$. U is a normalization factor and C are angular momentum coefficients. The factor Ω_n is the overlap of the relative motion wave function of the transferred pair $\phi_{no}(\xi_x)$ on the triton or ^{3}He wave function. The normalised oscillator wave function and the overlap Ω_n are defined in Appendix A1(ii). The final integration of the matrix element in eqn.(1.1) is simplified by reducing the interaction potential to the zero-range form.

This method of describing I^{eff} has been used, with one modification, in a number of analyses (Glendenning,1965; Donău et al.,1967; Kollveit, 1968). The modification has been necessary because the asymptotic form of the oscillator wave function does not reflect the correct binding energy of the transferred nucleons. The tail of the oscillator

wave function is therefore replaced at a matching radius MR by a spherical Hankel function of the first kind $-i^L h_L^1(i\kappa r_{xA})$ where κ^2 is proportional to the correct binding energy. This procedure suffers from the disadvantage that the matching radius and hence indirectly the magnitude of the predicted cross section, is critically dependent on the oscillator parameter ν.

This section will be concluded with a summary of the selection rules that can be derived from the theory. The quantum numbers of the transferred nucleons have been given as L,S and J. The isobaric spin is T and ℓ and j refer to the single particle orbits.

Angular momentum transfer: $|j_1 - j_2| \leq J \leq j_1 + j_2$

$|J_A - J_B| \leq J \leq J_A + J_B$

$|\ell_1 - \ell_2| \leq L \leq \ell_1 + \ell_2$

Parity change: $\Delta\pi = (-1)^{\ell_1+\ell_2}$

$= (-1)^{\lambda+\Lambda}$

$= (-1)^L$ Equations 1.8

Spin and isobaric spin rules: (for transferred nucleons)

(t,p) : S = 0, T = 1

(^{3}He,p): S = 0, T = 1 or S = 1, T = 0

Finally, the differential cross section for stripping is given by

$$\frac{d\sigma}{d\omega} = \frac{\mu_a\mu_b}{(2\pi\hbar^2)^2}\frac{k_b}{k_a}\frac{2J_B+1}{2J_A+1}\sum_J |\Sigma_{LS} b_s \Sigma_N S F_J^{\frac{1}{2}} \mathcal{S}_{LSJ}|^2 \qquad 1.9$$

where the amplitude $\mathcal{S}$ is what remains of the matrix element M of eqn.(1.1)

after the spectroscopic amplitude SF has been extracted. The reduced mass is given by μ and N refers to the summation over the configurations of the transferred nucleons. The pick-up cross section is related to the stripping cross section by

$$\frac{d\sigma}{d\omega} = \frac{k_a^2}{k_b^2} \frac{2J_A+1}{2J_B+1} \frac{2J_a+1}{2J_b+1} \frac{d\sigma}{d\omega}_{\text{(Stripping)}} \qquad 1.10$$

ii) Application of two nucleon transfer theory to experiment.

The wealth of spectroscopic information that can be obtained from the analysis of two nucleon transfer reactions is partly a consequence of the stringent selection rules that are applicable to these processes. The theoretical angular distribution is dependent on the form of the amplitude β of eqn.(1.9) and as in the case of single nucleon transfer reactions, the shape of the distribution will be characterised by the value of the orbital angular momentum transferred. A comparison between theory and experiment invariably allows this value to be determined unambiguously. In the case of (t,p) and (^{3}He,n) reactions when the two transferred nucleons are identical, the restriction of the spin of the pair to S = 0 implies that the total spin transfer is given by J = L. If the target nucleus has zero spin it is at once clear that the spin and parity of the final state can be assigned uniquely. This property of the two nucleon transfer reaction provides a sharp contrast to the uncertainty in spin determination of the final state which is a characteristic of the (d,p)

process. The difference in the isobaric spin selection rules between the (p,t) and (p,^{3}He) reactions and the relation between the cross sections for the two processes given by the values of b_s in eqn.(1.9) have been elegantly exploited by several workers to locate the components of isobaric spin multiplets (Détraz et al.,1965; Hardy and Skyrme,1966).

One of the outstanding features of the two nucleon transfer reaction is the coherent sum over all configurations of the transferred nucleons as expressed in eqn.(1.3). Yoshida (1962) has shown how this coherence can lead to considerable enhancement of the cross section when the reaction leads to collective states. The signs of the components of wave functions used for the initial and final states can be checked by comparing theoretical and experimental magnitudes of relative cross sections. The theoretical predictions should depend very sensitively on these signs through the coherence effect and Hardy and Towner (1967a) have demonstrated this in a conclusive manner in their analysis of the ^{28}Si(t,p)^{30}Si reaction, using the theory described in part (a) of the last section. An example of the examination of calculated wave functions and spectroscopic amplitudes made by the use of (p,t) and (p,^{3}He) reactions and the theory of part (b) of the last section, is contained in an extensive report on the levels of ^{13}C and ^{13}N (Fleming et al.,1968a).

Although the success of two nucleon transfer reactions in the field of nuclear spectroscopy has been demonstrated in several cases, a number

of important assumptions made in previous analyses have not been adequately considered. Perhaps the most significant of these is the neglect of spin-orbit forces in the entrance and exit channels. This has been a common feature of the spectroscopic analyses reported in the literature. The omission of spin-orbit forces has not been made without some justification. The triton and ^{3}He optical model potentials have not been systematically studied as will become evident later on. Very few ^{3}He elastic-scattering-polarization measurements, and no triton polarization measurements at all, have been reported. The almost total absence of information on the spin-orbit strength of the triton and ^{3}He optical potentials has therefore been responsible for the use of spin-independent DWBA theory in the analysis of experimental data. It has long been realised that the differential cross section for single nucleon transfer reactions is insensitive to the strength of the spin-orbit potential (Hodgson,1962) and the two nucleon transfer cross section is expected to be equally as insensitive to this term. The spin-independent differential cross section for stripping is given by

$$\frac{d\sigma}{d\omega} \propto \Sigma_{LSJ} b_s^2 \left| \Sigma_N \, SF_J^{\frac{1}{2}} \, g_{LSJ} \right|^2 \qquad 1.11$$

and the form of this equation should be compared with the spin-dependent cross section given by eqn.(1.9). The two equations differ notably by the replacement of a coherent sum over L and S in the spin-dependent case, with an incoherent sum in the spin-independent case. When two

identical nucleons are transferred to or from a spin-zero nucleus, the selection rules specify that only one L and S value will contribute to the cross section. In this instance, which covers (t,p) and (^{3}He,n) reactions, the coherence or incoherence of the sum is irrelevant and a spin-independent theory can be used. However, when a (^{3}He,p) reaction is considered, or a (t,p) reaction on a non spin-zero target, then in general more than one L value can contribute to the cross section and the subsequent use of a spin-independent theory in the analysis may be in error if the spin-orbit coupling is not negligible.

While the effect of spin-dependent distortions on the cross section is in doubt in certain circumstances, the relation between spin distortions and the polarization of the reaction products is much better known (Goldfarb and Johnson,1960). One result which is particularly relevant, is that if the spin S of the transferred particles is zero, then the polarization of the outgoing particle will be entirely dependent on the strength of spin-orbit coupling in the entrance and exit channels. The observation of proton polarization in a (t,p) reaction in which the selection rules restrict S to be zero, will clearly underline the presence of spin-orbit forces and the inadequacy of the spin-independent theory. The importance of coherence effects in the (^{3}He,p) reaction can be examined by comparing the predictions of spin-dependent theory with the experimental observations of the polarization of the outgoing protons. This discussion indicates the importance of polarization phenomena in this investigation. The subject will be developed in the next chapter.

The simple form of the interaction potential has been extended to include spin and isospin dependant terms (Abul-Magd and El-Nadi,1966). The effects on the cross section of this more general potential have not been studied within the framework of a theory which explicitly accounts for the interference of different L and S terms in the matrix element. An investigation of the general potential has been made but with a spin-independent theory (Hardy and Towner,1967b). However, Fleming and his collaborators (1968b) have shown that the combination of a spin-dependent interaction potential and a theory which neglects spin-orbit distortions is not able to account for experimental observations of the ratio of (p,t) and (p,^{3}He) cross sections with odd mass targets. Provided that a reaction is chosen so that the selection rules restrict each of S and T to one value only then it can be shown that the effect of the introduction of spin-dependence in the interaction potential is to reduce the absolute cross section. At the present time the development of two nucleon transfer theory has not reached the stage where absolute cross sections can be predicted reliably. This report will deal with reactions where the absolute magnitude of the cross section is not an important factor in the analysis and the use of a spin-independent interaction potential is therefore justified when reactions are chosen within the limits specified above.

Two significant factors have been mentioned which should be accounted for in any analysis. A third factor, the consequences

of the zero range approximation, must also be examined. This procedure is invariably adopted to reduce the 6 dimensional integral of eqn.(1.1) to 3 dimensions, the physical implication of the approximation being that the emitted particle leaves the nucleus at the same point where the incident particle is 'absorbed'. The complete integration has been attempted for the (d,p) calculation (Austern et al.,1964), but the complexities are such that the full treatment will probably remain an exception. Buttle and Goldfarb (1964) have shown for the case of deuteron stripping that it is possible to simulate the effects of a finite-range interaction by the use of a multiplicative factor which modifies the wave function of the transferred nucleon. Both the magnitude of the cross section and the shape of the angular distribution are affected when the correction is applied and the important result is that the agreement between theory and experiment is usually improved, thus lending greater credence to the spectroscopic information derived in the analysis. The zero-range approximation in two nucleon transfer reactions is obviously a more far reaching assumption than in the case of single nucleon transfer reactions and it is clearly of interest to examine whether similar finite-range corrections can be applied to the two nucleon transfer process. The effects of a finite-range interaction can be crudely estimated by the use of a lower cut-off in the radial integral of eqn.(1.1) (Rook and Mitra,1964). This is not wholly satisfactory and in fact Bencze and Zimanyi (1966) demonstrated that the use of a cut-off to simulate finite-range corrections is likely to give rise

to errors in the detailed reaction analysis. Finite range calculations based on the WKB approximation will be given in this report and their relevance to two nucleon transfer analyses will be discussed.

In this brief review of the application of two nucleon transfer theory to the analysis of experimental data, the observation of polarization phenomena has been shown to be a necessary adjunct to the measurement of differential cross sections if spin-orbit forces and interference effects are to be investigated. The methods by which polarization phenomena can best be studied will be described in the next chapter.

CHAPTER 2. POLARIZATION AND PICK-UP REACTIONS.

The observation of polarization effects, that is, the non-uniform population of magnetic substates, has proved to be an invaluable aid in testing nuclear reaction mechanisms and theories. The early plane wave Born approximation theory was known to be seriously inadequate and its limitations were emphasized when reaction products were observed to be polarised contrary to theoretical predictions. In 1953 Newns suggested that the sign of the polarization of the outgoing particle could give information about the total spin of the transferred nucleon in deuteron stripping reactions. The theory was developed to include optical model distortions in the description of the incoming and outgoing waves to account for nuclear interactions and semi-classical arguments were used to calculate the upper limits of the resultant polarization. When these limits were found to be exceeded, the optical model potential was extended by incorporating a spin-dependent term ($\underline{l}\cdot\underline{s}$ form) and the spin-dependent theory has since been used to predict angular distributions and polarization in deuteron stripping reactions (eg. Miller,1965).
It has been suggested in previous sections that the observation of polarization effects could, in a similar way, give information about the two nucleon transfer process and in this chapter a method of making these observations will be described.

i) The polarization-asymmetry theorem.

The description of polarization in direct reactions has been covered in a general paper by Goldfarb and Johnson (1960) and to avoid unnecessary repetition, those results which are relevant to the discussion will simply be quoted and will not be derived. The stripping process has been the main subject of the theoretical discussion because of the nature of the computer programme that will be used in the analysis. To simplify the notation, the triton stripping reaction A(t,p)B will now be taken as a specific example. The incident beam is unpolarised. In general, the interaction of the incident or emitted particle with the nucleus will polarise the outgoing particle. The proton polarization is defined as the expectation value of the Pauli spin operator and is a vector parallel to the normal of the reaction plane. The positive direction of the normal is parallel to the vector $k_t \times k_p$ where k_i are momentum vectors. The proton polarization P_p can be measured by using a second reaction as an analysing process. The differential cross section for the analysing reaction is given by

$$\frac{d\sigma}{d\omega} = \frac{d\sigma}{d\omega}\Big|_o \{1 + P_p \cdot P'_A(\theta)\} \qquad 2.1$$

where $\frac{d\sigma}{d\omega}\Big|_o$ is the differential cross section for the analysing reaction when the incident beam is unpolarised, ie $P_p = 0$. The efficiency of the process for the measurement of polarization is given by $P'_A(\theta)$, and is called the polarization analysing power.

This type of experiment, which involves a double scattering, is notoriously difficult because of the very small counting rates observed in the analysing reaction. It is plainly desirable to deal with one reaction only and this requires that instead of being examined after the interaction, any polarization phenomenon must be introduced before the reaction takes place. When the incident beam is polarised, the differential cross section for the inverse reaction B(p,t)A is given by the use of eqn.(2.1):

$$\frac{d\sigma}{d\omega} = \frac{d\sigma}{d\omega_o} \{1 + P \cdot P_A(\theta)\}$$

where $\frac{d\sigma}{d\omega_o}$ is the unpolarised pick-up cross section and is related to the stripping cross section by eqn.(1.10). The polarization of the incident proton beam is denoted by P and must be measured before the reaction takes place. The unknown quantity $P_A(\theta)$ is the analysing power of the reaction B(p,t)A. The product $P \cdot P_A$ is the asymmetry of the distribution and is the quantity actually measured in an experiment.

The polarization phenomena in the stripping and pick-up reactions are related by an important theorem first proposed by Blin-Stoyle (1951). The so-called polarization asymmetry theorem states that for the reactions mentioned in this discussion, the proton polarization P_p in the (t,p) reaction is equal to the polarization analysing power in the inverse, polarised proton induced (p,t) reaction:

$$P_p = P_A \qquad 2.2$$

The result is valid if the reaction B(p,t)A is the time inverse of A(t,p)B (Satchler,1958). This stringent condition can be relaxed without invalidating eqn.(2.2) so that the reactions need only be reciprocal in the sense that the inverse reaction is obtained by reversing the signs of the momentum vectors (Biedenharn,1959).

The polarization-asymmetry theorem is the link between the two nucleon stripping theory discussed previously and the double pick-up experiments that are to be described. The observation of polarization of the emitted particle in a double stripping reaction has been shown to provide a means of investigating the effects of spin-orbit forces in the entrance and exit channels, and also of studying interference effects in two nucleon transfer reactions. This observation can now be made by measuring the asymmetry in the angular distribution of the inverse pick-up reaction when the incident beam is polarised. The stripping theory can be used to predict both the analysing power of the pick-up reaction and the unpolarised differential cross section.

The polarization of the emitted particle in the double stripping reaction A(t,p)B is given by

$$P_p(\theta) = \frac{2\sum\{(\tfrac{1}{2}-m_p)(\tfrac{1}{2}+m_p+1)\}^{\frac{1}{2}}\ \mathrm{Im}\{B^{LM m_p m_t}_{SJ}\ B^{L'\ M+1\ m_p+1\ m_t+1^*}_{S'J}\}}{\sum B^{LM m_p m_t}_{SJ}\ B^{L'M m_p m_t}_{S'J}} \qquad 2.3$$

where m are the magnetic substates of the proton and triton and $B^{LM}_{SJ} = SF^{\frac{1}{2}}_{J} \times \delta^{M}_{L}$ where $SF^{\frac{1}{2}}$ and δ are the spectroscopic and transition

amplitudes respectively, and appear in eqn.(1.9). The summation is over all quantum numbers and the sensitivity of the polarization to interference effects is due to the interference between terms with different orbital angular momentum L and transferred spin S.

Sufficient theoretical detail has been given to allow the discussion to conclude with a summary of the particular problems of two nucleon transfer theory that are of interest and the reactions that would provide a suitable basis for their study.

ii) Pick-up reactions with polarised protons.

The widespread use of spin-independent DWBA theory in analyses of two nucleon transfer reactions is a matter that warrants close examination, especially for those reactions where interference between different orbital and spin angular momentum contributions can arise and is neglected. The interference only arises if spin-orbit forces are present in the entrance and exit channels. Since the effect of spin-orbit forces in two nucleon transfer reactions is unknown, it is essential to choose reactions for this study in such a way that the importance of spin-orbit coupling can be examined in isolation from the possible resultant interference effects. The spin-independent theory predicts that the asymmetry in the angular distribution of a double pick-up reaction induced by polarised protons will be zero if the spin angular momentum of the transferred particles is zero. This angular momentum condition is guaranteed for the (p,t) reaction by the selection rules given

in the last chapter, and an asymmetry measurement for such a process will constitute a stern test of the theory. The single value of the spin transfer avoids the otherwise mandatory use of a spin-dependent interaction potential, the exact form of which is, in any case, not fully established. Furthermore, if a zero-spin target is used, the selection rules restrict the transferred angular momentum L to a unique value. These conditions, which are satisfied by the following reactions, ensure that the examination of the direct effects of spin-orbit coupling will not be complicated by the indirect effects of any consequent interference between different L and S terms.

$^{12}C(p,t)^{10}C$	(ground state)	L = J = S = 0
$^{12}C(p,t)^{10}C$	(3.34 MeV)	L = J = 2, S = 0
$^{16}O(p,t)^{14}O$	(ground state)	L = J = S = 0
$^{16}O(p,^{3}He)^{14}N$	(2.311 MeV)	L = J = S = 0

The results of asymmetry measurements for these reactions will be described in detail. In addition, the differential cross sections, measured with an unpolarised beam, will also be discussed.

The use of spin-independent theory in any analysis has been shown to be most suspect when more than one L and S value can contribute to the reaction being studied. The reaction $^{16}O(p,^{3}He)^{14}N$ to the ground state has been chosen for an investigation of these effects. The angular momentum transfers are limited to S = J = 1 and L = 0 and 2. The use of a spin-dependent interaction potential is again avoided since there is only one S value, and the effects of

the interference between different L values can be assessed without additional interference due to a multiplicity of S values.

The ^{16}O target was chosen for a second reason. The reaction leading to the first excited state of ^{14}N is the analogue of the $^{16}O(p,t)^{14}O$ ground state reaction. If the interaction is charge independant, then the differential cross sections for the two processes should be related by a certain multiplicative factor. The polarization analysing powers of the two reactions should be identical. The relation between the cross sections has already been confirmed (Cerny and Pehl,1964), but the identity of the analysing powers has not, and their measurement will provide an interesting comment on the charge independence theory.

The $^{28}Si(p,t)^{26}Si$ ground state reaction in the s-d shell has been selected in order to study the coherence effects of the various configurations of the transferred nucleons. This coherence is expressed in the configuration sum in eqn.(1.3). These effects are expected to be more pronounced for this reaction where the configuration sum extends over more than 1 shell, than for the previous reactions where only the p-shell is dominant. The differential cross section is known to be sensitive to this coherence, and this measurement, while presenting a further test of the spin-independent theory, will allow the coherence effects on the polarization analysing power to be studied.

The DWBA analyses of all these reactions will be used to compare

the usefulness of the two methods that are generally employed to describe the two nucleon transfer process. The zero-range approximation will be examined as well as the relevance of effective non-local potentials.

iii) A general spin-dependent computer programme.

The theoretical analysis requires the use of a two nucleon transfer DWBA programme which has spin-orbit coupling included in the description of the optical model potentials. No such code was available and it was necessary to consider existing DWBA programmes with a view to their modification. The Rook-Mitra theory (point particle approximation) has been incorporated by M.J.L. Yates in a spin-independent DWBA programme. The modifications required to extend this double stripping code to include spin-orbit distortions in the optical potentials, and to alter the angular momentum coupling routines, are so extensive that it was decided instead to re-arrange an existing spin-dependent code written specifically for deuteron stripping by Macefield (1967). The full details of this converted programme will be published at a later date, but the essential modifications include:

a) the removal of the restrictions on the spins of the incident, emitted and transferred particles from the routines which calculate the radial integral and the angular momentum coupling,

b) the coding of the point particle and harmonic oscillator approximations to describe the effective interaction I^{eff},

c) the extension of the calculation of the differential cross section and polarization to include the coherent or incoherent sum over the orbital angular momentum L,

d) the provision of finite range corrections for two nucleon transfer reactions,

e) the extension of the calculation of the bound state wave function to include the coherent sum over the configurations of the transferred nucleons and lastly,

f) a re-organisation of the programme to reduce the required computer storage by half and to increase the execution speed by approximately 100%.

The cross section calculations of the completed programme were checked by comparison with the Yates code and calculations made with the Glendenning code (Hardy,1968) for the case of zero spin-orbit coupling. The polarization predictions were identical to those calculated with the unmodified programme for single nucleon transfer. The predictions were also found to satisfy the following theoretical constraints for two nucleon transfer reactions (Goldfarb and Johnson,1960).

For zero spin-orbit coupling:

1) Transferred spin S = 0: zero polarization for all values of L,

2) Transferred spin S = 1: the polarizations for the different allowed values of J are related by:

$$-\frac{P_+}{L} = P_o = \frac{P_-}{L+1}$$

where the polarization for $J = L \pm 1$ and $J = L$ is denoted by $P_{\pm}$ and P_o,

3) the limits on the magnitude of the polarization when $S = 1$ are given by:

$$|P_o| \leq \frac{1}{L+1} \quad ; \quad |P_-| \leq 1 \quad ; \quad |P_+| \leq \frac{L}{L+1}$$

4) and finally the magnitude of the polarization was checked for a variety of L values with $S = 0$ and 1, and with different values of the spin-orbit strength for the incident and emitted particles. The calculated polarization never exceeded ±1.

The apparatus and experimental techniques required for measurements of analysing powers and differential cross sections will now be described.

CHAPTER 3. EXPERIMENTAL APPARATUS.

The experiments were performed at the Rutherford High Energy Laboratory of the Science Research Council, where the 50 MeV linear accelerator was the source of the proton beam. The salient features of the machine, supplementary beam facilities and pulse analysis electronics are described below.

i) The accelerator

The proton linear accelerator is based on the designs of Alvarez et al. (1955) and consists of a series of 3 vacuum tanks, each containing a radio frequency cavity excited in the TM_{olo} mode at a resonant frequency of 202.5 MHz. Drift tubes are arranged on the axis of each cavity and the length and spacing of the tubes is chosen to provide a field-free region for the proton during that part of the r.f. cycle which is non-accelerating. Protons from a 500 keV Cockroft-Walton accelerator are injected into the first cavity and leave it with an energy of 10 MeV. Each of the remaining two cavities increases the proton energy by 20 MeV and intermediate energies can therefore be obtained by switching off the r.f. power to one or more cavities, and if necessary, by degrading the beam by means of aluminium and carbon foils. The technical difficulty of producing and dissipating the 3.2 megawatts of r.f. power required to generate the necessary electric fields within the cavities is such that the machine cannot be operated continuously. The r.f. pulse, which is repeated 25 times per second, is 800 μsecs long, 600 μsecs of which are used for proton acceleration. The duty cycle

is thus 1.5%.

The development of the polarised proton ion source can be followed in the annual PLA Progress Reports of the Rutherford Laboratory. The Mark 3 source presently in use has been fully described by Broad and McAlush in the 1964 Report and only an outline of its operation will be given here. A collimated atomic hydrogen beam from an r.f. dissociator is allowed to pass through the inhomogeneous field of a sextupole magnet which is transparent to only 2 of the 4 hyperfine states of the hydrogen atom ground state. If the emergent beam is ionised in a weak magnetic field, the maximum proton polarization will be less than 0.50. This limitation is overcome in the Mark 3 source by means of the adiabatic passage technique which employs r.f. and shaped DC fields after the sextupole magnet to induce transitions between hyperfine states. The atomic beam is then ionized in a strong magnetic field and the resultant proton beam can be fully polarised. The direction of polarization can be inverted if the field in the ionizer is reversed. The ion source is at a potential of 500 KV above ground, and the restrictions on its dimensions limit the efficiency by reducing the proton current and increasing the background of unpolarised protons. The intensity of the accelerated beam is about 7 to 12 $\times 10^8$ protons per second, with a polarization of between 45% and 55% depending on the adjustment of the source.

The absolute beam energy is determined by means of a range

measuring device employing aluminium degraders (Hanna and Hodges, 1965). In principle, since a 77° bending magnet is part of the beam transport system, the beam energy could be deduced from a measurement of the magnetic field and a suitable calibration experiment. The beam energy monitor, which has been calibrated by measuring proton energies in a time-of-flight experiment, is a permanent facility on the accelerator and so the calibration of the bending magnet was considered to be unnecessary.

The phase acceptance of the machine is about 10° on either side of the stable accelerating phase and the resultant phase oscillations cause the final beam to have an energy spread of approximately 250 keV at 50 MeV. In the next section, a description will be given of the methods used to improve the beam energy spread, and subsequent beam handling.

ii) Beam transport system.

The function of the beam transport system is to provide, at the target, a beam of well-defined energy, which is focussed to a small spotand is not so divergent that loss of beam occurs between the target and the Faraday cup at the end of the line. The beam transport was designed by Scott (1963) and is shown in Figure 3.1. The object for the system is aperture S_1, an image of which is formed at S_2 by means of the quadrupole pair Q_2 and a 77° bending magnet. The image at S_2 is broadened because of the natural energy spread of the beam and so the dimensions of the slit S_2 are chosen to select

a 70 keV 'bite' of this 250 keV spread. The quadrupole pair Q_4 then forms an image of S_2 on the target. The line is terminated with a Faraday cup. The system is optically aligned so that the magnetic axis of the quadrupole pair Q_4 coincides with the axis of the beam line as defined by a datum point in the pole gap of the bending magnet, the slit S_2, the centre of the target and a datum point at the 0° counter position.

The currents in the quadrupole pairs and the bending magnet were set to predicted values and final small adjustments were then made with the aid of closed circuit television cameras and retractable scintillators situated in the target position and at the points TV_1 to TV_3. A proton current of some 15 to 20 nanoamps could be readily focussed to a 3mm by 3mm spot on the target with a divergence of 0.005 radians. The focussing of the low intensity polarised beam was accomplished with ease by the same monitoring techniques, even though the beam current was little more than 100 picoamps.

(iii) Scattering chamber, counters and targets.

The target is situated at the centre of a 55 cm diameter scattering chamber which has been constructed so that two counter telescopes can be independently rotated about the centre. A view of the chamber, target ladder and one of two identical counter telescopes is shown in Plate A. The second telescope is suspended from the lid of the chamber. The counter telescope is fixed on to

a machined guide so that the angular calibration does not alter when the telescope is removed and replaced. The guide is graduated to allow the telescope-target distance to be measured to an accuracy of 0.3 mm.

The four components of each counter telescope are a tantalum collimator, which defines the angular acceptance of the telescope and the solid angle it subtends at the target, and three silicon semi-conductor counters. The first of these detectors must be transparent to all particles of interest and will be referred to as the ΔE counter. The second, called the E counter, must be thick enough to stop the particles of interest which enter it. The role of this pair of detectors in the mass analysis of reaction products will be discussed in section v. The last element in the telescope, the AC counter, is used to detect the presence of any particles that are not stopped by the first two.

Preliminary investigations of the differential cross sections showed that thick targets would be required if the duration of the experiments was to be kept within reasonable bounds when the low intensity polarised proton beam was used. The energy level diagrams of the residual nuclei in the reactions being studied, are shown in Figure 3.2. The large energy spacings between the ground state and first excited state in each case do not impose critical limits on the energy resolution of the experiments and hence on the thickness of the targets. A polyethylene film 0.001" thick was used as a carbon

target and a sample of the film was analysed by the Dyson Perrins Laboratory with the following result.

Table 1.

Composition of polyethylene target.

C	85.25%
H	14.09%
N	0.51%

The analysis confirms that the composition of the target is well defined by the formula for polyethylene $(CH_2)_n$. The effective carbon surface density of 2.1 mg.cm^{-2} was determined by weighing the film on a micro-balance and measuring the surface dimensions with vernier calipers.

An organic film was also used for an oxygen target. The analysis of a sample of tricellulose acetate, $C_6H_7O_2(OOCCH_3)_3$, is given in Table 2.

Table 2.

Composition of tricellulose acetate target.

O	36%
C	51.11%
H	5.93%
N	4.40%
S	1.12%

The percentage of oxygen was determined by a subtraction method and is subject to an error of ±1.5. The oxygen surface density was found by weighing and area measurement to be 0.81 mg.cm^{-2} for a 0.001" thick target.

The target used for the $^{28}Si(p,t)^{26}Si$ experiment had been prepared by etching a slice of natural silicon to a thickness of approximately 25 microns. The mean surface density was found by weighing and area measurement to be 6.0 mg.cm^{-2}. The possible non-uniformity of the target does not affect the measurement of the polarization analysing power.

iv) The beam monitor.

The Faraday cup at the end of the beam line is a 4" diameter, carbon-lined cage with a secondary electronsuppressor near the entrance. The beam current is integrated by the Harwell Type 3008 monitoring equipment. Instrumental dead time corrections to the integrated current can easily be made when a DC beam is used, but since the 100 μsec dead time of the instrument is comparable with the 600 μsec length of the beam pulse from the accelerator, some precautions must be taken to avoid an erroneous measurement of total beam charge.

Suppose the instrumental dead time, which arises from the discharge of a storage capacitor, is t_d, and let t_p be the duration of the beam pulse. Then if the integrator cycle terminated during the n_{th} beam pulse, the fractional loss L in integrated current will be such that

$$0 < L < t_d/nt_p .$$

If the beam current is constant, this loss will be the same for each integrator cycle. However, the beam intensity varies and

therefore it can be assumed that the integrator cycle will end at any point during the n_{th} beam pulse. In this case, the average fractional loss is clearly

$$\langle L \rangle = \frac{t_d (t_p - t_d)}{n\, t_p^2} + \frac{t_d^2}{2n\, t_p^2}$$

$$= \frac{11}{72n}$$

If the integrator cycle is completed once a second, then with n = 25 beam pulses per second, the average percentage loss will be 0.61%. Beam currents between 10^{-10} amps and 2 or 3 x 10^{-9} amps were used in the experiments and with the integrator operating at 10^{-8} coulombs per cycle, dead time losses never exceeded 0.3%. The internal leakage of the instrument amounts to about 3.5 picoamps and therefore adds to the total integrated charge. The integrator was calibrated with a current generator which provided known currents with an accuracy of 0.2%. These three corrections, namely, average dead time loss, spurious additional charge due to leakage current, and absolute calibration, were applied to the observed total charge for each experiment.

v) Electronics.

The information contained in the charge pulses from the semi-conductor counters must be analysed to provide a separate energy spectrum for the product of each reaction being studied. The different types of particles are identified by means of a mass

analyser (Fisher and Scott,1967), which is based on the empirical range-energy relation for charged particles in silicon $R = aE^{1.67} + b$ where a and b are constants and depend only on the type of particle being considered.

Suppose a particle with energy T_o enters the counter telescope. It will deposit an energy T_1 in the first detector (the ΔE counter), and the remainder, T_2, in the second counter. If d is the thickness of the ΔE counter then it can be shown from the application of the range-energy relationship that

$$d/a = (T_1 + T_2)^{1.67} - T_2^{1.67}$$

The mass analyser provides two output pulses. The 'mass pulse' is proportional to the function $(T_1 + T_2)^{1.67} - T_2^{1.67}$ and is dependent on the constant a and therefore on the mass of the particle. The 'analogue pulse' is proportional to the sum $(T_1 + T_2)$ which is the total energy of the particle. A typical voltage spectrum of the mass pulses is shown in Figure 3.3. By using several discriminators with triggering levels set at the voltages indicated by the arrows, it is possible to obtain a set of routing pulses so that energy spectra corresponding to deuterons, tritons, ^{3}He and ^{4}He ions can be stored in different subgroups of a multi-channel pulse height analyser.

The separation of the particle groups shown in Figure 3.3 can be enhanced if non-uniformities in the thickness of the ΔE counter and fluctuations in the energy loss T_1 due to the Landau-Simon effect, are kept to a minimum. This is achieved by using a ΔE counter which

is as thick as possible and yet is transparent to all the particles of interest. The ΔE counters used in the $^{12}C(p,t)^{10}C$ and $^{28}Si(p,t)^{26}Si$ experiments were 300μ to 400μ thick, but the kinematics of the $^{16}O(p,^{3}He)^{14}N$ reactions are such that ^{3}He ions would not be able to penetrate these ΔE counters at laboratory angles greater than 35°. For this experiment, 150μ to 200μ ΔE counters were used instead. The manner in which the mass analyser is used in the pulse electronics system will now be described.

A block diagram of the electronics system for one counter telescope is shown in Figure 3.4. The pulses from the three counters in each telescope are amplified by charge-sensitive pre-amplifiers. These are mounted on the scattering chamber itself so as to keep the signal leads from the counters as short as possible. The remainder of the pulse analysis is carried out in the counting room 150 feet away. The incoming pulses from the ΔE, E and AC counters are clipped by double delay lines and amplified. The bipolar output of the amplifiers in the ΔE and E lines is now split, the prompt output being used for coincidence and logic purposes while the delayed output is fed to the mass analyser through a bipolar-unipolar converter. The performance of the mass analyser, which requires unipolar inputs, would be adversely affected by poor base-line recovery at the high count rates that could be expected if the entire output from the counter telescopes were to be fed to it. The gate of the bipolar converter is therefore opened only on receipt

of a pulse which is generated by the logic circuit if the particle comes to rest in the E counter. The AC counter provides an anticoincidence signal to block the gate pulse should particles pass through the E counter. Since the mass analyser requires signals from the ΔE and E counters, false mass analysis is avoided by ensuring that the gate pulse is generated only if these two signals are coincident. A further restriction is necessary because while the r.f. field is building up (this takes about 200 μsecs due to the very high Q of the cavities), spurious pulses picked up by the signal lines could open the gates and initiate unwanted analysis. This is prevented by having a third gating requirement which is only fulfilled when the r.f. field has reached its operating level. This additional gate pulse is provided by the accelerator master trigger circuits.

The analogue output of the mass analyser is fed to a Laben 4096 channel pulse height analyser (PHA) which is divided into 8 subgroups, 4 subgroups for each telescope. The mass output is fed to a 4 channel (variable width) pulse height analyser where each channel corresponds to a particle group in the mass spectrum. The presence of a pulse in a channel is detected by a selective storage unit (SSU) which generates a suitable routing pulse for the 4096 channel PHA. The SSU also provides a gate pulse (marked code present in the block diagram) for the PHA, to prevent analysis of analogue pulses that are unaccompanied by routing pulses.

The system is relatively simple to set up. The gains of the ΔE and E lines must be identical otherwise the analogue pulse from the mass analyser will not be proportional to the total energy of the detected particle. A convenient energy reference is provided by 5.5 MeV alpha particles from ^{241}Am deposited on anti-scattering apertures mounted in the counter telescope. The gains of the ΔE and E lines are adjusted by altering the gains of the double delay line amplifiers. The timing of all the gating pulses can be observed on an oscilloscope when a mercury pulser is connected to test inputs on the ΔE and E preamplifiers.

In practice the system worked well. The ^{3}He-^{4}He particle groups were well separated so that no feed-through of ^{3}He particles into the ^{4}He spectrum could be detected. The separation of the deuteron and triton groups was less distinct and a slightly incorrect setting of the 4 channel analyser could result in the misrouting of tritons to the unwanted deuteron spectrum. Two procedures were followed to avoid this problem. The deuteron/triton discriminator level of the 4 channel analyser was set as low as possible without allowing the deuteron feed-through into the triton energy spectrum to provide an unwanted background. The mass spectrum was also monitored continuously with a 512 channel PHA, and the different particle groups were routed into subgroups of the PHA by a second selective storage unit connected to the 4 channel analyser. In this way, any maladjustment of the mass discriminator settings could be

detected without delay. It is difficult to determine with accuracy the extent of the triton loss to the deuteron spectrum due to misrouting. Since the separation of the groups in the mass spectrum is partly dependent on the thickness of the ΔE counter, the excellent reproducibility of cross section measurements when different ΔE counters are used, gives some indication of the small extent of this loss. An upper limit of 2% to 3% has been estimated for this loss, from the peak to valley ratio of the groups in the mass spectrum. The possible loss of tritons has been ignored in the calculations.

The observed yield of any reaction will differ from the true yield because of losses due to the dead time of the electronics system. The largest contribution to the dead time comes from the selective storage unit and the 4096 channel PHA, and is determined from the difference in the total counts displayed by two scalers connected to the ΔE logic discriminator. This point in the circuit was chosen because the ΔE count rate was the greatest and was representative of the beam intensity. One of the scalers is ungated but the second is inhibited when the analyser and SSU are busy. The coincidence circuitry is responsible for the remaining contribution, and the dead time loss is calculated from the known characteristics of the logic circuits. The derivation of a formula showing the complete dead time correction is given in Appendix 2.

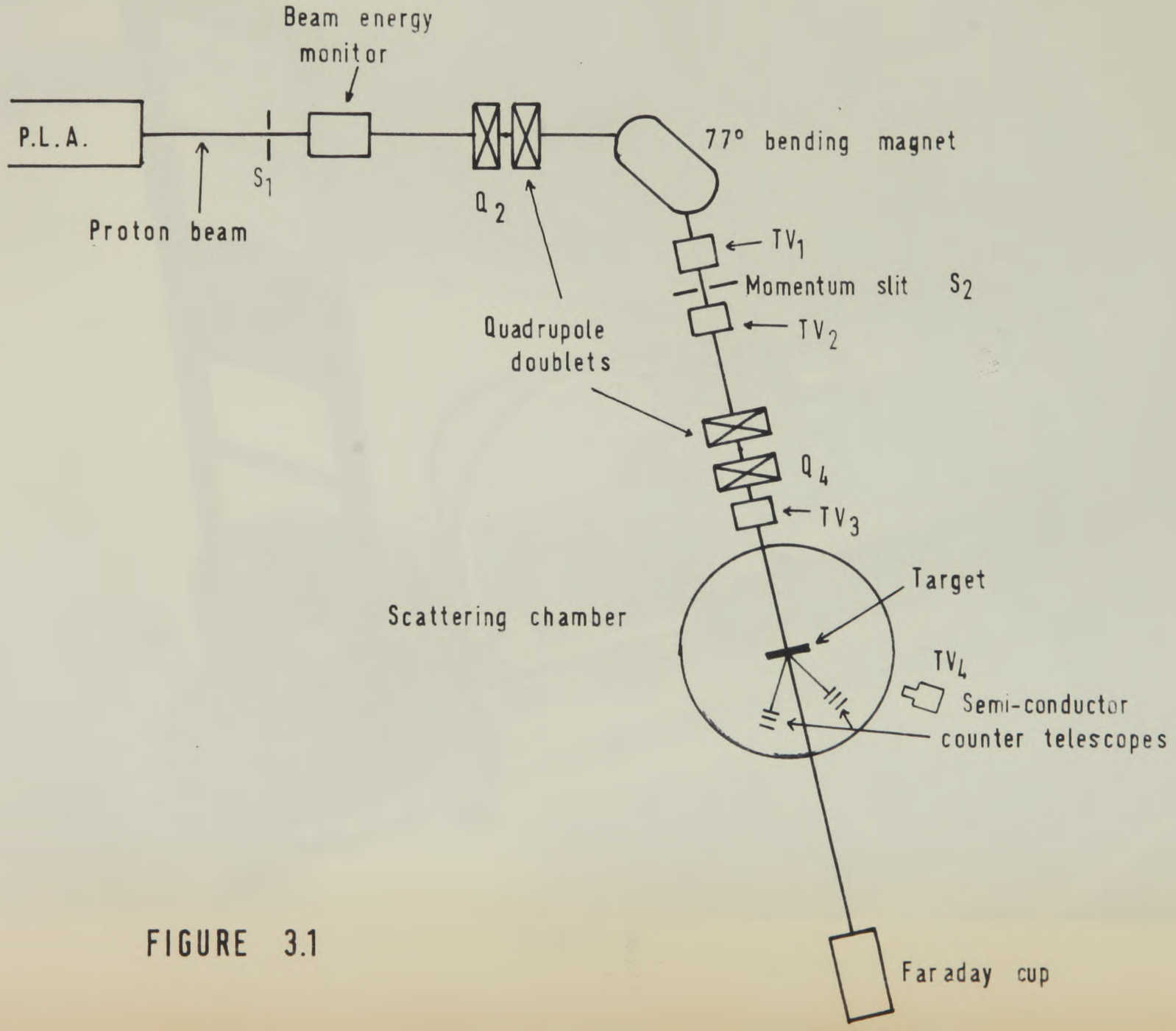

Beam energy
monitor
P.L.A.
S_1
Proton beam
Q_2
77° bending magnet
TV_1
Momentum slit S_2
TV_2
Quadrupole
doublets
Q_4
TV_3
Target
Scattering chamber
TV_4
Semi-conductor
counter telescopes
Faraday cup

FIGURE 3.1

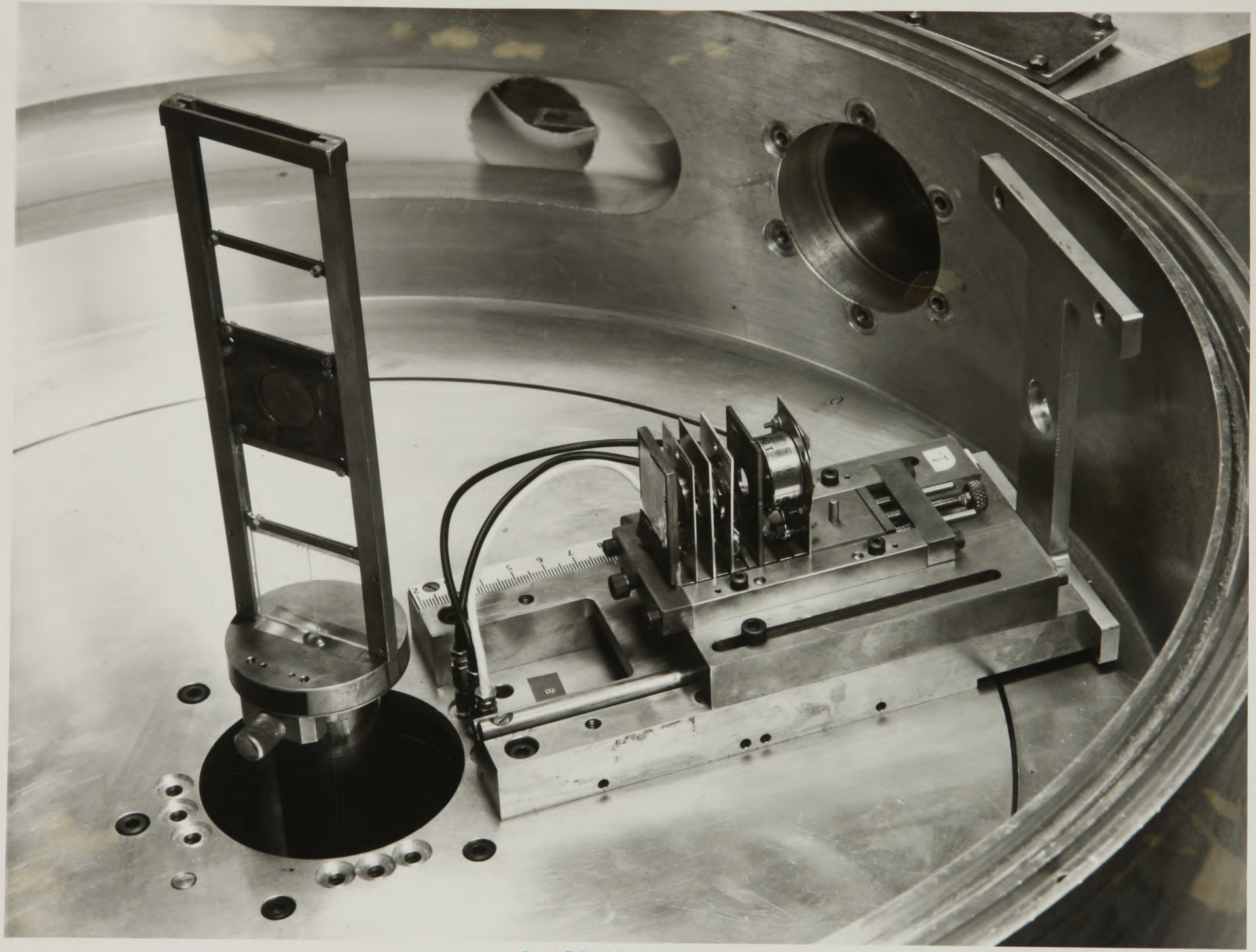


PLATE A

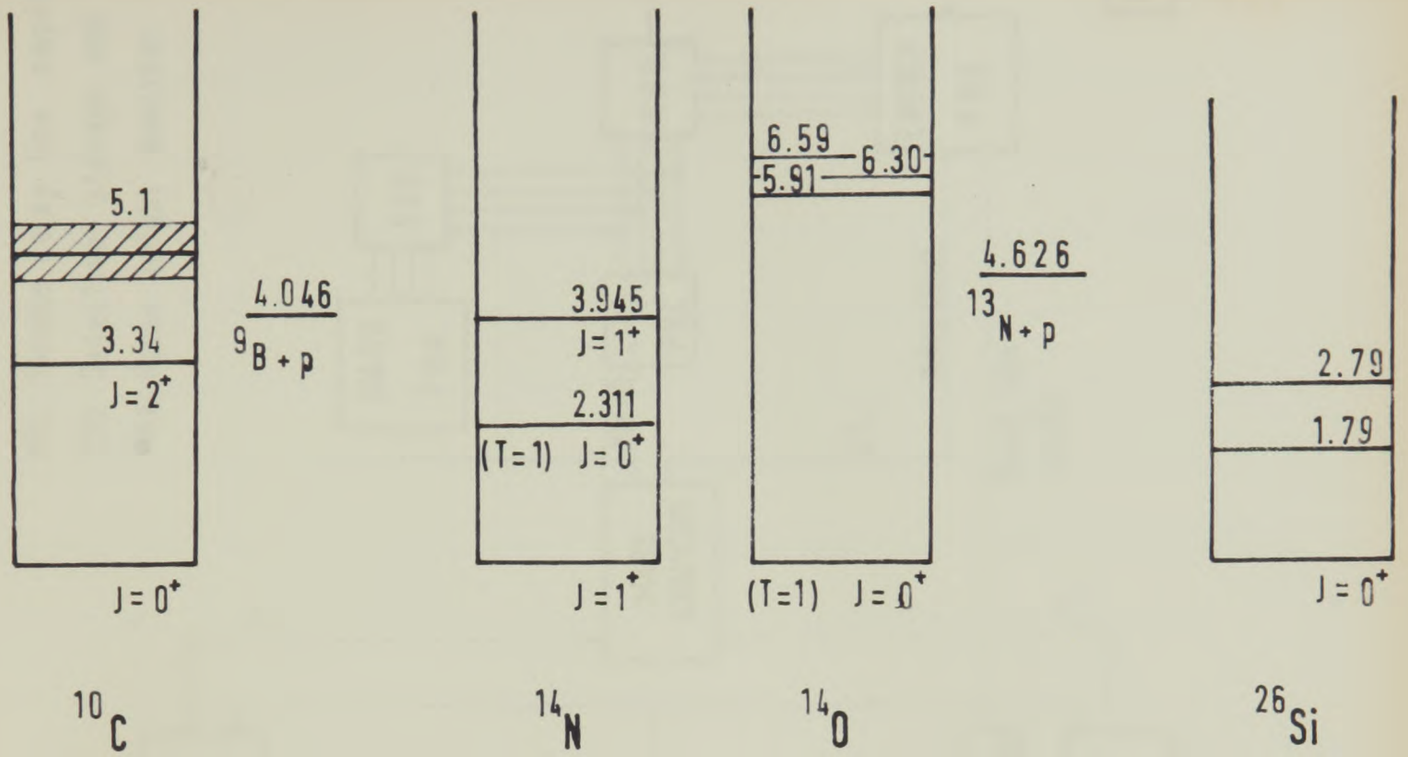


FIGURE 3.2

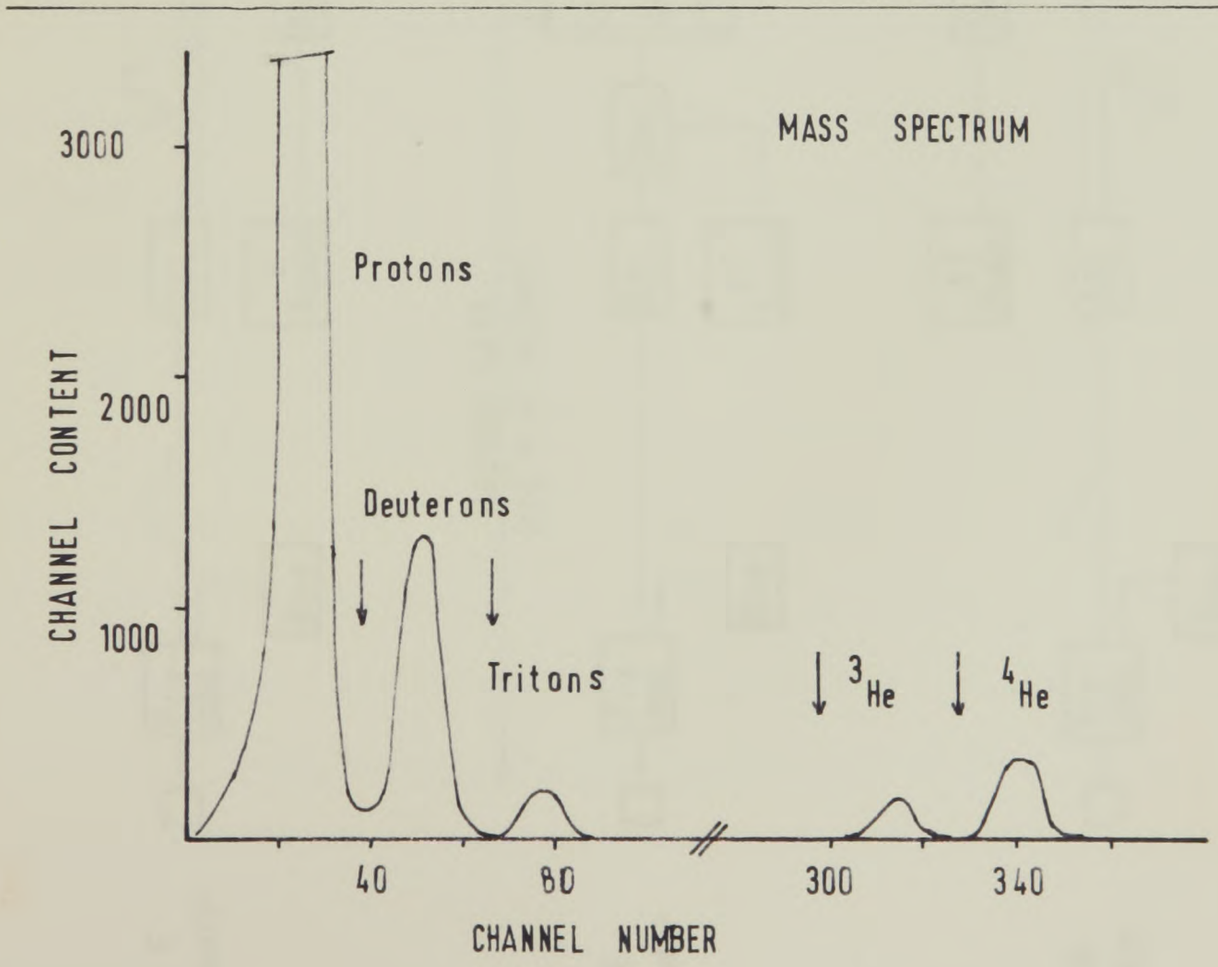


FIGURE 3.3

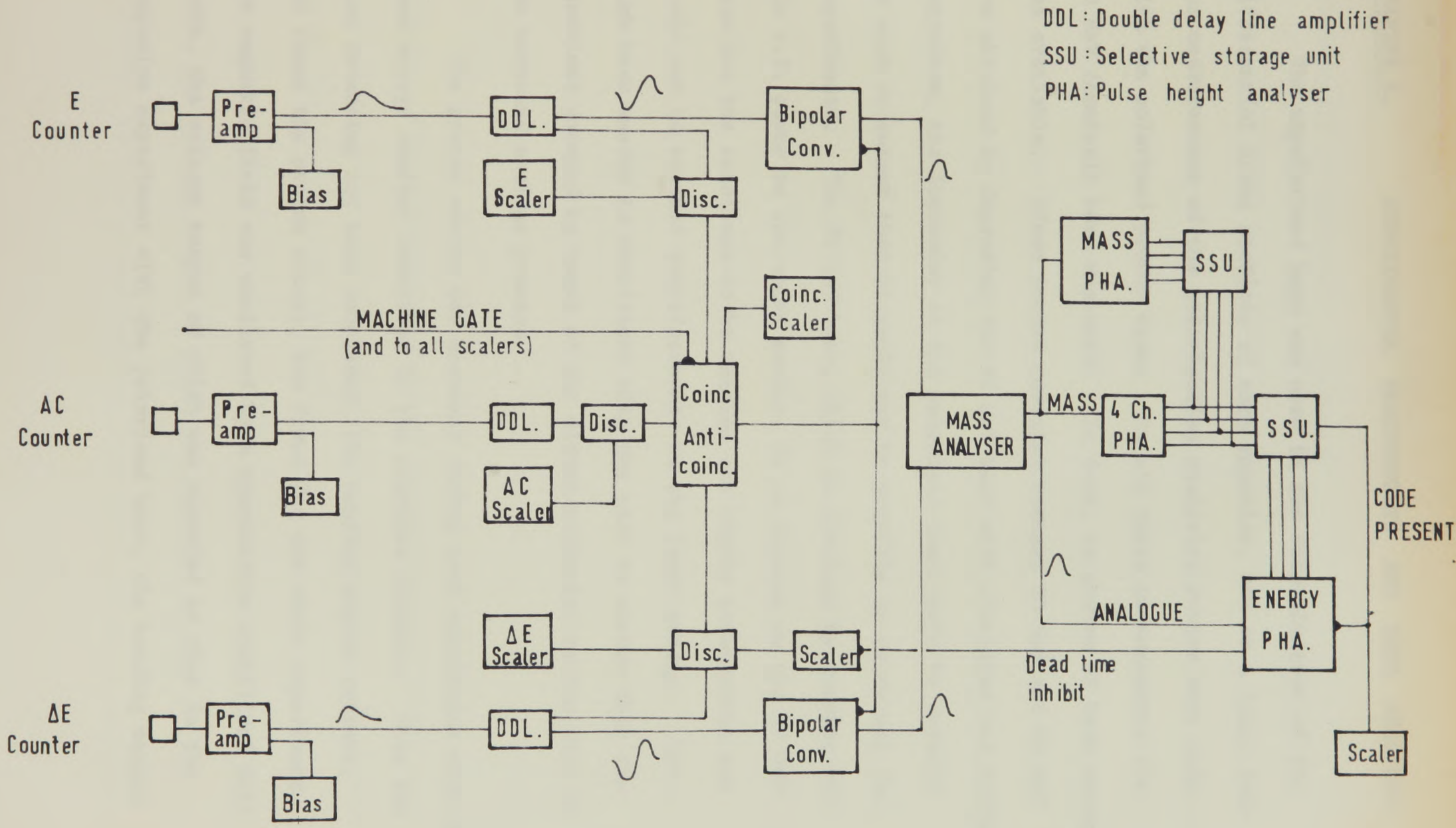

DDL: Double delay line amplifier
SSU: Selective storage unit
PHA: Pulse height analyser
E Counter
Pre-amp
Bias
DDL.
E Scaler
Disc.
Bipolar Conv.
MACHINE GATE
(and to all scalers)
Coinc. Scaler
AC Counter
Pre-amp
Bias
DDL.
Disc.
AC Scaler
Coinc Anti-coinc.
MASS ANALYSER
MASS PHA.
SSU.
MASS
4 Ch. PHA.
SSU.
CODE PRESENT
ΔE Scaler
Disc.
Scaler
ANALOGUE
ENERGY PHA.
Dead time inhibit
ΔE Counter
Pre-amp
Bias
DDL.
Bipolar Conv.
Scaler

FIGURE 3.4

The unpolarised beam was used in the determination of the differential cross sections of each reaction, and at a later date the measurements of the polarization analysing powers were made with the polarised proton beam. In all these measurements the 50 MeV (nominal) beam was used. In fact, no choice of beam energy was available. Since proton energies between 30 MeV and 50 MeV are obtained by degrading the 50 MeV beam with aluminium and carbon degraders, the intensity of the polarised beam would be reduced to such an extent that it would not be possible to carry out the experiments. The 30 MeV beam, which is obtained by turning off the r.f. power to the third cavity, is as intense as the 50 MeV beam but the reactions to be studied are highly endothermic and could not be studied satisfactorily at the lower energy. The high beam energy is consistent with the need to ensure that the reactions proceed by means of the direct mechanism rather than by the compound nucleus process.

The proton energy was measured during each experiment with the beam energy monitor described in the previous chapter. Once the beam focussing had been completed, the bending magnet current, and hence the proton energy, was fixed for the whole experiment. The magnetic field was monitored by a temperature stabilised Hall probe, the voltage output of which was recorded so that in the companion experiment with the polarised beam, the bending magnet

field could be accurately reproduced.

A: Measurement of differential cross sections.

The energy resolution of the beam is defined by the momentum slit S_2 of Figure 3.1. For these measurements, a 1/16" slit in a tantalum plate corresponded to a 70 keV 'bite' of the natural 250 keV energy spread from the accelerator. After the beam transport and pulse electronics systems had been adjusted according to the procedure described in Chapter 3, the counter telescopes were set symmetrically on either side of the beam axis as a check on relative telescope efficiencies and solid angles. Thereafter they were set at different angles, thus doubling the rate of data collection. At angles greater than 40° or 50°, the counter telescope resolution decreased and it was necessary to alter the target normal from 0° to 40°. The 40° cross section was measured for both values of the target normal, so that non-uniformities in target thickness could be taken into account by using the normalization of the two cross sections to correct the measurements made at larger angles. Slit apertures in front of the ΔE counters defined the solid angle to be 1.70 millisteradians and the angular acceptance in the horizontal plane to be 1°.

i) $^{12}C(p,t)^{10}C$ Levels: ground state (0^+) and 3.34 MeV (2^+)

The polyethylene film that was used for a target in this experiment, is free of contaminants that would otherwise complicate

the triton spectrum. The ground state Q-value for the reaction is -23.330 MeV. The width of the peaks in the triton energy spectrum shown in Figure 4.1, is mostly due to the thickness of the target. The ground state and first excited state peaks are well separated and the triton yield was determined simply by summing the counts in each peak. The two peaks at approximately 5.3 MeV and 6.6 MeV were not analysed. These states are unbound since the binding energy of the last proton is 4.046 MeV. The low energy background is due to the ^{10}C nucleus having an excitation energy in the continuum.

The differential cross sections in the centre of mass system for the two states are shown in Figures 4.2 and 4.3 and are tabulated in Appendix 3. The errors shown are statistical errors and the error on the absolute value of the cross section is approximately 10% and is due to uncertainties in the target thickness and the solid angle of the telescopes. The method of calculation of the centre of mass cross section will be described in section v. These results are in good agreement with the measurements of Cosper et al. at 50.0 MeV (1967).

ii) $^{16}O(p,t)^{14}O$ ground state (0^+)

The ground state Q-values of the possible reactions that can take place with a target of tricellulose acetate are:
$^{16}O(p,t)^{14}O$ -20.408 MeV; $^{14}N(p,t)^{12}N$ -22.400 MeV and
$^{12}C(p,t)^{10}C$ -23.330 MeV.

An inspection of these values shows that the large amount of carbon present does not constitute a background problem. A triton energy spectrum from the acetate target is shown in Figure 4.4. The ^{14}O ground state peak is well isolated and the yield was determined by summing the counts in the peak. Triton groups from the ^{14}N reaction were not observed at all. The ^{10}C 3.34 MeV peak is situated in the continuum background from the breakup of ^{14}O and for this reason the cellulose acetate target was not used to study the (p,t) reactions on ^{16}O and ^{12}C simultaneously. The differential cross section of the $^{16}O(p,t)^{14}O$ ground state reaction is shown in Figure 4.5 and is tabulated in Appendix 3. The errors shown are statistical errors and the error on the absolute value of the cross section is approximately 14%, and is due partly to uncertainty in the amount of oxygen in the target. The differential cross section of the $^{12}C(p,t)^{10}C$ ground state reaction was also calculated and was found to agree with the measurements described in the previous section.

iii) $^{16}O(p,^3He)^{14}N$ Levels: ground state (1^+) and 2.311 MeV (0^+)

The measurement of the cross sections of these reactions was, of course, made at the same time as the triton data was accumulated from the $^{16}O(p,t)^{14}O$ reaction. The ground state Q-values of the possible $(p,^3He)$ reactions are $^{16}O(p,^3He)^{14}N$ -15.242 Mev; $^{14}N(p,^3He)^{12}C$ -4.779 MeV and $^{12}C(p,^3He)^{10}B$ -19.694 MeV.

The energy spectrum that is observed is shown in Figure 4.6. The ^{14}N ground state and first excited state groups are well separated from the large contribution from the $^{12}C(p,^{3}He)^{10}B$ reaction. The ^{14}N 3.945 second excited state cannot, however, be satisfactorily resolved from the tail of the ^{10}B ground state peak. The ^{3}He groups from the $^{14}N(p,^{3}He)^{10}C$ reaction were not observed.

The centre of mass differential cross sections of the reactions leading to the ground state and first excited state of ^{14}N are shown in Figures 4.7 and 4.8, and tabulated in Appendix 3. The source of the errors was discussed in the last section.

iv) $^{28}Si(p,t)^{26}Si$ ground state (0^{+})

The isotopic abundance of ^{28}Si in the natural silicon target that was used is 92.2%, and reaction products from the other two isotopes were not observed. The ^{26}Si ground state peak was clearly separated from the 1.79 MeV first excited state peak in spite of the very thick target that was used. The reaction yield was measured directly. The differential cross section is shown in Figure 4.9 and tabulated in Appendix 3. The errors shown are statistical but do not include the error on the absolute value of the cross section due to uncertainty in the uniformity of the target thickness. This error is estimated to be about 20%.

The experiment was performed mainly to check the usefulness of the silicon targets that were to be employed in the polarised

run since the differential cross section had already been measured at 50 MeV (Montague,1967). The results of this experiment are in excellent agreement with the earlier measurement.

v) Calculation of the centre of mass differential cross section.

The differential cross section in the centre of mass system is given by

$$\frac{d\sigma}{d\omega} = \frac{N \times C_N \times \cos\theta_T \times A}{t \times L \times Q \times C_Q \times \Omega}$$

where N = yield of the reaction,

C_N = dead time correction factor derived in Appendix 2,

θ_T = angle between the target normal and the beam axis,

A = the atomic weight of the target nucleus,

t = the surface density of the target,

L = Avogadro's number,

Q = total integrated beam charge,

C_Q = beam integrator correction factor,

Ω = centre of mass solid angle subtended by the counter telescope at the target.

The solid angle transformation factor between the laboratory and centre of mass coordinate systems is well-known (eg. Baldin et al., 1961). The detection efficiency of the counter telescopes is assumed to be 100%. The statistical error on the cross section is given by the following formula where $\sigma^2(X)$ is the variance of X:

$$\sigma\{\frac{d\sigma}{d\omega}\} = \frac{d\sigma}{d\omega}\left(\frac{\sigma^2(N)}{N^2} + \frac{\sigma^2(C_N)}{C_N^2}\right)^{\frac{1}{2}}$$

The quantity $\sigma^2(C_N)$ is given in Appendix 2. If N is considered to follow a Poisson distribution, then $\sigma^2(N) = N$.

The calculation of the cross section and the statistical error, as well as the dead time correction factors and the relativistic transformation of solid angle and counter angle, are performed by computer.

B: Measurement of polarization analysing powers.

The examination of the differential cross section is fundamental to the study of reaction mechanisms. The techniques of its measurement are well known, as are the sources of systematic errors and consequently these have not been elaborated in the previous section. The methods of experimentation with polarised beams on the other hand, are relatively unfamiliar and therefore some of the elements of polarimetry will be considered in detail before the results of the polarised beam experiments are discussed.

i) Experimentation with polarised beams.

In Chapter 2, the differential cross section for a reaction initiated by a polarised beam, was given by the equation

$$\frac{d\sigma}{d\omega} = \frac{d\sigma}{d\omega_o}\{1 + P_B \cdot P_A(\theta)\} \qquad 4.1$$

where $\frac{d\sigma}{d\omega_o}$ is the differential cross section when an unpolarised

beam is used. The polarization of the incident beam is given by P_B, and the polarization analysing power of the reaction is P_A. Reaction products are detected by counter telescopes set at equal angles on either side of the beam axis. These two angles will be labelled LEFT and RIGHT with respect to the direction of the beam, and the following nomenclature will be used:

$\pm$ the possible spin states of the beam. (The direction of beam polarization is at right angles to the reaction plane).

$P_\pm$ the polarization of the beam in these two spin states,

L,R the reaction yields detected by the left and right counters,

$P_A(\theta_L)$, $P_A(\theta_R)$: the polarization analysing power as measured at each counter.

From eqn.(4.1): $$L_+ \propto \frac{d\sigma}{d\omega}$$

$$= k_+(1 + \vec{P}_+ \cdot \vec{P}_A(\theta_L))$$

where k_+ is proportional to the number of incident protons, and is defined by

$$k_+ = \frac{d\sigma}{d\omega_o} \frac{t \times L \times C_Q \times Q_+}{C_M \times \cos\theta_T \times A}$$

Since the direction of the beam polarization is perpendicular to the scattering plane, and is parallel (or anti-parallel) to the vector $P_A(\theta)$ representing the polarisation analysing power, the product $P_+ P_A$ can be replaced by

$$\vec{P}_\pm \cdot \vec{P}_A(\theta_L) \rightarrow \pm P_\pm P_A(\theta_L)$$

and $$\vec{P}_\pm \cdot \vec{P}_A(\theta_R) \rightarrow \mp P_\pm P_A(\theta_R).$$

The reaction yields can now be written in the form

$$L_+ = k_+\{1 + P_+P_A(\theta_L)\} \qquad 4.2a$$

$$R_+ = k_+\{1 - P_+P_A(\theta_R)\} \qquad 4.2b$$

$$L_- = k_-\{1 - P_-P_A(\theta_L)\} \qquad 4.2c$$

$$R_- = k_-\{1 + P_-P_A(\theta_R)\} \qquad 4.2d$$

If the polarization of the beam is very nearly the same in each of the two spin states, then the polarization $P_\pm$ can be written in terms of the mean beam polarization P_B:

$$P_+ = P_B(1 + \delta P_B) \qquad 4.3a$$

$$P_- = P_B(1 - \delta P_B) \qquad 4.3b$$

Furthermore, if the detectors are very nearly at the same angles, then

$$P_A(\theta_L) = P_A(1 + \delta P_A) \qquad 4.3c$$

$$P_A(\theta_R) = P_A(1 - \delta P_A) \qquad 4.3d$$

where P_A is the mean polarization analysing power at the angle θ. If eqns.(4.3) are substituted into eqns.(4.2), then the quantities $k_\pm$, which depend on several experimental parameters, can be eliminated in the evaluation of the so-called cross-product.

$$\frac{L_+ R_-}{L_- R_+} = C\,\frac{(1 + P_BP_A)^2}{(1 - P_BP_A)^2} \qquad 4.4$$

where C is a factor in which δP_A and δP_B appear in second and higher orders. If $\delta P_A = \delta P_B = 0$ then $C = 1$ and even if δP_A and δP_B are large, it can be shown that the correction to P_BP_A calculated from eqn.(4.4) is very much less than 1%. The factor

C will be taken to be unity. The asymmetry is therefore

$$P_B P_A = a = \frac{X - 1}{X + 1} \qquad 4.5$$

where $$X^2 = \frac{L_+ R_-}{L_- R_+}$$

Thus, if the beam polarisation P_B is known, the polarisation analysing power P_A can be determined from a measurement of the reaction yields in two experiments - one with the beam polarization positive and the other with the polarization negative. The form of eqn.(4.5) shows that systematic errors due to counter efficiencies, beam integration, dead time corrections, counter geometries, and target non-uniformities, are eliminated.

In the symetrical system that has been described with the target normal along the beam axis and counters on either side of the beam, reaction products travel through an amount d of target material, which varies such that

$$0 < d < t \sec \gamma$$

where t is the thickness of the target and γ is the difference between the counter angle and the target normal. When γ approaches 40°, the resultant energy straggle of the reaction products which is observed, especially in the case of ^{3}He ions, seriously impairs the experimental resolution. The target must then be rotated to reduce γ, and consequently only one counter telescope may be used. The simplicity of eqn.(4.5) is lost. Of the eqns.(4.2), only eqn.(4.2a) and eqn.(4.2c), for example, can be used.

$$L_+ = k_+(1 + P_+ P_A) = k_+\{1 + P_B P_A (1 + \delta P_B)\}$$
$$L_- = k_-(1 - P_- P_A) = k_-\{1 - P_B P_A (1 - \delta P_B)\}$$

These equations can be combined to give

$$\beta = \frac{Y - 1}{Y + 1} = \frac{P_B P_A}{1 + P_B P_A \delta P_B}$$

where $Y = \dfrac{L_+ k_-}{L_- k_+}$

Finally $$P_A = \frac{\beta}{P_B(1 - \beta\, \delta P_B)} \qquad 4.6$$

The quantity δP_B must now be determined as well as the ratio of the number of incident protons with spin up to the number with spin down (k_+/k_-).

This discussion underlines the simplicity of asymmetry measurements when a symmetrical geometry is used. In these experiments with the polarised beam, measurements with a single counter were made only when the observed energy resolution became unacceptable due to increased effective target thickness.

ii) The polarimeter and the gold foil monitor.

The polarization analysing power can only be determined from eqn.(4.5) or eqn.(4.6) if the beam polarization P_B is known. In this section, the method of measuring the beam polarization

will be described as well as a supplementary method of beam monitoring.

A simplified diagram of the beam transport system is shown in Figure 4.10. The polarimeter, which is situated at the exit of the third cavity, is a permanent facility on the accelerator and has been fully described by Hanna (1965). At the polarimeter, the beam is degraded to 15.7 MeV and protons scattered from a carbon target are observed by four plastic scintillator-photomultiplier detectors situated at angles of 45° to the left and right of the beam axis, as well as above and below it. The degrader and target are mounted on the circumference of a rotating disc so that the carbon target intercepts the beam once in every 10 bursts. The master trigger for the accelerator is taken from the motor drive to this disc to ensure that the target is accurately positioned on the beam axis when the beam burst is fired.

The pulses from these counters are analysed by an electronics system shown in block form in Figure 4.11 and the proton energy spectrum that is observed is plotted in Figure 4.12a. The two groups correspond to elastic scattering and inelastic scattering leading to the 4.43 MeV first excited state in ^{12}C. The analysing powers for these two reactions are known (Craig et al.,1964; Yamabe et al.,1960). The values are -0.609±0.015 for the elastic state and -0.326±0.033 for the inelastic state. Fast discriminators

are set so that the inelastic protons of lower energy are not counted and a proton spectrum, gated in this way, is shown in Figure 4.12b, where only the elastic peak is seen. The beam polarization can be determined by counting the number of protons elastically scattered to the left and right for the two spin states of the beam and then by making use of eqn.(4.5) with the known analysing power of the elastic process. The energy spectra from the four counters were monitored continuously during an experiment to ensure that the discriminator levels remained correctly set.

In order to determine δP_B, which is required when single telescope operation is employed, two polarimeter measurements must be made with an unpolarised beam. The yields from the Left and Right polarimeter counters are denoted by L_o and R_o where the subscript indicates zero beam polarization. The yields are

$$L_o = k_o \varepsilon_L \qquad 4.7a$$

$$R_o = k_o \varepsilon_r \qquad 4.7b$$

where ε are the counter efficiencies. If the yields from the polarimeter are labelled $L_\pm$ and $R_\pm$ when the beam is polarised, then from eqns.(4.2) and eqns.(4.7)

$$D = \frac{P_+}{P_-} = \frac{k_-}{k_+} \frac{L_+R_o - L_oR_+}{L_oR_- - L_-R_o}$$

$$\text{and } \delta P_B = \tfrac{1}{2}(P_+ - P_-) = \frac{D-1}{D+1} \qquad 4.8$$

The ratio (k_+/k_-) can be determined from the integrated charge for

spin up and spin down runs.

The gold foil monitor shown just downstream from the scattering chamber in Figure 4.10 was used as a monitor of the beam in addition to the Faraday cup charge integration system. The polarised proton current was usually about 5×10^{-11} to 10×10^{-11} amps. If the beam current falls much below these values, then it becomes comparable with the leakage current of the beam integrator. The incident proton current can then be monitored by observing proton scattering from a thin target downstream from the chamber. In this case, a 50 mg.cm^{-2} gold foil is used and plastic scintillator-photomultiplier detectors are placed at 20° to the left and right of the beam axis. If the number of counts observed are ℓ_+, r_+ and ℓ_-, r_- then from eqns(4.2) the quantity

$$\frac{\ell_+ \, r_+}{\ell_- \, r_-} = \frac{k_+^2}{k_-^2}$$

gives the square of the ratio of the number of incident spin up protons to the number with spin down and is independent of the polarisation of the beam or the analysing power of the proton scattering reaction. This ratio is required when single telescope measurements are taken. The monitor electronics are shown in Figure 4.13a with an integral bias curve for one of the counters in Figure 4.13b. The discriminator level is set as indicated, but provided this remains fixed for the whole experiment

and is not so high that the effective efficiency of the counter is adversely affected by small gain shifts, the setting is not critical.

iii) $^{12}C(p,t)^{10}C$ Levels : ground state (0^+) and 3.34 MeV (2^+)

The pulse electronics system was set up in the manner described in the last Chapter. The only additional equipment needed for the polarised beam experiments was the sampling polarimeter and the gold foil monitor. The width of the momentum slit was increased in improve the beam transmission at the expense of energy resolution. The 70 keV resolution obtained in the unpolarised beam experiments was increased to 160 keV but the beam intensity was trebled. The spacing of the energy levels in the residual nuclei are all sufficiently large so that poorer beam resolution and thicker targets could be tolerated. The time needed to study these reactions in better resolution would have been prohibitively long. The counter solid angle, defined by a slit aperture, was 6.5 millisteradians and the angular acceptance was 2°. These experimental conditions were used for all the experiments with the polarised beam. Each measurement consisted of two runs, one with the proton spin up and then, after the field current in the ionizer magnet had been reversed, a run with spin down. The two runs were roughly equal in duration.

The general methods of data reduction have already been described. The analysing powers were calculated by using eqn.(4.5)

or when necessary, eqn.(4.6) after dead time corrections had been applied to the yields from the counter telescopes. The methods of calculation and error estimation will be discussed in section vii. The final results are plotted in Figure 4.14 and Figure 4.15 and are tabulated in Appendix 4. The errors shown are statistical and include the 2% uncertainty in the beam polarization.

iv) $^{16}O(p,t)^{14}O$ ground state (0^+)

$^{16}O(p,^3He)^{14}N$ ground state (1^+) and 2.311 MeV (0^+)

The low intensity beam, coupled with the small differential cross section of the $(p,^3He)$ process, required the use of as thick a target as possible consistent with the need to resolve the ^{14}N ground state and first excited state. A 0.0014" tricellulose acetate target was used in this experiment. The analysing powers for the (p,t) reaction are shown in Figure 4.16, and for the $(p,^3He)$ reactions in Figures 4.17 and 4.18. All the results are tabulated in Appendix 4. The errors shown are statistical and include the error in the determination of the beam polarization. Some indication of the duration of these experiments is given by the fact that when the differential cross section is in the region of 10 to 20 μb/sr, the analysing power cannot be determined to within about ±10% without running the experiment for more than 12 hours.

The triton yield from the contaminant $^{12}C(p,t)^{10}C$ ground

state reaction was determined as well, and the analysing powers are plotted in Figure 4.14 together with the results from the previous measurement using a 'pure' carbon target. The good agreement that is obtained between these two quite separate measurements is a comment on the absence of random errors in this technique of measuring polarization analysing powers.

v) $^{28}Si(p,t)^{26}Si$ ground state (0^+)

The small cross section and the limited beam time available precluded the use of a target sufficiently thin that the 1.78 and 2.79 MeV levels could be resolved. The polarization analysing powers for the ground state reaction were measured with a 10.5 $mg.cm^{-2}$ natural silicon target, and are plotted in Figure 4.19 and tabulated in Appendix 4. The measurement was limited at wider angles by the small cross section,while at forward angles, the new counters that were used were not thick enough to stop the high energy tritons. The errors shown in Figure 4.19 are statistical and include the uncertainty in the beam polarization.

vi) Possible sources of systematic error.

A measurement of the polarization analysing power requires two complete runs to be made, and it is important that no experimental parameters change during these two runs except for the spin state of the beam. If for some reason beam conditions change on account of the spin reversal at the ion source, then the

calculation of the analysing power and the beam polarization may be subject to a systematic error.

The analysing power is calculated from eqn.(4.4)

$$X = \frac{L_+ R_-}{L_- R_+} = \frac{(1 + P_B P_A)^2 (\epsilon_L/\epsilon_R)_+}{(1 - P_B P_A)^2 (\epsilon_L/\epsilon_R)_-}$$

where ϵ is an efficiency factor and is proportional to the product of the unpolarised differential cross section and the counter solid angle -

$$\epsilon \propto \frac{d\sigma}{d\omega_o} \times \Omega .$$

The ratio of the relative efficiencies is taken to be unity in the calculation. If the horizontal position of the beam or its direction at the target is dependent on the spin state, then the counter solid angle and the differential cross section as observed by the telescope will also be dependent on the spin state. The ratio of the relative efficiencies will then be different from unity. This error can be detected by using as a monitor, a reaction process which is known to have a very small analysing power. For such a reaction

$$X = \frac{L_+ R_-}{L_- R_+} = \frac{(\epsilon_L/\epsilon_R)_+}{(\epsilon_L/\epsilon_R)_-}$$

and any observed asymmetries, that is, when X is different from unity, would be spurious and a consequence of beam shifts. A

possible reaction that could be used in this context is proton scattering at small angles from heavy nuclei where, in general, the analysing powers for angles less than 10° do not exceed 1%. The gold foil monitor would have provided a useful check in this respect were it possible to reduce the counter angle from 20° to about 5°.

The position of the spot at the target can only change with spin reversal if the beam moves on a different trajectory through the beam transport system. A single beam 'ray' which is a distance x in the horizontal plane from the axis at the momentum slit, will be at a distance Mx from the axis at the target where M is the horizontal magnification of the system. If the beam profile at the momentum slit is much smaller than the width of the slit, then slight changes in the position at this point will have a marked effect on the position of the beam at the target. The dispersion of the beam once it has passed through the bending magnet, ensures that the momentum slit is uniformly illuminated and since the width of the slit has been chosen to be considerably smaller than the dimensions of the beam, the position of the beam focus at the target will not be affected by movement of the beam spot at the momentum slit. This argument is based on the assumption that the quadrupole pair between the momentum slit and the target is non-dispersive, and this is valid only when the pole faces are properly aligned so that the beam is paraxial.

Before every experiment, therefore, the axis of the beam line and the quadrupole pair was aligned to within 0.003" in the manner described in section ii of Chapter 3.

The very good agreement between the two separate determinations of the analysing powers of the $^{12}C(p,t)^{10}C$ ground state reaction demonstrates the reproducibility of the experimental techniques which range from optical alignment to data collection and reduction. Additional confirmation of the absence of systematic errors due to beam shift as been obtained in experiments performed at 30 MeV (Chant and Nelson,1968). At this energy the gold foil monitor can be used at 20° to detect the presence of false asymmetries. None was observed.

vii) Calculation of the polarization analysing power.

The analysing powers were calculated with a computer programme based on eqns.(4.5) and (4.6). When single counter operation was used, the yields from the counter telescopes were corrected for the electronic dead time losses using the formula given in Appendix 2. The beam polarization was calculated from eqn.(4.5) using the yields from the polarimeter.

The standard deviation σ of the analysing power P_A is given by the following expressions.

a) Double counter operation.

$$\sigma^2(P_A) = \frac{X^2}{P_B^2(X+1)^2}\left\{\frac{1}{L_+} + \frac{1}{L_-} + \frac{1}{R_+} + \frac{1}{R_-}\right\} + \frac{(X-1)^2\,\sigma^2(P_B)}{(X+1)^2\,P_B^2}$$

The cross product X is defined in eqn.(4.5). The standard deviation of the beam polarization is given by a similar expression involving the polarimeter yields and the polarimeter analysing power.

b) Single counter operation.

The standard deviation in this case is rather a long expression and with reluctance it is given as

$$\sigma^2(P_A) = P_A^2 \left\{ \frac{\sigma^2(P_B)}{P_B^2} + \frac{1}{(1-\beta\,\delta P_B)^2} \frac{\sigma^2(\beta)}{\beta^2} + \frac{(P_A P_B)^2 \sigma^2(\delta P_B)}{} \right\}$$

where $\sigma^2(P_B)$ can be calculated from the double counter equation and

$$\sigma^2(\beta) = \frac{4Y^2}{(Y+1)^4} \left\{ \frac{1}{L_+} + \frac{1}{L_-} + \frac{1}{4\ell_- r_-} + \frac{1}{4\ell_+ r_+} + \frac{\sigma^2(f_+)}{f_+^2} + \frac{\sigma^2(f_-)}{f_-^2} \right\}$$

where Y is defined in eqn.(4.6) and the quantities $\ell_\pm$ and $r_\pm$ are the yields from the gold foil monitor. The standard deviation $\sigma(f)$ of the dead time correction factor, f, is given in Appendix 2. Finally

$$\sigma^2(\delta P_B) = \frac{4X^2}{(X+1)^4} \left\{ \frac{1}{4\ell_+ r_+} + \frac{1}{4\ell_- r_-} + \frac{L_+ R_o (L_+ + R_o) + L_o R_+ (L_o + R_+)}{(L_+ R_o - L_o R_+)^2} \right.$$

$$+ \frac{L_o R_- (L_o + R_-) + L_- R_o (L_- + R_o)}{(L_o R_- - L_- R_o)^2}$$

$$\left. + \frac{2(L_+ L_- R_o + R_+ R_- L_o)}{(L_+ R_o - L_o R_+)} \frac{1}{(L_o R_- - L_- R_o)} \right\}$$

where X is the cross product calculated with the polarimeter yields: $L_\pm$ and $R_\pm$, and L_o and R_o are defined in eqn.(4.7) and eqn.(4.8).

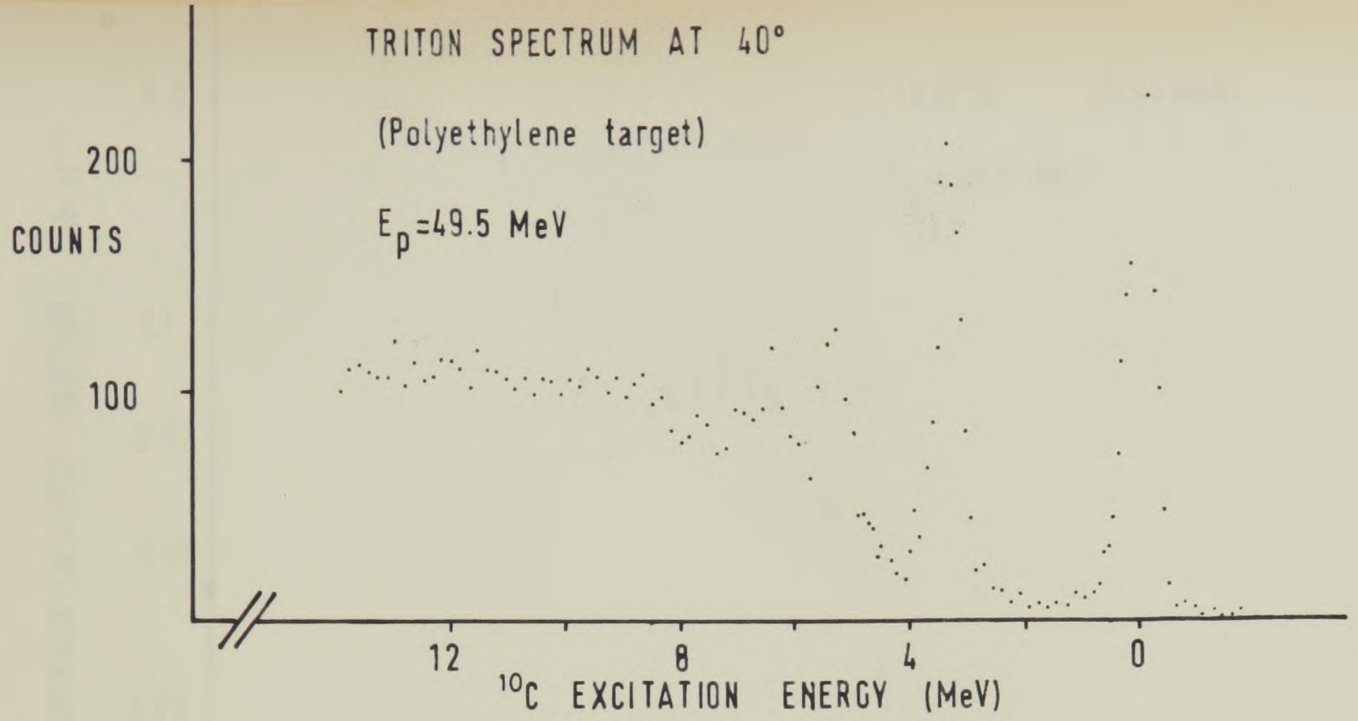


FIGURE 4.1

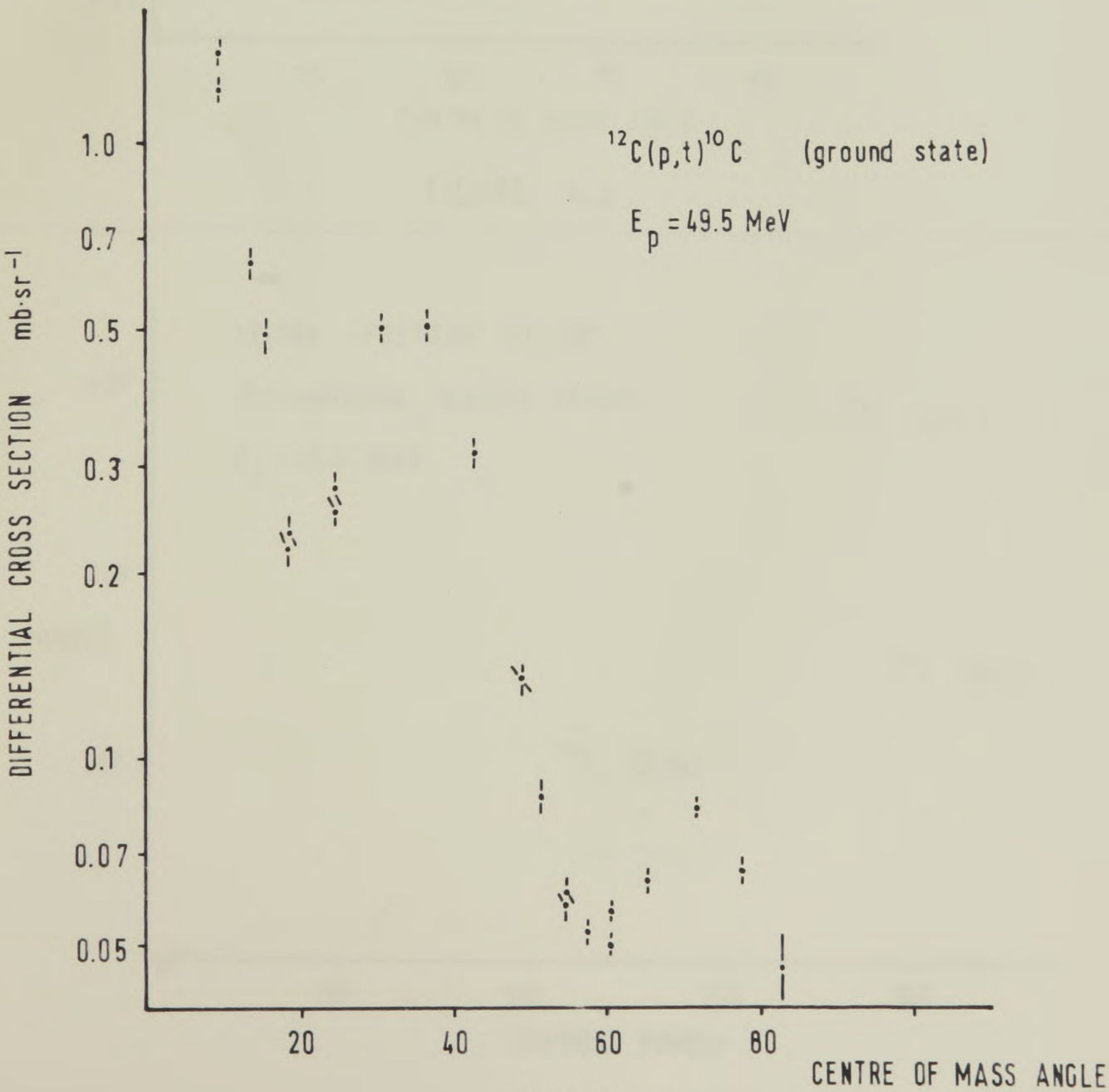


FIGURE 4.2

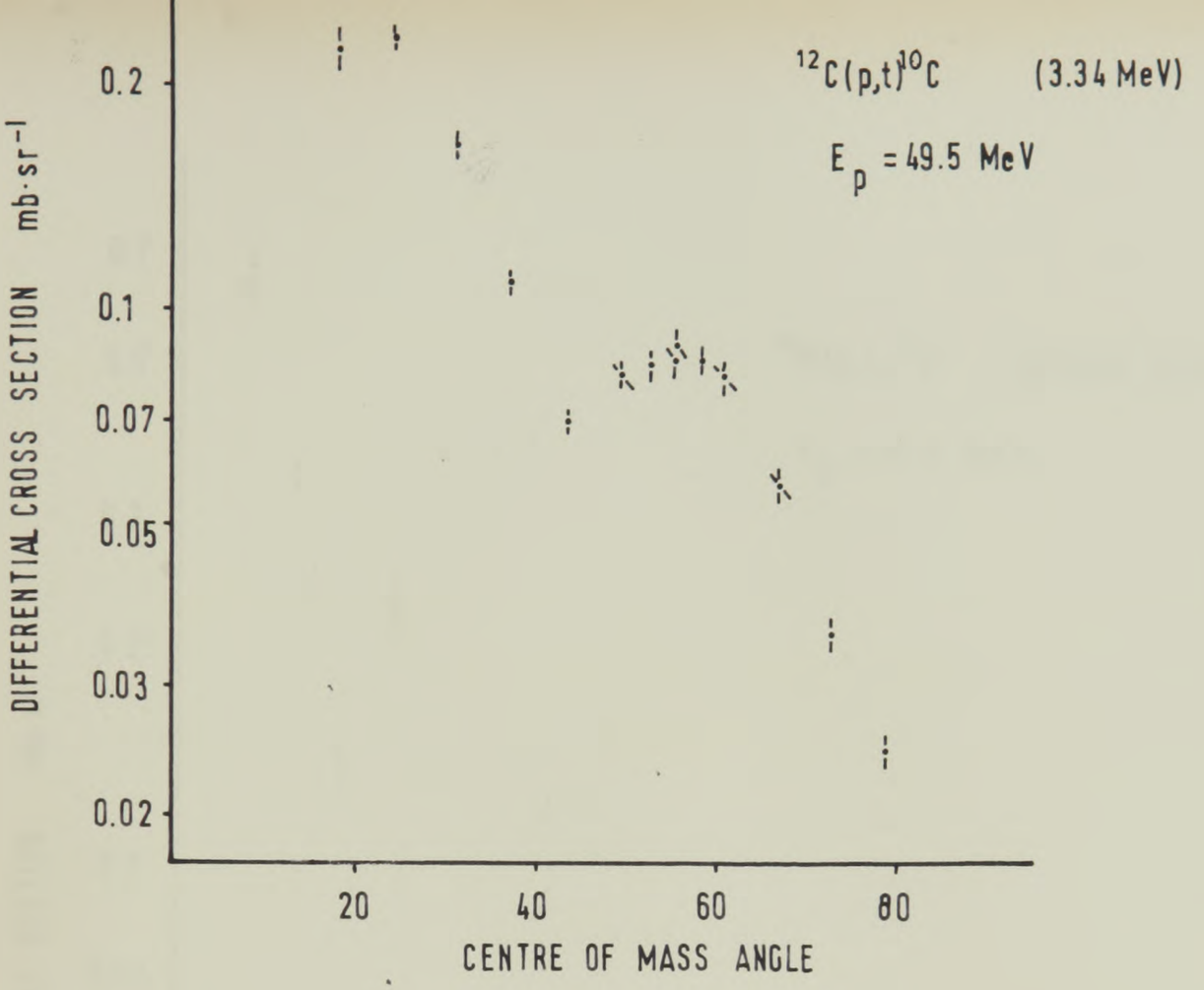


FIGURE 4.3

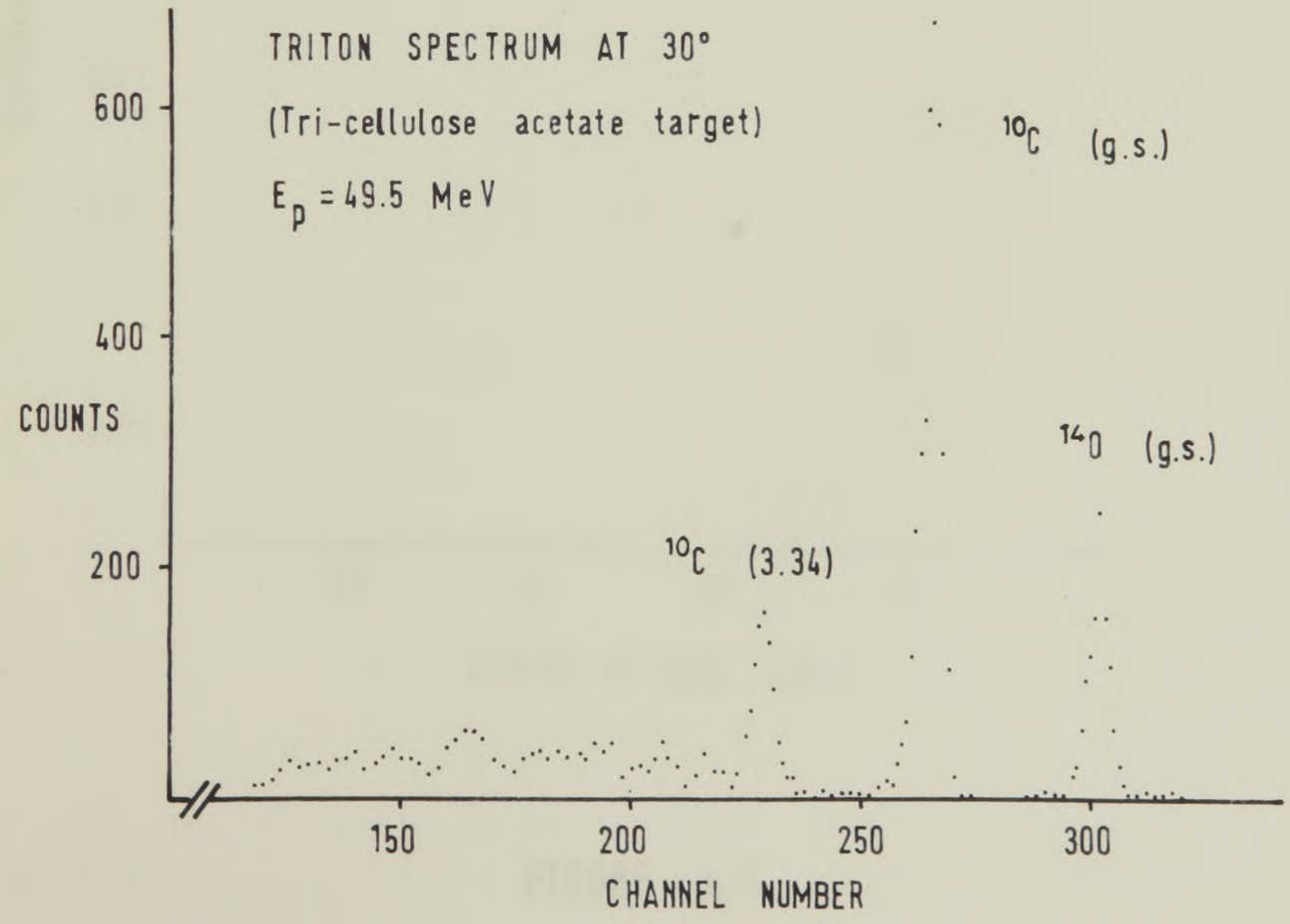


FIGURE 4.4

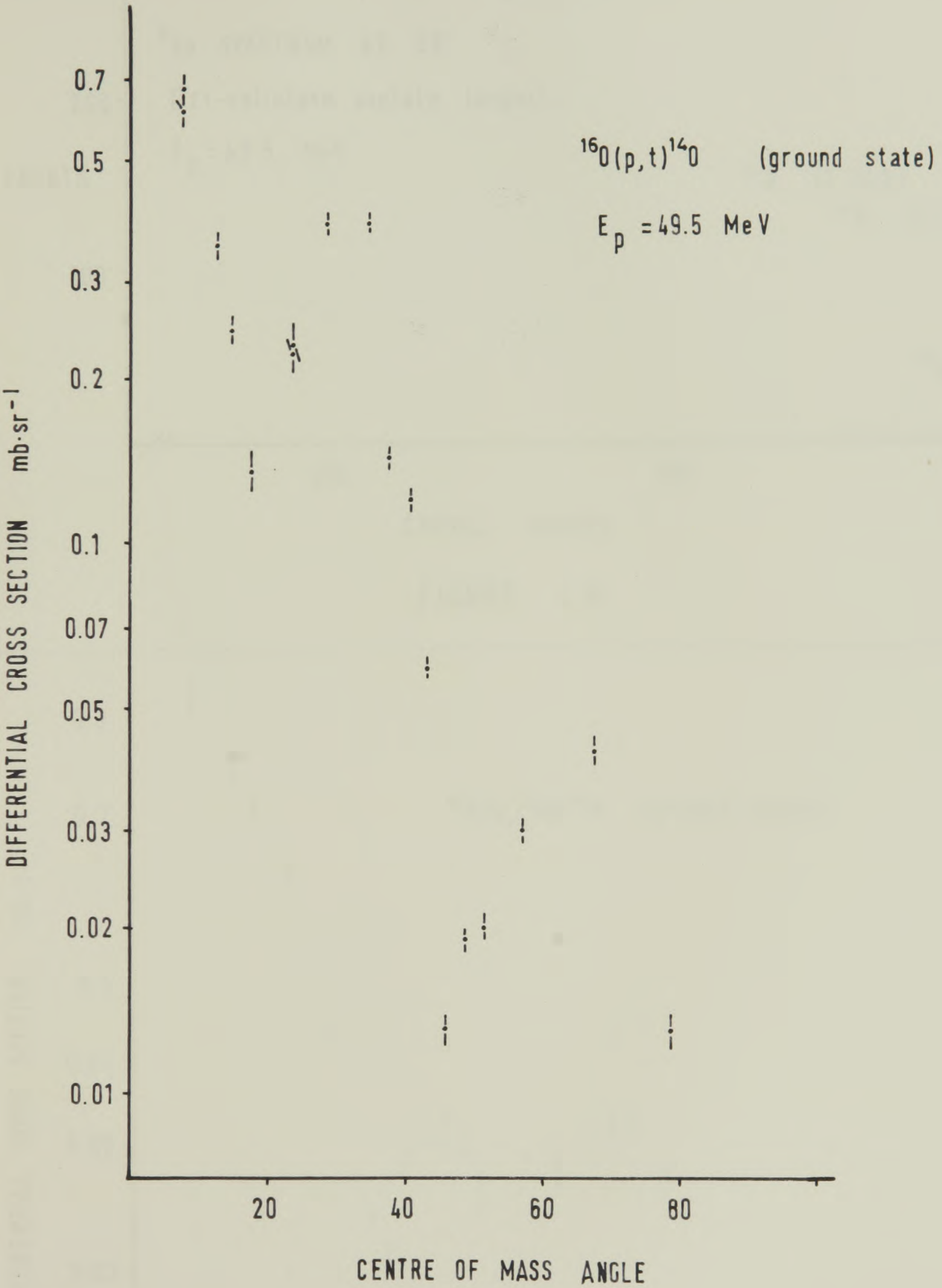

$^{16}O(p,t)^{14}O$ (ground state)
E_p = 49.5 MeV
DIFFERENTIAL CROSS SECTION mb·sr⁻¹
0.7
0.5
0.3
0.2
0.1
0.07
0.05
0.03
0.02
0.01
20
40
60
80
CENTRE OF MASS ANGLE

FIGURE 4.5

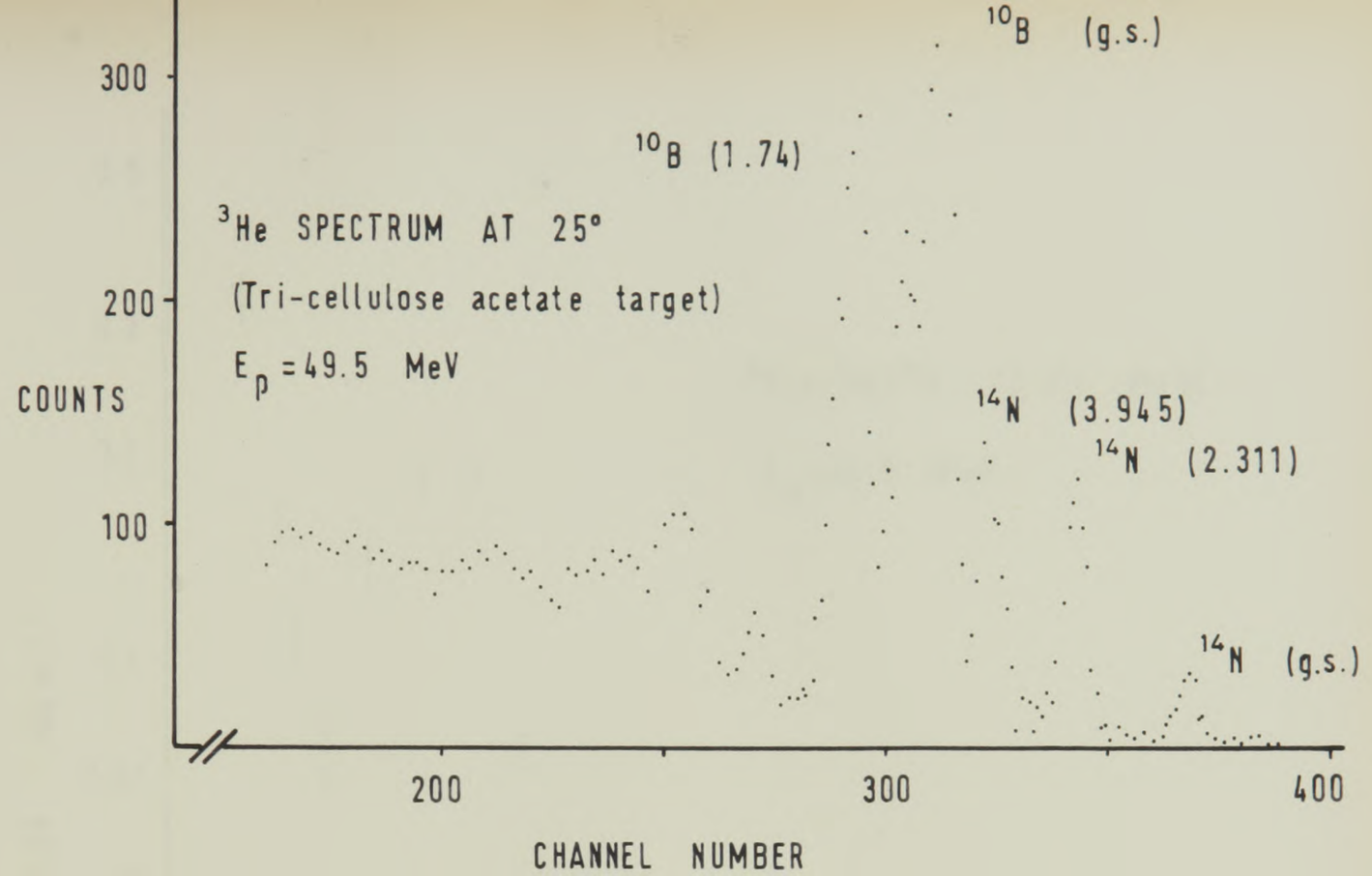


FIGURE 4.6

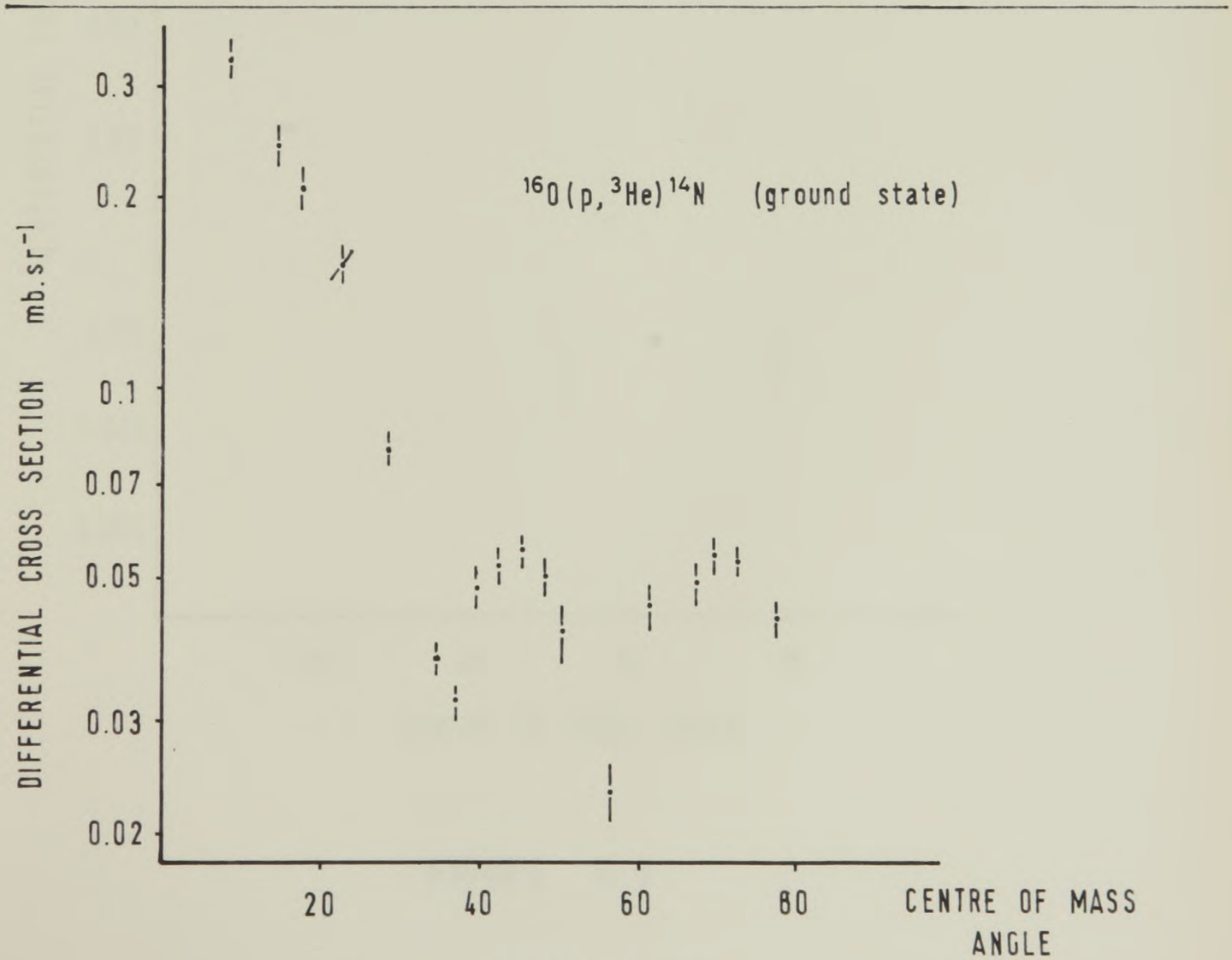


FIGURE 4.7

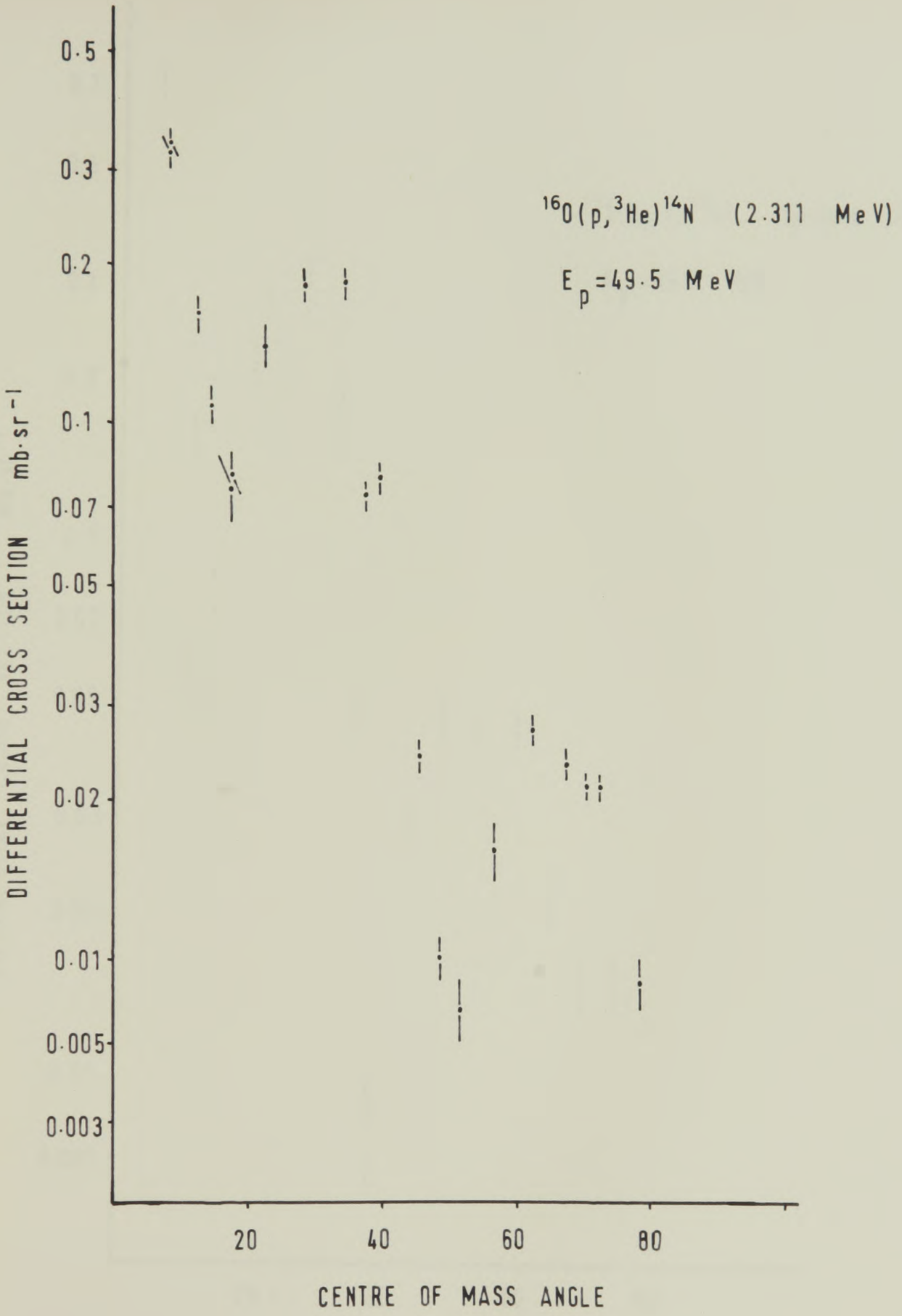

$^{16}O(p,^{3}He)^{14}N$ (2.311 MeV)
$E_p = 49.5$ MeV
DIFFERENTIAL CROSS SECTION mb·sr⁻¹
0·5
0·3
0·2
0·1
0·07
0·05
0·03
0·02
0·01
0·005
0·003
20
40
60
80
CENTRE OF MASS ANGLE

FIGURE 4.8

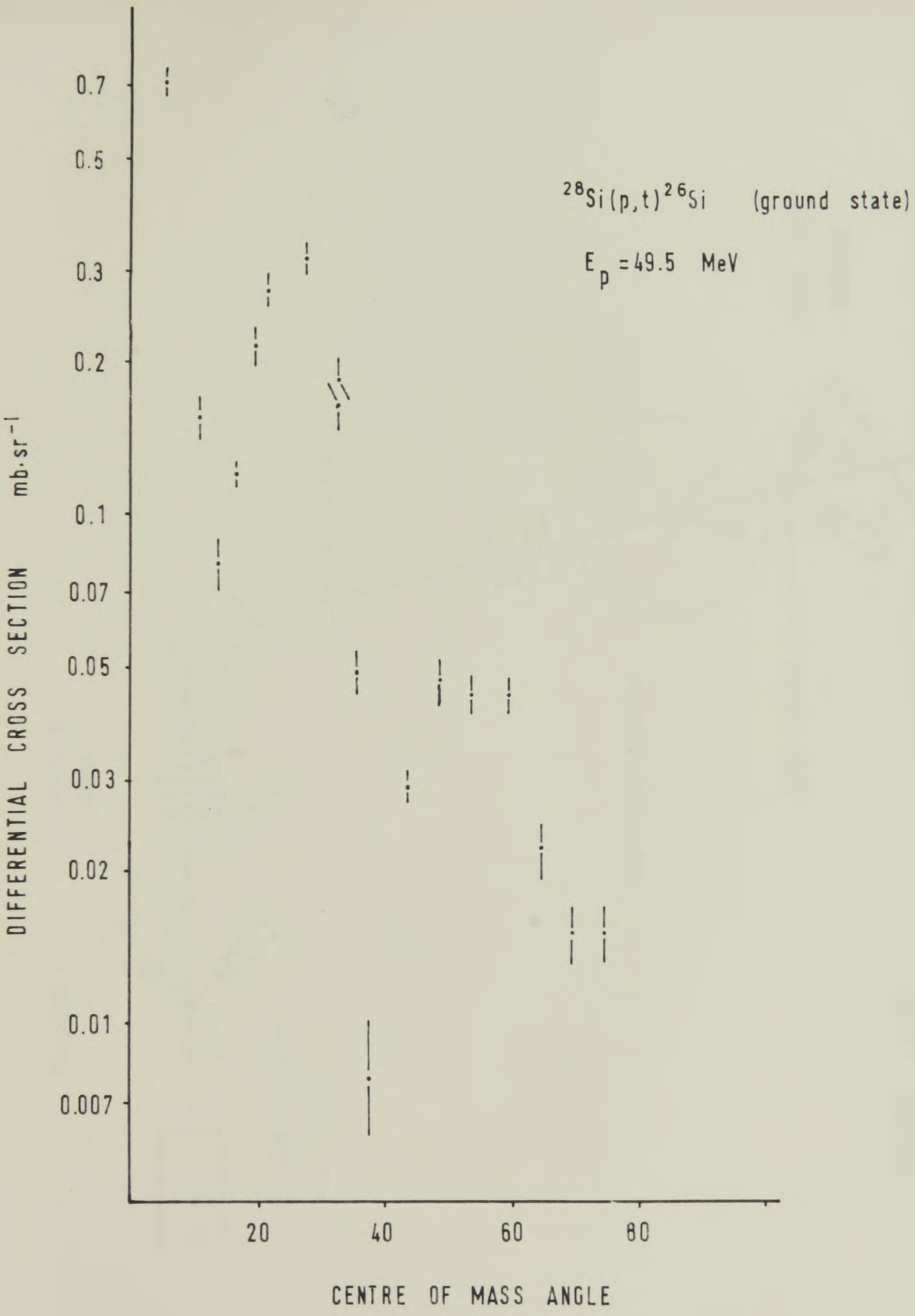

$^{28}Si(p,t)^{26}Si$ (ground state)
$E_p = 49.5$ MeV
DIFFERENTIAL CROSS SECTION mb·sr^{-1}
0.7
0.5
0.3
0.2
0.1
0.07
0.05
0.03
0.02
0.01
0.007
20
40
60
80
CENTRE OF MASS ANGLE

FIGURE 4.9

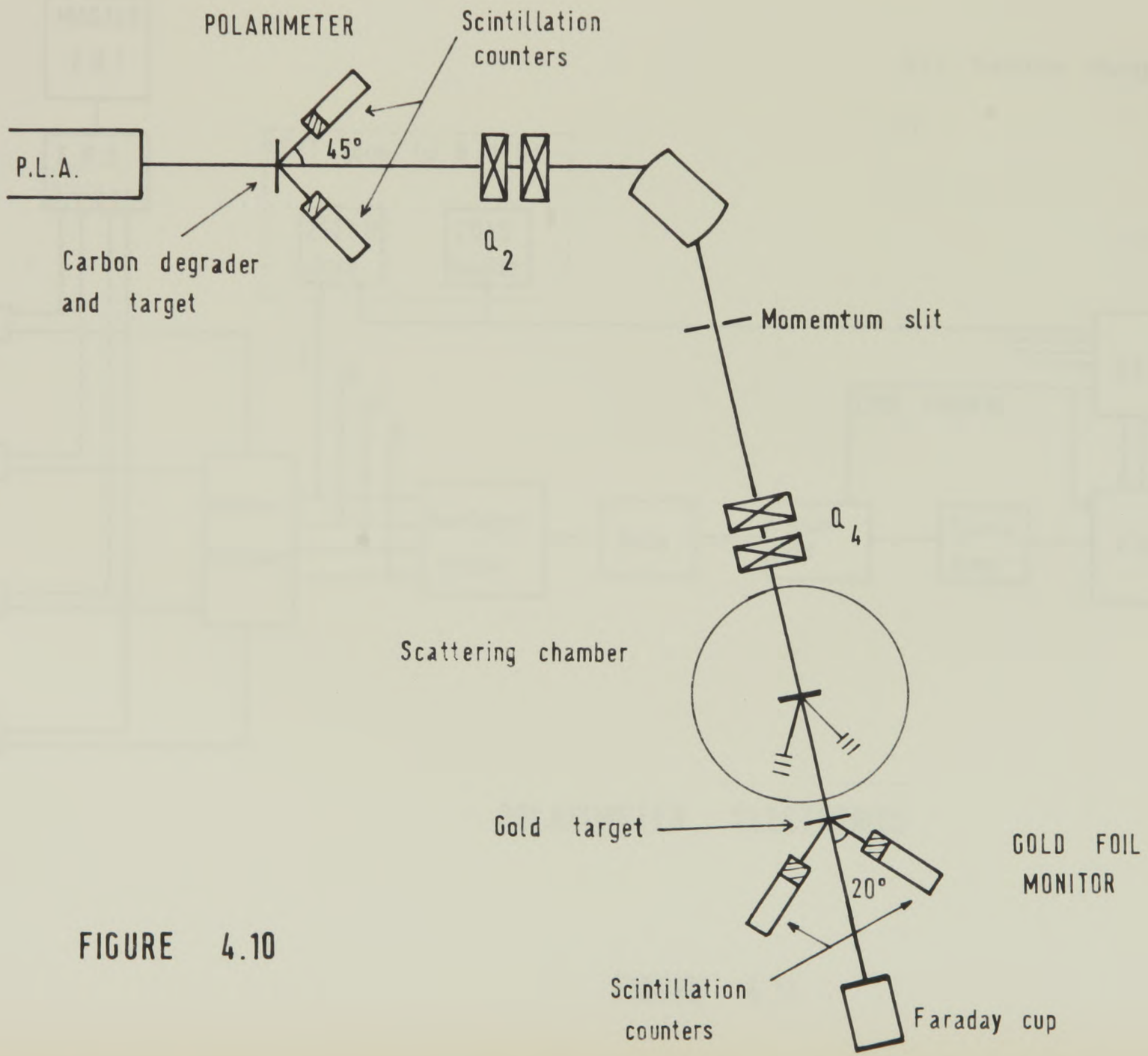
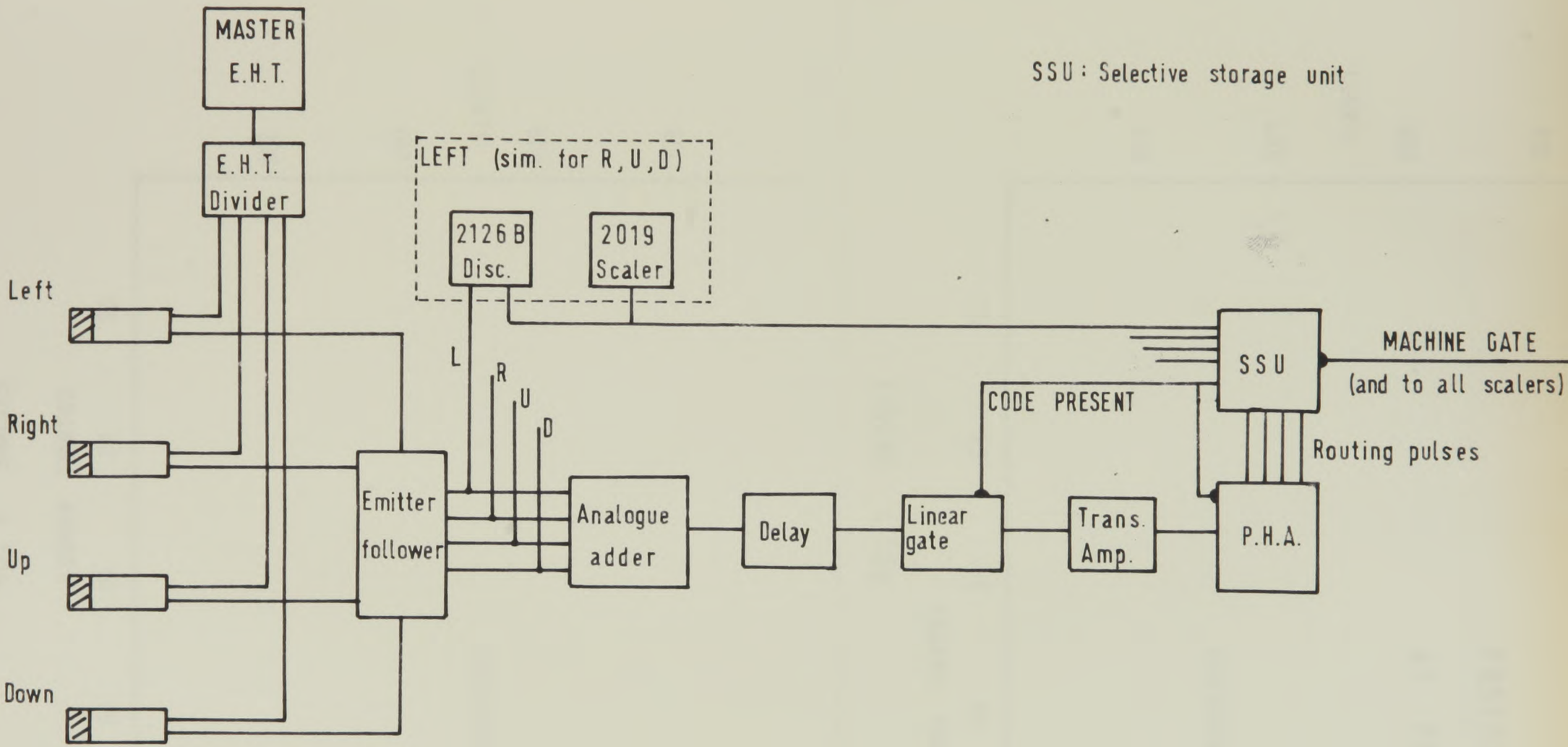

POLARIMETER
Scintillation counters
P.L.A.
45°
Carbon degrader and target
Q2
Momemtum slit
Q4
Scattering chamber
Gold target
GOLD FOIL MONITOR
20°
Scintillation counters
Faraday cup

FIGURE 4.10



POLARIMETER ELECTRONICS

FIGURE 4.11

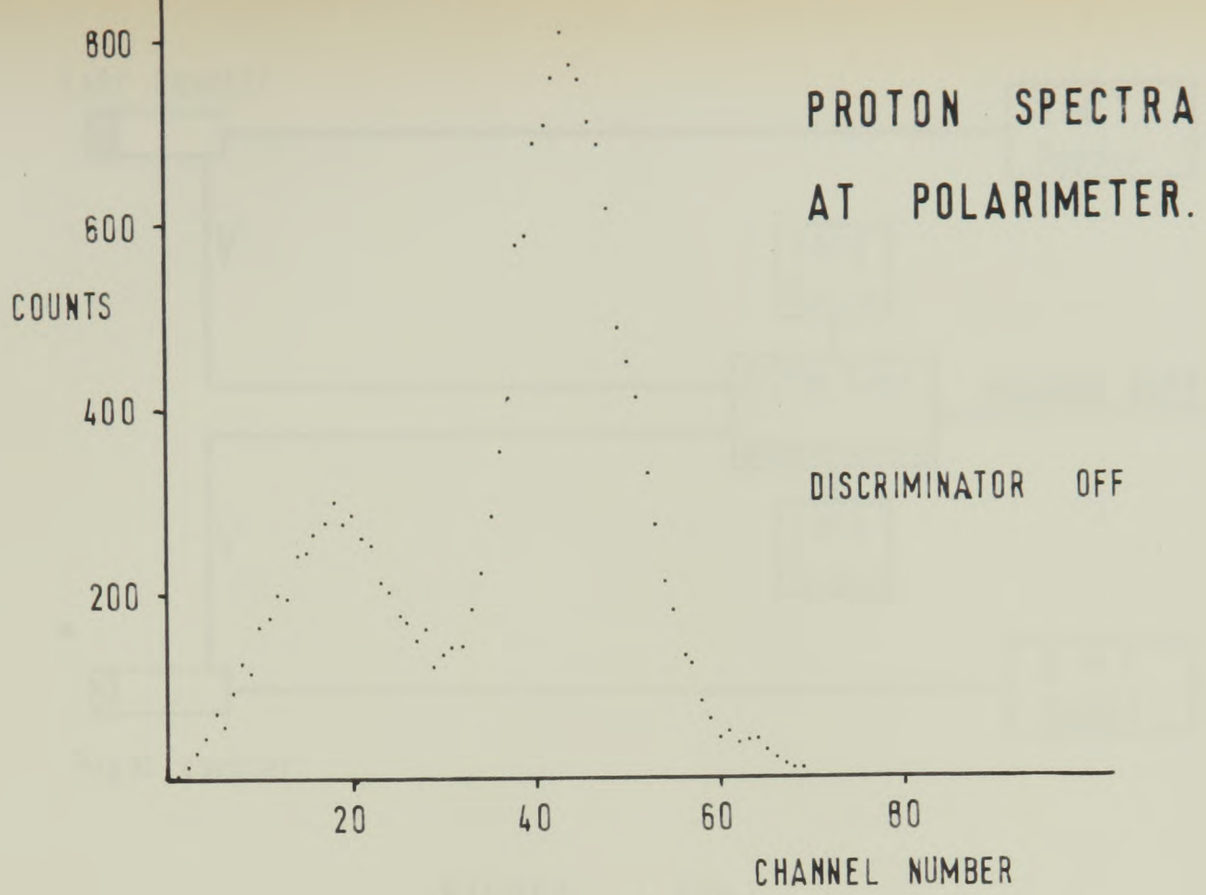


FIGURE 4.12a

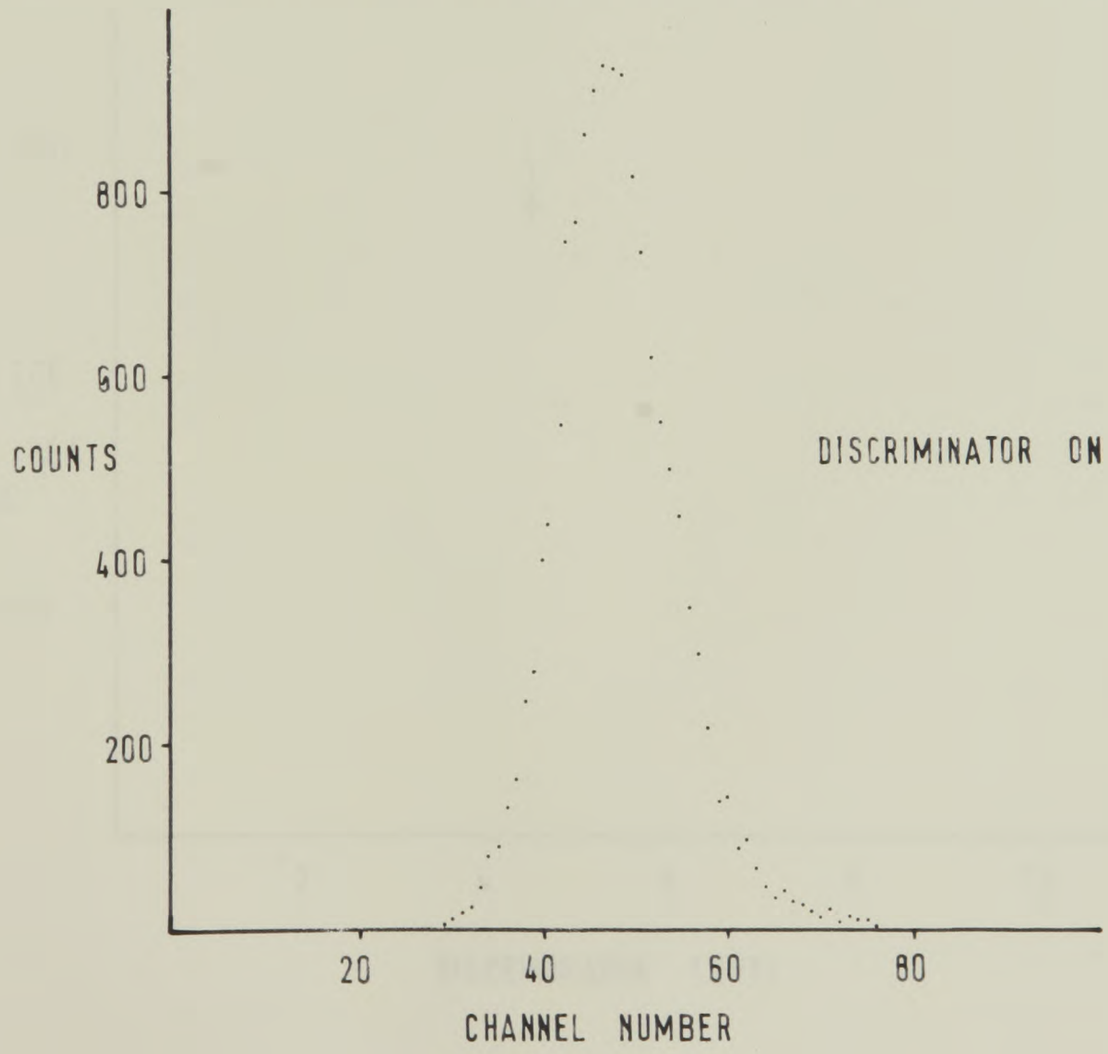


FIGURE 4.12b

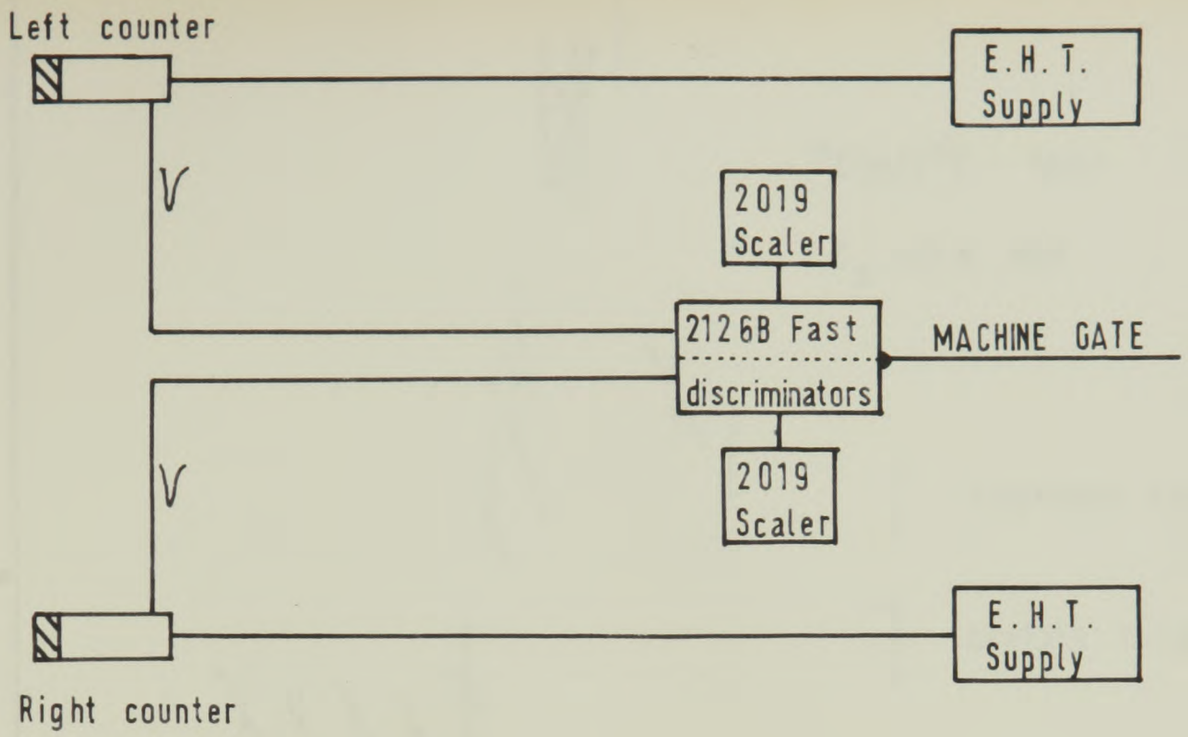


FIGURE 4.13a

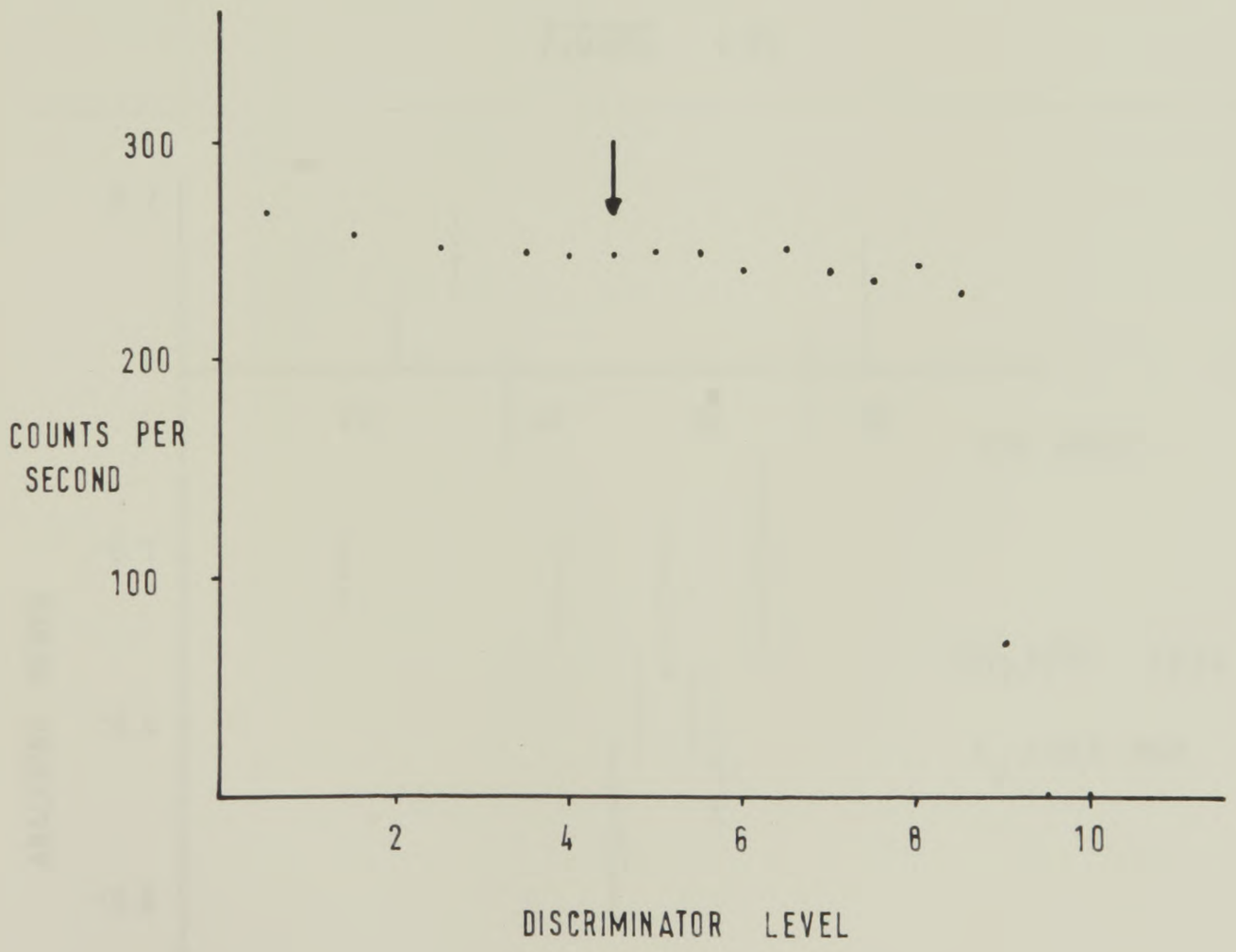


FIGURE 4.13b

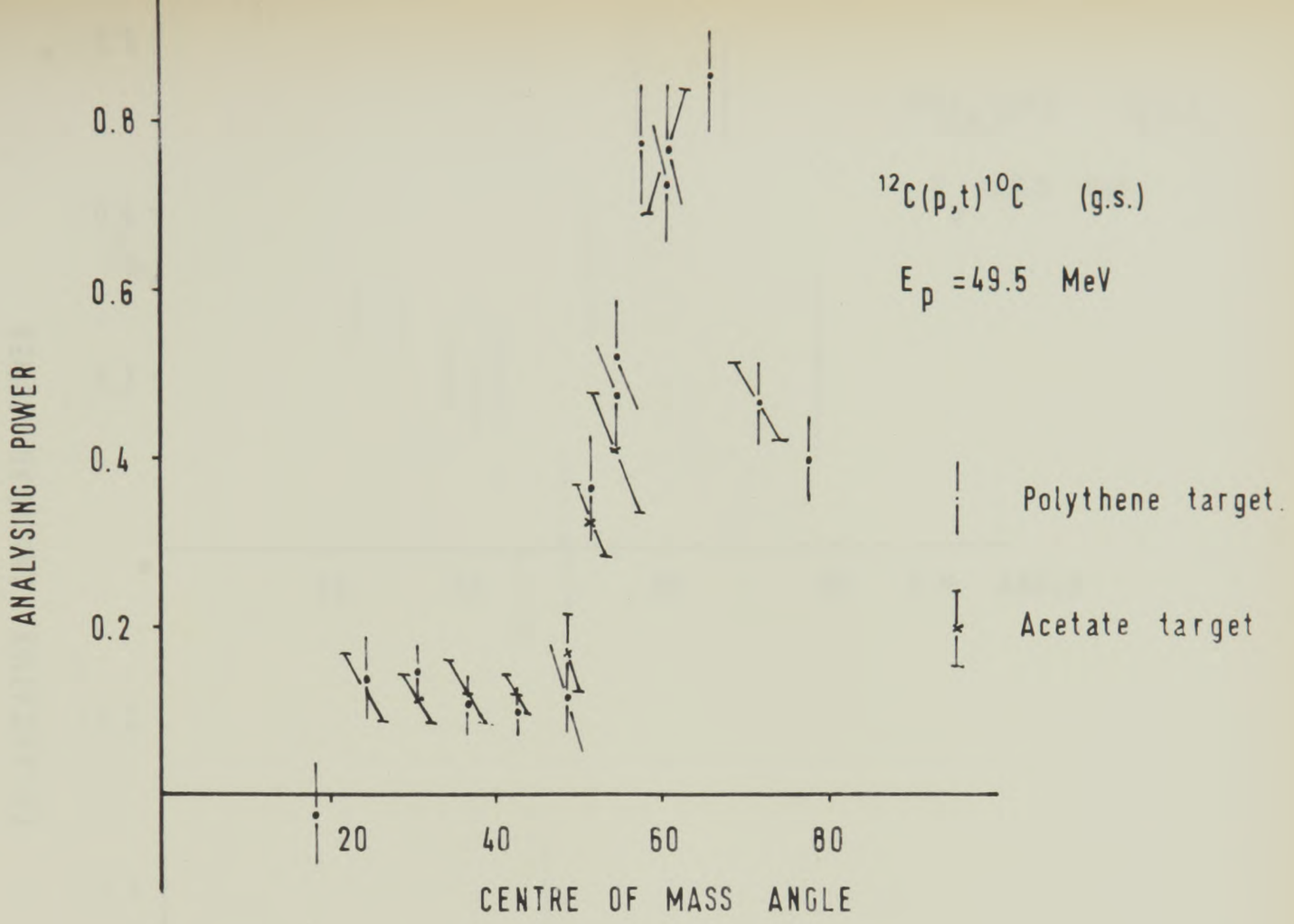


FIGURE 4.14

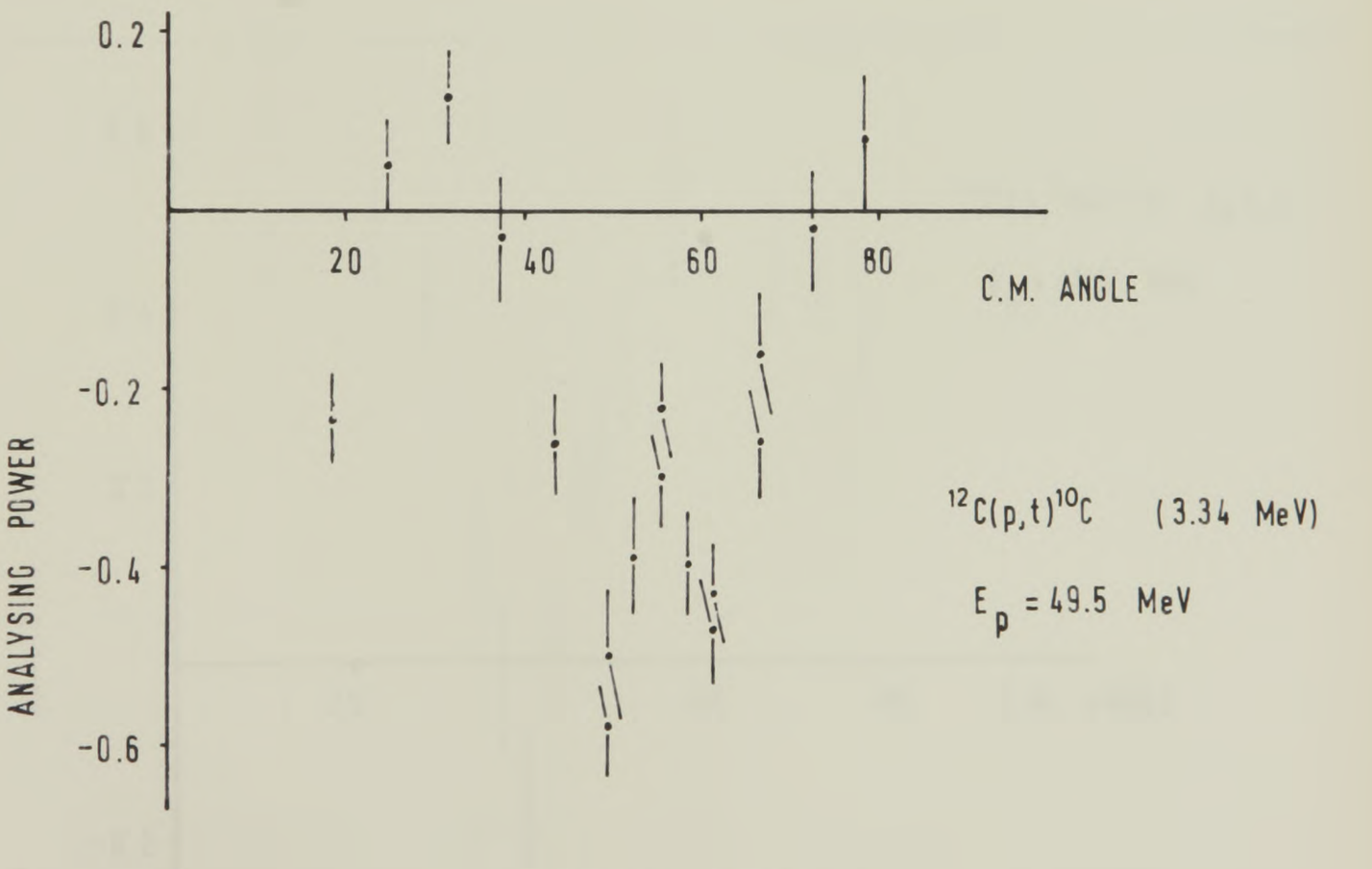


FIGURE 4.15

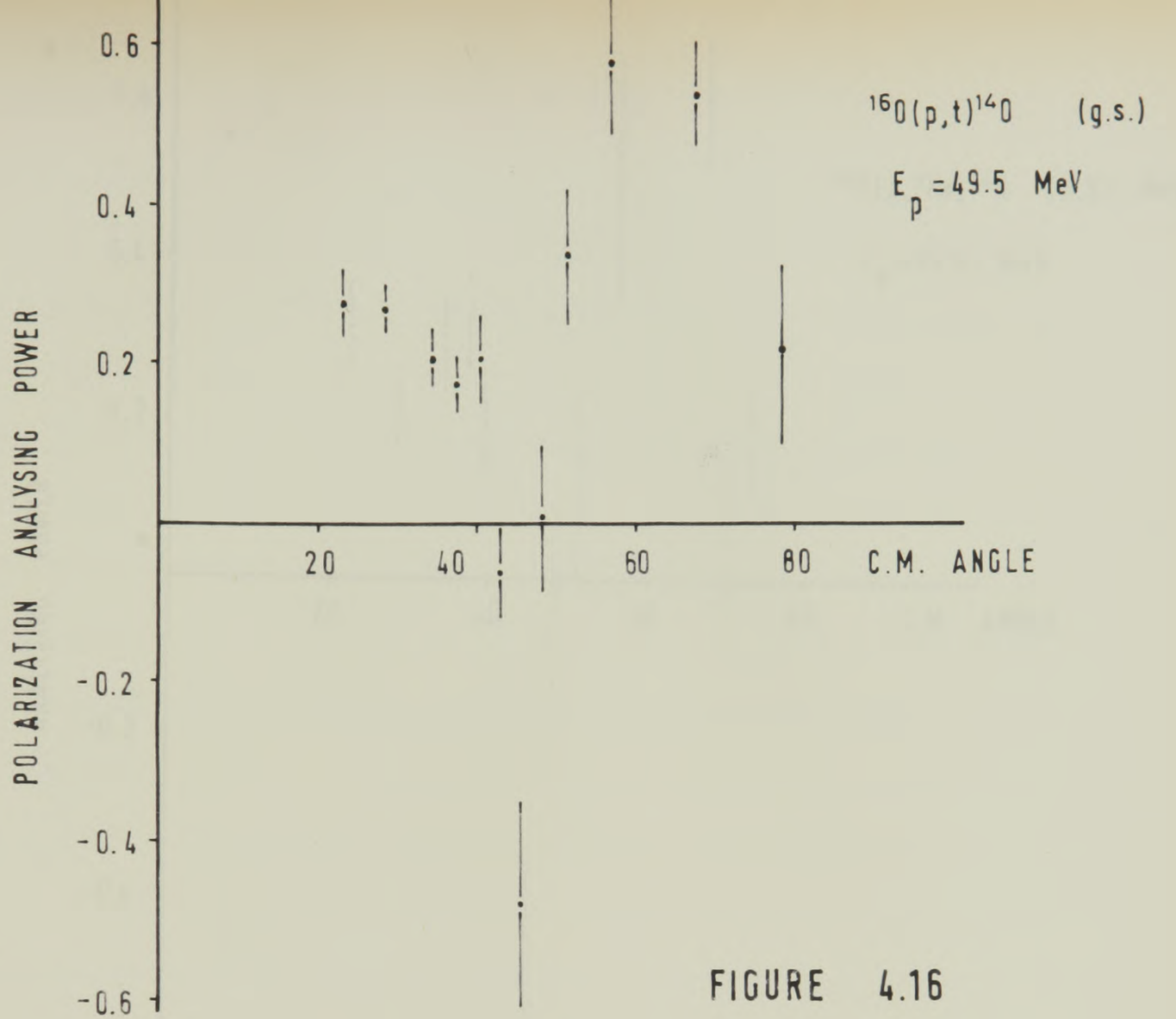


FIGURE 4.16

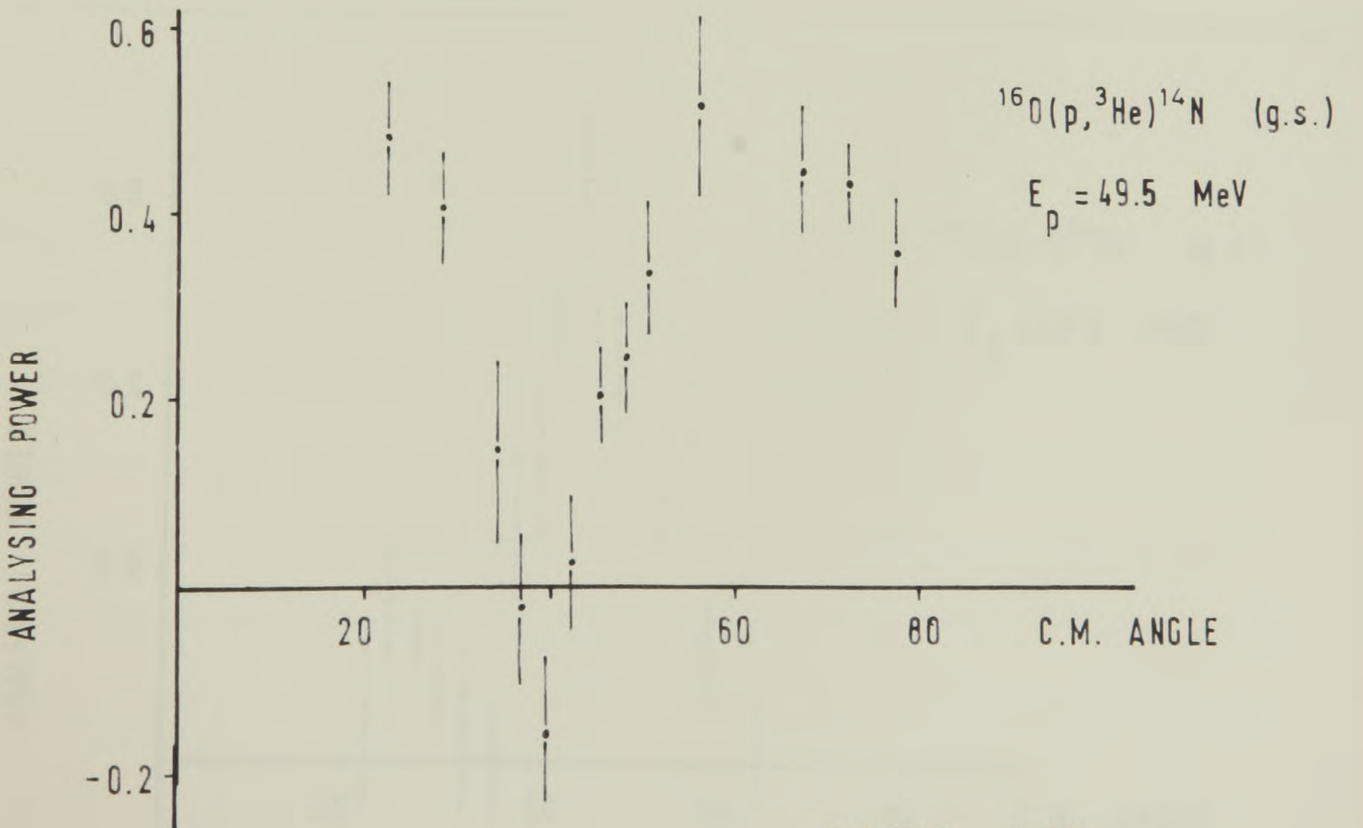


FIGURE 4.17

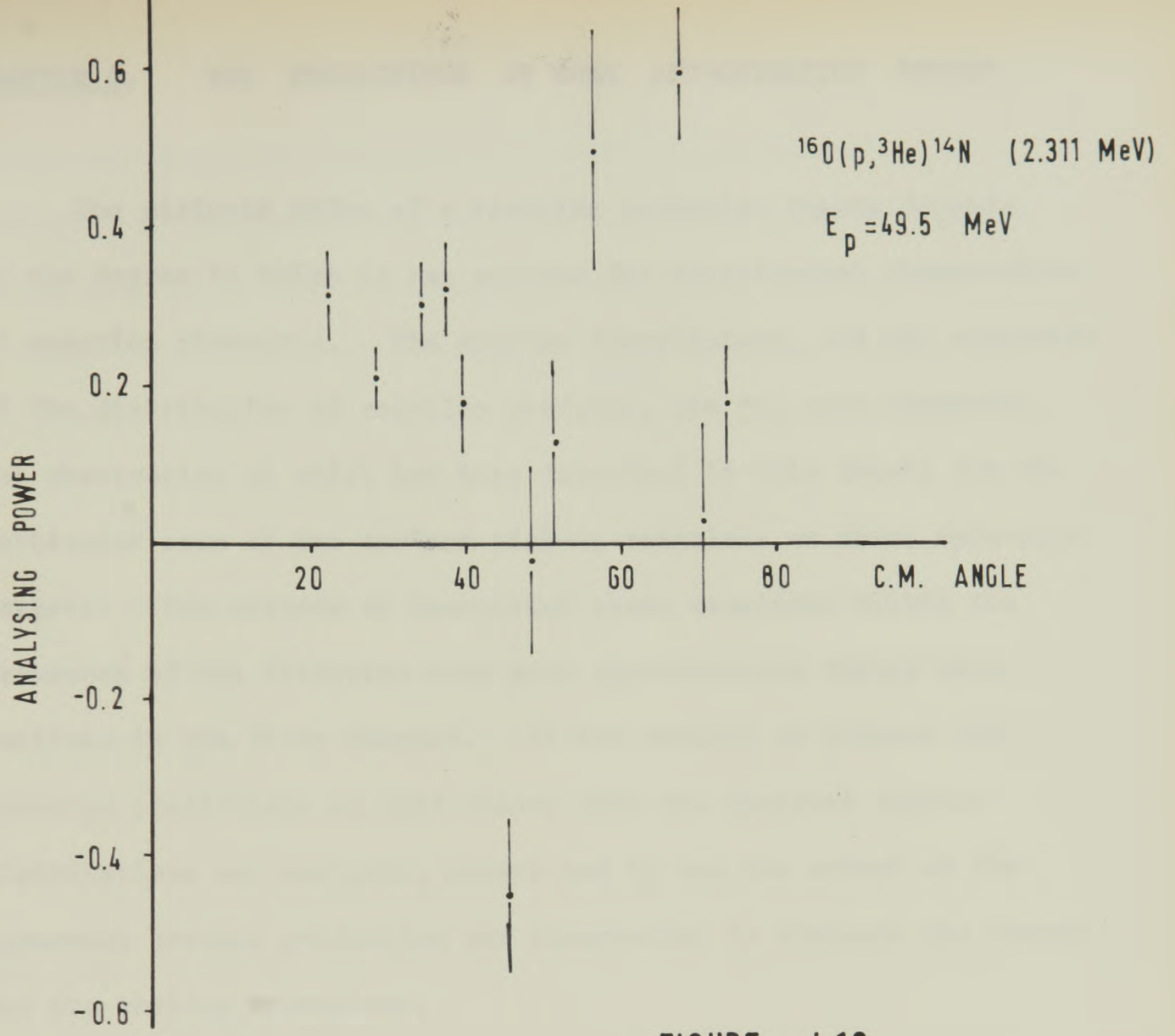


FIGURE 4.18

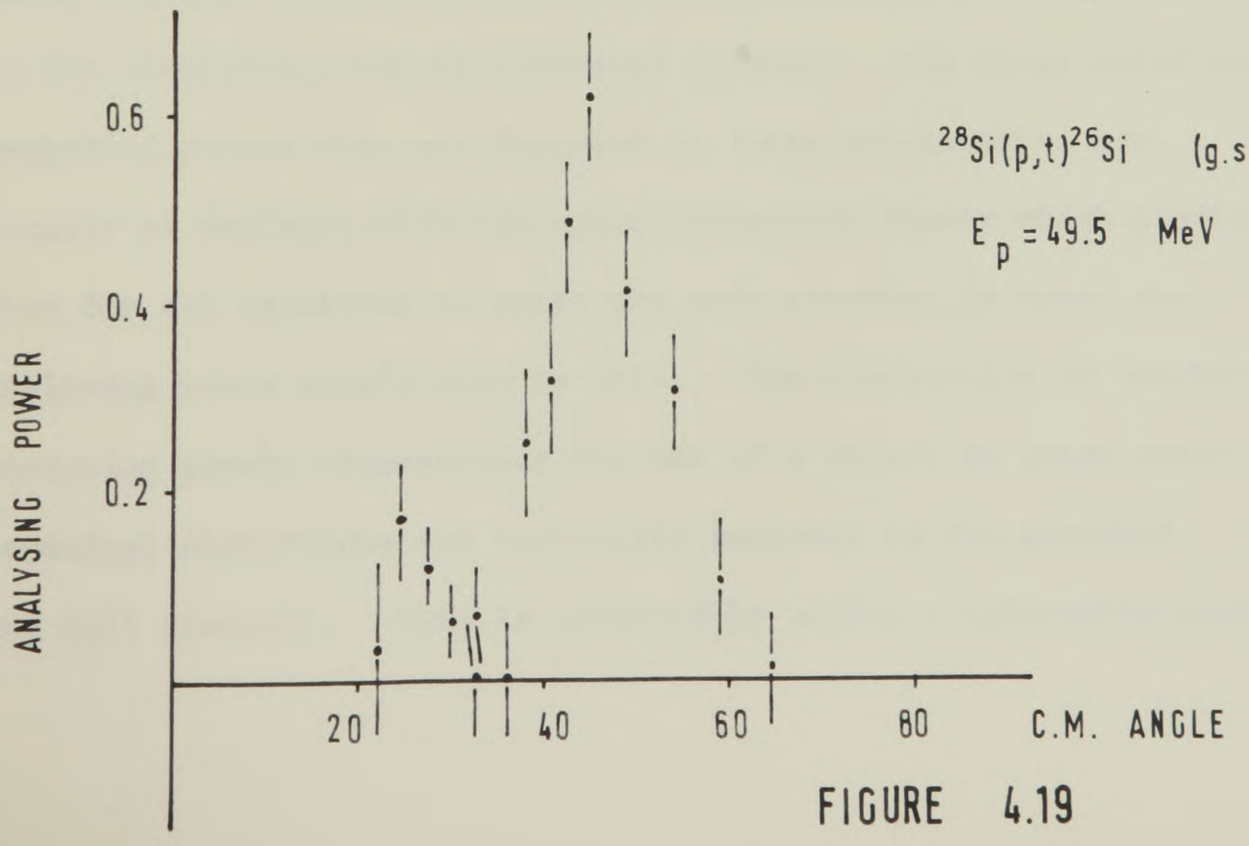


FIGURE 4.19

CHAPTER 5. THE PREDICTIONS OF BORN APPROXIMATION THEORY.

The ultimate value of a reaction mechanism theory depends on the degree to which it can account for experimental observations of reaction phenomena. The angular distribution, and the asymmetry of the distribution of reaction products, are two such phenomena, the observation of which has been described in this thesis for the particular case of two nucleon pick-up reactions on three spin-zero targets. Two methods of describing these reactions within the framework of the distorted wave Born approximation theory were outlined in the first chapter. It now remains to compare the computed predictions of this theory with the observed angular distributions and analysing powers and to use the extent of the agreement between prediction and observation to evaluate the theory and its various extensions.

The usual spin-independent theory, which has provided the basis for the analyses of two nucleon transfer reactions reported in the literature, can be dismissed at once. The large polarization analysing powers that are observed in these experiments, are totally at variance with the spin-independent theory which predicts that for all reactions in which the spin transfer is zero, the analysing power should also be zero. The observation of non-zero analysing powers necessitates the use of a theory in which spin-dependent distortions are explicitly included in the incident and exit channels. This is achieved by adding a spin-orbit term

to the optical model potential relevant to each channel. The solutions of the Schrodinger equations in which these potentials appear are, of course, the distorted waves that describe the incident and emitted particles. The wave functions appear in the matrix element given in eqn.(1.1) which is repeated here.

$$M_{ab} = \int \chi^{*}_{bB}(k_b, r_{bB})\ I^{eff}\ \chi_{aA}(k_a, r_{aA})\ dr_{aA}\ dr_{bB} \qquad 5.1$$

The form of the effective interaction I^{eff} has already been described and in the next section the optical model potentials used to generate the distorted waves χ_{bB} and χ_{aA} will be discussed.

i) Optical model potentials.

Analyses of proton elastic scattering at or near 50 MeV have been published for the three targets of interest, namely, ^{12}C, ^{16}O, and ^{28}Si and these will be discussed briefly in terms of their usefulness in DWBA calculations. The spin-dependent term in the optical potential can only be defined adequately if a polarization measurement forms part of the elastic scattering experiment, and this requirement limited the number of analyses that were considered. For the case of ^{12}C at 46 MeV proton energy, an extensive analysis has been reported by Satchler (1967), and at 50 MeV by Craig et al.(1966), and Fannon et al. (1967). A number of these optical potentials were used in DWBA calculations with comparable results, a not unexpected outcome since the potentials are very similar. The proton potential that was used for the ^{12}C

DWBA calculations was taken from Table 8 of Fannon's analysis and is tabulated here in Table 3 with the label PFC.

Table 3.

Proton optical potentials.

	Tgt	En.	V_o	r_o	a_o	W_V	r_V	a_V	W_D	r_D	a_D	V_s	r_s	a_s
PFC	^{12}C	50	35.2	1.15	0.68	4.87	1.10	1.14	0			3.42	0.62	0.24
PFO	^{16}O	50	35.4	1.25	0.65	3.31	1.25	0.65	3.70	1.25	0.47	5.48	0.96	0.65
PBO	^{16}O	52	31.4	1.25	0.7	0			3.60	1.20	0.44	5.7	1.25	0.7
PCS	^{28}Si	50	36.4	1.16	0.7	6.8	1.47	0.61	1.4	1.47	0.7	5.4	1.0	0.7
PFS	^{28}Si	40	44.6	1.13	0.73	1.39	1.41	0.54	4.41	1.41	0.54	5.84	1.01	0.63

All energies are in MeV and lengths are in fermis.

The general form of the optical modal potential used in the calculations is defined by

$$V = V_c(r_c) - V_o f(r_o,a_o) - iW_V f(r_V,a_V) + 4iW_D a_D \frac{d}{dr} f(r_D,a_D)$$

$$+\left(\frac{\hbar}{m_\pi c}\right)^2 \frac{1}{r} V_s \mathbf{l}\cdot\boldsymbol{\sigma} \frac{d}{dr} f(r_s,a_s) \qquad 5.2$$

where $f(r_j,a_j) = \{1 + \exp(\frac{r - r_j A^{1/3}}{a_j})\}^{-1}$,

and V_c is the coulomb potential due to a uniformly charged sphere of radius $r_c A^{1/3}$,

V_o is the real central potential strength,

W_V is the volume absorption potential strength,

W_D is the surface absorption potential strength,

V_s is the spin-orbit potential strength.

The symbol σ denotes the Pauli spin operator. The coulomb radius for the potentials listed in the Table is 1.25 fm except for potential PFS where the value is 1.2 fm.

Two analyses of proton scattering on ^{16}O were considered. The work of Fannon et al. does not include a polarization measurement and hence the magnitude of the spin-orbit term may not be accurately defined. The result of an elastic scattering polarization measurement at 52.5 MeV reported by Boschitz et al (1965) yields a potential almost identical to that of Fannon et al. Both potentials are tabulated in Table 3 with the labels PFO (Fannon) and PBO (Boschitz). When used in DWBA calculations, the potentials were indistinguishable, and in so far as it is now known that the spin-orbit radius should be less than the radius of the real central potential, the Fannon potential was preferred.

The optical potential used by Craig et al. (1966) to describe elastic scattering and polarization of 50 MeV protons on ^{28}Si is tabulated in Table 3 with the label PCS together with the result, PFS, of an analysis by Fricke et al. (1968) at 40 MeV. The results of DWBA calculations using these two potentials were similar and the 50 MeV potential PCS was chosen for the complete analysis. In general, all the DWBA calculations were found to be insensitive to the particular proton potential that was used.

When the point 'tri-nucleon' approximation was used in the

effective interaction, the two transferred particles were assumed to have been bound in single particle orbits described by a Saxon-Woods well:

$$V = V_c(r_o) - V_o\{f(r_o,a_o) - \lambda\left(\frac{\hbar}{2M_pC}\right)^2 \frac{1}{r}\, \ell\cdot\sigma \frac{d}{dr} f(r_o,a_o)\}$$

where $r_o = 1.2$ fm, $a_o = 0.65$ fm and $\lambda = 25$. The other terms have already been defined except M_p, which is the proton mass. The depth V_o is adjusted so that the asymptotic behaviour of the bound state wave function for each transferred nucleon is consistent with the binding energy of the nucleon. (The total binding energy is shared equally between the two nucleons.)

The optical model potential in the exit channel is not very well defined. The results of triton elastic scattering polarization measurements are required at energies of 26 MeV to 29 MeV for the targets ^{10}C, ^{14}O and ^{26}Si, and ^3He elastic scattering polarization measurements are required at 33 MeV for ^{14}N. Triton elastic scattering measurements have not been performed at energies greater than 20 MeV and even at this energy, the lightest target used was ^{52}Cr (Hodgson,1968). No triton polarization measurements have been reported at all. Since triton and ^3He optical potentials at a particular energy and for the same target nucleus are not expected to be appreciably different, ^3He potentials will be used in place of the missing information. The study of triton and ^3He elastic scattering has not reached the

stage where systematic variations of the potentials over energy and target mass can be defined accurately, so that a sensible extrapolation of potentials to the required energy and mass values cannot be made.

Although a few measurements of ^{3}He polarization have been made, no analyses of these data have been published, and the only information about the strength of the spin-orbit potential has come from elastic scattering analyses in which the spin-orbit term was included in the search procedure. This method of analysis does not always lead to an accurate determination of the spin-orbit strength. A more serious uncertainty is connected with the strength of the real central potential. Hodgson's survey of ^{3}He potentials shows that the real central potential varies from 13 MeV to 200 MeV and while the elastic cross sections predicted in calculations using these potentials may be similar because of the optical model potential depth ambiguity, DWBA predictions are certainly not similar. Evidence summarised by Hodgson and arguments proposed by Glover and Jones (1966), and Jones (1965), indicate that the depth of the potential should be roughly equivalent to the sum of the three individual nucleon potentials. The many analyses of deuteron elastic scattering and deuteron stripping reactions show that for the case of the deuteron-nucleus optical potential, this addition rule is meaningful and this criterion has been used as a basis for accepting or rejecting ^{3}He potentials for the

present DWBA calculations. The ^{3}He potentials will be discussed further at the same time as the calculations in which they were used. The special case of the $^{16}O(p,^{3}He)^{14}N$ ground state reaction where two L values are allowed, will be left to the end.

ii) The reaction $^{16}O(p,^{3}He)^{14}N$ (2.311 MeV)

It is convenient to consider first a reaction for which a ^{3}He potential is properly required in the analysis rather than as a substitute for an unavailable triton potential. The four potentials that were used are listed in Table 4.

Table 4.

^{3}He optical potentials

	Tgt	En.	V_o	r_o	a_o	W_V	r_V	a_V	r_c
TS	^{14}N	29	62	1.62	0.57	60.0	1.62	0.57	1.3
THN	^{14}N	29	169	1.14	0.67	32.1	1.62	0.57	1.4
THO	^{16}O	29	190	1.14	0.67	11.2	2.17	0.43	1.4
TG	(N)	≈30	153	1.25	0.65	16.0†	1.25	0.54	1.3

† Surface absorption.

All energies are in MeV and lengths are in fermis.

As far as can be ascertained, only two ^{3}He - ^{14}N elastic scattering analyses have been published for the required energy region. These were at 29 MeV and 25.7 MeV (Sen Gupta et al.,1962;1964). The 29 MeV potential, which closely resembles the 25.7 MeV potential, is labelled TS. Although this is a shallow potential, it is included for the sake of comparison and will not be considered in detail.

Hiebert and collaborators (1967) used the potentials TBW and TBO in an analysis of the (d,^{3}He) pick-up reaction on oxygen. The parameters were obtained by unspecified extrapolation of existing potentials. The potential TC was constructed by summing appropriate low energy (10 MeV) nucleon optical potentials and was used in a study of (p,t) and (p,^{3}He) reactions on ^{15}N (Fleming et al.,1968). The consideration of the applicability of the distorted wave theory to the present work is limited by the paucity of information not only about the spin-orbit strength of the ^{3}He potential, but about the ^{3}He potential as a whole. In spite of this difficulty, it is felt that an illustration of the features of the theory that was described earlier will be of value, and furthermore, it may be possible to deduce some limit for the strength of the ^{3}He spin-orbit potential. Although the theoretical analysing powers will be shown in the diagrams, the discussion will be centred on the differential cross sections until such time as the effects of the spin-orbit forces are considered. The addition of a spin-orbit term to the ^{3}He potential is not expected to have a marked effect on the cross sections.

The results of zero-range calculations, which employed the proton potential PTO and the ^{3}He potentials listed above, are shown in Figure 5.1 and Figure 5.2. The potentials were assumed to be local, and the transferred nucleons were both assumed to have been picked up from the $1p_{\frac{1}{2}}$ shell and were described by Saxon-Woods wave functions in the manner discussed in Chapter 1. The selection rules

restrict L, S and J to be zero. The absolute magnitude of the theoretical cross section is dependent on the spectroscopic amplitude and the factor D_o contained in eqn.(1.6a). In all the calculations, the spectroscopic amplitude is unity unless otherwise specified and for the Saxon-Woods formulation of the effective interaction, D_o is given the value $D_o^2 = 3 \times 10^7$ MeV^2.fm^6 (Mathur and Rook,1967). The factor N used to normalise the theoretical predictions to the experimental data is shown in the diagrams.

The agreement between theory and experiment is poor and though the inadequacies of the ^{3}He optical potential and uncertainty in the form of the effective interaction I^{eff} may be partially responsible, it is considered that an important reason for the discrepancy is due to the range of integration of eqn.(5.1) which extends from the origin to infinity. This is a problem which has been encountered in many DWBA analyses and is essentially a question of the meaning to be attached to the existence, as described by optical model wave functions, of a loosely bound particle such as the ^{3}He ion in the interior of the nucleus. Recently the subject has been studied in detail for the case of deuteron elastic scattering on ^{40}Ca where the break-up of the deuteron in the nuclear interior has been explicitly included in the calculations (Rawitscher,1968). It is more common however, to assume that optical model functions have little significance inside the nucleus and this region should therefore be excluded from the calculation by reducing the range of

the integration with a lower cut-off. The necessity of using a cut-off has been demonstrated by Rook and Mitra (1964) in their analysis of the reaction $^{40}Ca(p,t)^{42}Ca$ and indeed, the use of a lower cut-off is an integral part of Glendenning's formulation of the double stripping theory (1965). Although it would appear that there are good physical grounds for damping the contributions from the nuclear interior to the radial integral, the choice of a cut-off radius and even whether the cut-off should be sharp or smooth, is largely arbitrary, and since the shape and magnitude of the differential cross section is strongly dependent on the value of the cut-off radius, this procedure can be little more than an unsatisfactory solution to the problem. The results of zero-range calculations in which sharp cut-off radii of 4 fermis and 5 fermis were used, are shown in Figure 5.3. The ^3He potential TC was used, and similar results are obtained when the other potentials are used. The agreement with the experimental cross section is improved when the cut-off radius is greater than that of the nucleus thus supporting the physical argument for excluding the nuclear interior from the calculations. However, a more satisfactory method of damping the interior contributions must be sought.

The effective interaction I^{eff} which has been used in the calculations so far, is based on the point 'tri-nucleon' approximation in which a δ-function is used to describe the ^3He particle. The integral in eqn.(5.1) is also simplified by assuming that the interaction

has zero range. The assumption permits dr_{aA} to be written in terms of dr_{bB} and in this way the 6 dimensions of the integral are reduced to 3. Various forms of the effective interaction have been used in the literature but the zero-range approximation has invariably been a common feature. Finite-range corrections are known to be important in analyses of deuteron stripping and they should be at least as important in two nucleon transfer reactions. The point 'tri-nucleon' and zero-range approximations are both avoided in a formulation of the matrix element described by Bencze and Zimanyi (1966). Instead, Gaussian forms are used for the interaction and the tri-nucleon wave function, and the local WKB approximation is employed in the evaluation of the radial integral. The net result is that whereas in eqn.(1.5) the transferred nucleons are described by the product of two Saxon-Woods wave functions, in the finite-range formula, this product is modified by a second term and an overall multiplicative factor. The forms of the interaction and the ^{3}He wave function are given by

$$V_I = V_{b1} + V_{b2} = V\{\exp(-\beta^2\{r_b - r_1\}^2) + \exp(-\beta^2\{r_b - r_2\}^2)\}$$

and $$\psi_{J_a} = N \exp(-\tfrac{1}{2}\gamma^2\{(r_1 - r_2)^2 + (r_1 - r_b)^2 + (r_2 - r_b)^2\})$$

where N is a normalisation constant and β and γ are range parameters which are chosen to be equal. The product of the two bound state wave functions is replaced by

$$\phi_{\ell_1}(r_1)\phi_{\ell_2}(r_2) \rightarrow \exp\left(\frac{\kappa^2(R)}{12\beta^2}\right) \times \left\{\phi_{\ell_1}(R)\phi_{\ell_2}(R) - \frac{1}{24\beta^2}\left\{\frac{d\phi_1}{dR}\ \frac{d\phi_2}{dR}\right\}\right.$$

$$- \frac{\phi_1\phi_2}{24\beta^2}\ \frac{\ell_1(\ell_1+1)+\ell_2(\ell_2+1)-L(L+1)}{2R^2}$$

$$\left. + \text{higher order terms.}\right\} \qquad 5.3$$

where $R = r_{xA} = \frac{1}{2}(\bar{r}_{1A} + \bar{r}_{2A})$

and $\kappa^2(R) = \frac{2m}{\hbar^2}\left(V_p(R) - V_H(R) + 5/4\ V_1(R) + 5/4\ V_2(R) + BE/A\right)$

In this last equation V_p and V_H are the proton and ^3He optical potentials respectively and V_1 and V_2 are the Saxon-Woods potentials used to generate the bound state wave functions ϕ_{ℓ_1} and ϕ_{ℓ_2}. The quantity BE is the total binding energy of the transferred pair.

These corrections, with two simplifications, were included in the computer programme. The terms containing second and higher order derivatives were neglected since Bencze and Zimanyi indicated that these terms do not make an appreciable contribution to the total correction. A considerable increase in computing time is required if the spin-orbit terms in the proton and ^3He optical potentials are retained in the exponential multiplicative factor in eqn.(5.3). They were therefore omitted from the calculation. During the course of the development of the programme, it was found that the inclusion of the spin-orbit terms in the finite-range correction had very little effect on the final predictions and their omission is not considered to be a serious modification of

the formulation.

The results of electron scattering measurements (Collard et al.,1965) have been used to determine the following values of the size parameter β for the ^{3}He ion and triton.

$$\text{He:}\quad \beta = 0.31\ \text{fm}^{-1}$$
$$\text{t:}\quad \beta = 0.34\ \text{fm}^{-1} \qquad 5.4$$

These values are preferable to the size parameter quoted by Bencze and Zimanyi and the values used by Clendenning (1965) as these values were deduced from electron scattering measurements which Collard et al. have acknowledged to be incorrect.

The results of a calculation in which these finite-range corrections were included are shown in Figure 5.4. The ^{3}He potential TC was used. The agreement with experiment is considerably improved in comparison with the zero-range predictions shown in Figure 5.2. It is of interest to study the form of the correction term. The unmodified product of the bound state wave functions is shown in Figure 5.5 as well as the product modified by the first correction term. The real part of the exponential multiplicative factor is shown at the bottom of the diagram. It can be seen that the bound state wave function is reduced in the nuclear interior and a certain degree of cancellation is effected by the change in sign. The wave function in the interior is reduced further by the damping effect of the multiplicative factor. The improvement in the agreement between theory and

experiment is most likely due to the fact that the finite range formulation gives a better description of the reaction process than the zero-range point particle approximation. That this formulation also has the effect of reducing the contributions from the nuclear interior to the radial integral is particularly important in view of the earlier discussion on the significance of optical model wave functions in this region. This is achieved in a consistent manner and not by the arbitrary use of a radial cut-off.

One further aspect of the distorted wave calculation that was considered, was the use of non-local potentials since there are theoretical and experimental grounds for believing that the optical model potential should be non-local (Perey and Buck,1962; Preston,1962) and that the Schrodinger equation should be written as:

$$\nabla^2\phi(r) + \int V(r,r')\ \phi(r')\ dr' = E\ \phi(r).$$

The solution of this integro-differential equation is complex and it has been suggested that an equivalent local potential V_L should be used in DWBA calculations, the relation between the local and non-local potentials being

$$V_L = V_{NL} \exp\{-\mu\beta^2(E - V_L)/2\hbar^2\}$$

where β is the range of the non-locality. A simpler method is now used in DWBA analyses and makes use of a result given by Perey (1962) which indicates that the effects of using non-local potentials

can be simulated quite accurately by a factor which is applied to the wave functions generated by a local potential. This factor is

$$C\{1 - \mu\beta V_L(r)/2\hbar^2\}^{-1}$$

where β is the range of the non-locality and μ is the reduced nucleon mass. The factor C is unity except for the bound state when C is chosen to preserve the normalisation of the wave function. It is arguable whether the non-local correction can have much meaning for the ^{3}He channel when the local optical potential is so ill-defined, but the simplicity of the correction warrants some consideration to be given to the effects of applying it to the DWBA calculation as a whole.

The finite range non-local predictions shown in Figure 5.6 used non-locality ranges of 0.85 fm for nucleons and 0.22 fm for the ^{3}He ion. The label FRNL' refers to a calculation in which the non-local correction was not applied to the bound state wave functions since it has been suggested that the non-locality correction should only be applied to the scattered wave functions (Hiebert et al.,1967 and refs. therein). The shapes of the angular distributions are not very different from the results of the local calculations shown in Figure 5.4 since the damping effect of the non-local corrections is probably overshadowed by the effect of the finite-range correction. The magnitude of the cross section is reduced by about 30%. Since it is the ratio of cross

sections that is compared in nuclear spectroscopy studies with two nucleon transfer reactions, this reduction in the absolute cross section may not be significant. However, although the magnitude of the effect and the simplicity of the correction suggest that the effects should, in general, be considered in analyses of two nucleon transfer reactions, it is clear that in this analysis, the use of non-local corrections must await the proper definition of the ^{3}He optical potential.

The Gaussian 'tri-nucleon', harmonic oscillator formula for the effective interaction can now be compared with the Saxon-Woods formula which has just been illustrated. To recapitulate briefly the discussion of Chapter 1: the use of harmonic oscillator wave functions to describe the transferred nucleons, permits the relative motion and centre of mass motion of the transferred pair to be formulated exactly in contrast to the Saxon-Woods prescription in which the relative motion is ignored completely. The asymptotic region of the oscillator wave function is replaced by a hankel function so that the binding energy of the transferred pair is described correctly. The internal wave function of the ^{3}He particle has a Gaussian form with a size parameter given in eqn.(5.4). The predictions of zero-range local (ZRL) calculations in which the ^{3}He potentials TC and TMN were used, are shown in Figure 5.7. The oscillator parameter ν was chosen to be 0.32 fm^{-2} since this value has been used in shell model calculations in the p shell. The two

components of the harmonic oscillator expansion in eqn.(1.7) are shown in Figure 5.8 and also the bound state wave function which is the weighted sum of these components.

The agreement with the experimental differential cross section is poor and is insensitive to slight changes in the oscillator parameter or the application of non-local corrections to the optical potentials. A series of calculations which contain Glendenning's requirement of a lower cut-off, are shown in Figure 5.9 for the potential TG. It is apparent that large values of the cut-off radius must be used in order to obtain some measure of similarity between theory and experiment. The same conclusion is obtained when the potential THM is used in a cut-off calculation. These calculations permit an interesting comparison of the two formulations to be made. In the zero-range approximation, the Saxon-Woods and harmonic oscillator effective interactions differ only in the form of the bound state wave function in the nuclear interior since in both cases, the asymptotic form of the wave function has been determined uniquely by the binding energy of the transferred pair. Consequently, calculations in which the two different formulations are used, will be almost completely similar if a lower cut-off is used to exclude the nuclear interior. Slight differences will remain because of different radii chosen to match the asymptotic and the interior parts of the bound state wave function

in the two cases. This similarity is evident from a comparison of the predictions shown in Figure 5.3 (Saxon-Woods) and Figure 5.9 (harmonic oscillator). Calculations in which a lower cut-off has not been used, but where the nuclear interior has been effectively excluded from the calculation by very large absorption strengths in the optical potentials, display the same similarity. This effect is clearly illustrated in Figures 5.1 (Saxon-Woods) and 5.7 (harmonic oscillator) for the potential THU which has a 32 MeV absorption potential. The predictions of the two calculations are almost identical despite the considerable difference in the bound state wave functions for the two cases shown in Figure 5.5 and Figure 5.6.

A proper comparison of the two formulations should be made with calculations in which finite-range corrections have been included in both cases. These corrections cannot be made in the local WKB approximation because of the use of the infinite harmonic oscillator potential. It may be possible to calculate a finite-range correction factor if the potential is suitably modified in the same region that the oscillator wave functions are altered. The accuracy of such a method would have to be checked against the results of a full finite range calculation with the proper six dimensional radial integral. For this work, the Saxon-Woods finite-range corrected theory is preferred to the zero-range theory in either form, and the zero-range forms will be mentioned only briefly

when the remaining reactions are described.

It has been necessary to delay the consideration of spin-orbit effects, and the comparison of DWBA predictions with the experimental polarization analysing powers, until the cross section predictions and the two theories had been closely examined. The theoretical analysing powers shown in the diagrams are entirely due to the presence of the spin-orbit term in the proton optical potential. The analysing power predictions do not compare favourably with the data except, possibly, in those cases where the nuclear interior is excluded from the calculation. The only calculations which give an acceptable account of both differential cross section and analysing power, are the finite-range predictions shown in Figure 5.4 and Figure 5.6. The patterns of the analysing powers have roughly the correct shape but are shifted towards negative values. This disagreement may be due to the absence of a spin-orbit term in the ^{3}He optical potential, and with no elastic scattering or polarization data available there is no alternative to an arbitrary addition of a spin-orbit term to the potential. Since the potential TG has been constructed from nucleon optical potentials, it is consistent to use this potential for the addition of a spin-orbit term. The three nucleons in the ^{3}He ion are coupled to spin-$\frac{1}{2}$, and an immediate conclusion is that the spin-orbit strengths of the ^{3}He ion and the spin-$\frac{1}{2}$ nucleon should be approximately equivalent. A theoretical calculation by Frahn and

Wiechers (1965) supports this conclusion. The predictions shown in Figure 5.10, are finite-range local calculations in which the potential TG has been extended to include a spin-orbit term with the geometrical parameters r_s = 1.1 fm and a_s = 0.65 fm, and with strengths between 4 and 10 MeV. In these calculations, the proton spin-orbit potential has been set to zero so that the theoretical analysing powers are, again, the consequence of spin-orbit coupling in one channel only. In Figure 5.11, the calculations contain spin-orbit coupling in both channels.

As expected, the shape and magnitude of the angular distribution is not very sensitive to the strength of the spin-orbit term, while the effect on the analysing powers is to raise the pattern to more positive values although the forward angle data is not well accounted for. The calculations show that the spin-orbit strength saturates at values greater than about 8 MeV and that the best agreement between theory and experiment corresponds to a ^{3}He spin-orbit strength of 4MeV to 6 MeV which is indeed equivalent to the strength of the nucleon spin-orbit potential. For the sake of comparison, a series of calculations is shown in Figure 5.12 for the case of the harmonic oscillator formulation and spin-orbit coupling in the ^{3}He channel only. Lower cut-offs between 3 fm and 5 fm were used.

It has not been possible to obtain detailed agreement between

theoretical and experimental analysing powers in these calculations. At best, the agreement is broad in that the main peak in the pattern at 60° is roughly reproduced. The lack of detailed agreement does not permit a realistic assessment of the two formulations to be made in terms of their ability to predict experimental analysing powers, but it does appear that the fit to the data when the harmonic oscillator formulation is used, is not as good as when the finite-range Saxon-Woods formulation is used. This is, perhaps, to be expected, since the finite-range calculation is a more sophisticated description of the process.

The reasons for the discrepancies are not clear. Distorted wave predictions of polarization phenomena in single nucleon transfer reactions have not been in good agreement with observation, and although this problem has been examined (eg. Chant and Nelson, 1968) it has not been solved. The two nucleon transfer process is much more complex, and the greater uncertainty with respect to the optical model potentials may be an important factor in the lack of detailed agreement. However, in view of the difficulties experienced in analyses of single nucleon transfer, there may be a more fundamental reason. The analysing powers are sensitive to changes in the form of the effective interaction, and a more detailed study of other formulations of the interaction may lead to a better fit to the data. It is important, however, to note that some agreement does exist with the finite-range corrected theory.

The effects of non-local corrections on the analysing powers are shown in Figure 5.13. The label FRNL' indicates that the correction was not applied to the bound state wave function. The ^{3}He spin-orbit potential was 4 MeV. The analysing power, like the differential cross section, is not very sensitive to these additional corrections and this is doubtless for the same reason given earlier. It is not possible to place any emphasis on the non-local calculations or assess their importance until the local ^{3}He optical potential is defined with greater precision.

The discussion of this reaction concludes with the consideration of the coherent sum over the configurations of the transferred nucleons as expressed in eqn.(1.3). The calculations have so far been based on a $(1p_{\frac{1}{2}})^2$ pick-up configuration, so that the coherent sum has contained only one term and the analysis has been simplified as a result. However, the $(1p_{3/2})^2$ configuration is also allowed since the ground state of ^{16}O is known to contain particle-hole excitations, (Brown and Green,1965). Spectroscopic amplitudes have been calculated on the basis of the wave functions of Cohen and Kurath for $(1p_{\frac{1}{2}})^2$ and $(1p_{3/2})^2$ pick-up, and they are, respectively, -1.584 and -0.702 (Towner,1968). A finite-range local calculation, which contains the coherent sum, is compared in Figure 5.14 with a similar calculation which neglects the $(1p_{3/2})^2$ component. The ^{3}He potential TC was used with a 4MeV spin-orbit potential. The presence of the $(1p_{3/2})^2$ component in

the coherent sum does not significantly affect the shape of the angular distribution or the polarization analysing powers, although the extreme forward angle differential cross section predictions are improved. The p shell was chosen for the initial study of these reactions in anticipation of this result. The coherent sum can contain only one term if the spin-orbit force in the bound state is removed, since in that case the wave functions describing $1p_{\frac{1}{2}}$ and $1p_{3/2}$ states will be identical. Even when a spin-orbit potential of approximately 6 MeV is present in these calculations, the potential wells for the $1p_{\frac{1}{2}}$ and $1p_{3/2}$ particles are not so different that the resultant wave functions lose their basic similarity. The coherent sum of the configurations is expected to be important only when two shells are involved in the nucleon transfer, or when the cross sections of reactions leading to different states in the residual nucleus are being compared.

iii) The reaction $^{16}O(p,t)^{14}O$ (ground state)

The charge independence theory of nuclear forces can be tested by a comparison of reactions which populate mirror final states from the same initial state, with the proviso that the particular reactions should be free from compound nucleus interference. Examples of two such reactions are the $^{16}O(p,t)^{14}O$ ground state (T = 1) reaction and the $^{16}O(p,^{3}He)^{14}N$ 2.311 MeV (T = 1) reaction, which have been studied at 43.7 MeV (Cerny and Pehl,1964) and at 50 MEV (the present work). The relation between the differential cross sections of the

two reactions can be obtained from eqn.(1.9) and eqn.(1.10), which define the differential cross section. Thus:

$$\frac{d\sigma}{d\omega}_{p,t} = \frac{d\sigma}{d\omega}_{p,^3He} \times \frac{k_t}{k_{^3He}} \times \frac{b_s^2(^3He)}{b_s^2(s)} \times \frac{|\Sigma\, SF^{\frac{1}{2}}\, \beta_{^3He}|^2}{|\Sigma\, SF^{\frac{1}{2}}\, \beta_t|^2}$$

$$= 1.90 \times \frac{d\sigma}{d\omega}_{p,^3He}$$

Differences in coulomb energies have been ignored in the cancellation of the transition amplitudes. The $(p,^3He)$ differential cross section, multiplied by the factor 1.90, is compared with the (p,t) cross section in Figure 5.15. The very good agreement between the two cross sections supports the assumption that the interaction responsible for the transition is charge independent, and this confirms the findings of Cerny and Pehl at 43.7 MeV. In this present work, additional confirmation of charge independence is provided by the comparison of polarisation analysing powers. The analysing powers of the two reactions, which are defined by eqn.(2.3), should be identical, provided again, that coulomb differences in the transition amplitudes are neglected. The (p,t) and $(p,^3He)$ analysing powers are shown in Figure 5.16 and it can be seen that, within experimental errors, this identity is confirmed. This identity, reported here for the first time for two nucleon transfer reactions, demonstrates how the measurement of polarization phenomena can assist the search for the components of isobaric spin multiplets.

The considerable difference in the r.m.s. radii of the triton and the ^{3}He ion led Mathur and Rook (1967) to examine the validity of the cancellation of the transition amplitudes. They showed that the use of Gaussian wave functions to describe the triton and ^{3}He ion is incorrect, and that the wave functions of the particles must have mixed symmetry. This requirement enormously complicates the present analysis and it will not be considered. The general use of the convenient Gaussian form in this context is a contributory factor to the uncertainty in the absolute magnitude of the theoretical cross section.

The equivalence of the differential cross sections, and the analysing powers of the two reactions, permit the discussion of the last section on the (p,^{3}He) reaction to be applied without exception to the ^{16}O(p,t)^{14}O ground state reaction. Distorted wave calculations for the two cases are not identical because of kinematic differences, but the dissimilarity is so slight as to be negligible for the purposes of the present analysis.

iv) The reactions ^{12}C(p,t)^{10}C (ground state and 3.34 MeV)

Elastic scattering data cannot be obtained for a ^{10}C target, and since triton elastic scattering data does not exist for neighbouring targets at the relevant energy, ^{3}He elastic scattering data will be used as was mentioned earlier. The beryllium isotopes have been the subject of ^{3}He scattering analyses at 31 MeV but the

resultant shallow potentials, which range in depth from 13 to 70 MeV, are not considered to be satisfactory for use in DWBA calculations (Hodgson,1968). The deepest of these potentials is labelled TW in Table 5. Several analyses of ^{3}He - ^{12}C elastic scattering have been reported (Sen Gupta et al.,1964; Hodgson,1968), but none of the potentials is deeper than 80 MeV. In one case, the cross sections have been tabulated (Baugh et al.,1967), and this data has been used in an analysis made in terms of deeper optical potentials.

The starting parameters used by Baugh et al. invariably caused the optical model search code used in the present work to produce a shallow potential and for this reason the geometrical parameters were replaced by

$$r_o = 1.14 \text{ fm}, \quad a_o = 0.72 \text{ fm}, \quad r_V = 1.6 \text{ fm}, \quad a_V = 0.81 \text{ fm}$$

and the starting value of the well depth was increased from 100 MeV to 150 MeV. A six parameter search of a more elaborate nature than that of Baugh et al. was used in which the spin-orbit and surface absorption potentials were zero. The result of one of these searches is listed in Table 5 with the label CN together with the published potential of Baugh et al. which is labelled TB. The quantity Δ is a measure of the goodness-of-fit and is defined by

$$\Delta = \frac{1}{N} \Sigma \frac{\{\sigma_{th}(\theta_i) - \sigma_{exp}(\theta_i)\}^2}{\{\delta(\theta_i)\}^2}$$

where N is the number of experimental points, $\sigma_{th}(\theta)$ and $\sigma_{exp}(\theta)$

are the theoretical and experimental differential cross sections respectively and $\delta(\theta)$ are the experimental errors. The summation is from i = 1 to N.

Table 5.

^{3}He optical potentials.

	Tgt	En.	V_o	r_o	a_o	W_V	r_V	a_V	V_s^*	r_c	Δ
TW	^{9}Be	31	69.5	1.18	0.76	20.3†	1.18	0.76	0	1.18	-
TB	^{12}C	29	76.6	1.05	0.88	16.61	1.78	0.74	0	1.06	7.12
CN	^{12}C	29	138.6	1.11	0.71	23.71	1.38	0.97	0	1.3	4.15
CN5	^{12}C	29	130.2	1.15	0.69	24.27	1.35	0.98	5	1.3	3.27
CN10	^{12}C	29	125.0	1.20	0.65	24.02	1.37	0.96	10	1.3	1.26
CN15	^{12}C	29	135.9	1.12	0.69	20.93	1.57	0.83	15	1.3	2.53

† Surface absorption * $r_s = r_o$, $a_s = a_o$.

All energies are in MeV and lengths in fermis.

It is interesting to note that the deeper potential CN provides a better fit to the data than the shallow potential TB. The spin-orbit potential could not be examined directly since only cross section data were available, but various spin-dependent potentials were obtained from a series of calculations in which the spin-orbit strength was held fixed at values between 5 and 15 MeV while the remaining parameters were adjusted to minimise Δ. These potentials are labelled CN5, CN10, and CN15 in Table 5. The fit to the data shows an improvement when the spin-orbit term is added to the optical potential with a minimum in Δ corresponding

to a spin-orbit strength of 10 MeV. Without the proper polarization measurements however, it is not possible to differentiate with certainty between an improvement which is due to a more complete description of the relevant optical potential, or which is just a consequence of using more parameters to describe a particular situation. The re-analysis of the Baugh data was not extended beyond proving the existence of a more appropriate family of deeper potentials because the intended use of ^{3}He - ^{12}C potentials to describe the t - ^{10}C channel, though justified in the circumstances, is not strictly correct and further investigation of the ^{12}C data was not considered to be warranted.

The angular momentum transfers for the $^{12}C(p,t)^{10}C$ ground state reaction are L = S = J = 0. The transferred neutrons were assumed to have been bound in $(1p_{3/2})$ orbits. Zero-range DWBA predictions with the Saxon-Woods or harmonic oscillator formulations of the effective interaction and the potentials in Table 5 and Table 3, displayed the same lack of structure in the differential cross section as did similar calculations for the $^{16}O(p,^{3}He)^{14}N$ (2.311 MeV) reaction. Calculations with a lower cut-off improved the agreement between theoretical and experimental cross sections in both cases, but for the reasons already given, this procedure is thought to be inferior to the use of finite-range corrections. The results of finite-range local (FRL) calculations with the Saxon-Woods effective interaction are shown

in Figure 5.17 for the spin-independent potentials TW, TB and CN.

These predictions are typical of finite-range calculations using deep and shallow potentials, with the 35° peak being better defined with the deeper potential. The wider angle predictions are all smaller than the experimental data and this discrepancy could not be accounted for by using potentials deeper or shallower than those listed in Table 5. The use of spin-dependent potentials does not improve the fit as can be seen from the predictions shown in Figure 5.18. A slightly different method of normalisation is used in this diagram. Indeed, the agreement deteriorates when the spin-orbit strength exceeds 5 MeV. The theory is also unable to account for the observed polarization analysing powers even when zero-range cut-off calculations are used, and it is not possible to determine from the calculations whether it is necessary to have a spin-orbit term in the "triton" optical potential at all. The effects of non-local corrections are shown in Figure 5.19 where the label FRNL' indicates that the correction was not applied to the bound state. The spin-dependent potential CN5 was used in these two calculations. The differential cross section and the analysing power are practically unaltered when the non-locality correction is confined to the incident and exit channels. The effects of the correction are more pronounced, especially for the analysing power, when applied to the bound state as well although the overall agreement is only slightly improved. The basic discrepancies

however, are such that it is not possible to determine whether the non-local corrections are necessary or not. The contribution to the reaction of the $(1p_{\frac{1}{2}})^2$ pick-up configuration amounts to less than 14% and its omission from the calculations was found not to be important.

The optical potentials of Table 5 will be used without modification in calculations describing the reaction leading to the first excited state of ^{10}C which has $J^\pi = 2^+$. The angular momentum transfers are $L = J = 2$ and $S = 0$. Since the spectroscopic amplitude for $(1p_{\frac{1}{2}}\ 1p_{3/2})_{J=2}$ pick-up is only 0.003 compared with -1.909 for the pick-up configuration $(1p_{3/2})^2$, the former contribution will be ignored. Zero-range calculations with the Saxon-Woods or harmonic oscillator formulations were again unable to account for the experimental observations, and the calculations were repeated with finite-range corrections and the CN potentials. The results are shown in Figure 5.20. The agreement between theory and experiment is fair and is better in this case than for the ground state reaction. The pattern of the analysing powers is only broadly reproduced although, again, the discrepancies are not as marked as they are for the ground state predictions. In fact it is possible to estimate from the analysing power predictions that the strength of the "triton" spin-orbit potential should be at least 5 MeV. Non-local corrections do not affect the theoretical predictions to any noticeable extent.

An unsatisfactory, but unavoidable, feature of the analysis of these two reactions is the use of ^{3}He - ^{12}C optical potentials to describe the t - ^{10}C channel. The optical model is generally more successful with heavier nuclei and so the light nuclei involved in this reaction make the procedure all the more uncertain. The ^{3}He potential derived from the analysis of the Baugh data can be questioned, in any case. At angles greater than 65°, the form of the elastic cross section departs from the usual oscillatory behaviour. This portion of the data was ignored in both the Baugh analysis and the present analysis, but the unexplained behaviour of the data suggests interference from compound elastic processes and this may cast doubt on the results of the optical model search. The proton optical potential is also probably not defined with complete certainty in view of the difficulties and ambiguities revealed in Satchler's analysis at 46 MeV.

Similar difficulties in DWBA analyses in this mass region have been encountered before, for example in the analysis of the $^{12}C(p,d)^{11}C$ reaction at 30 MeV (Chant et al.,1967) and the $^{12}C(^{3}He,p)^{14}N$ reaction at 20 MeV (Mangelson et al.,1968) where ^{3}He - ^{12}C potentials derived from optical model analyses had to be discarded in favour of artificially constructed potentials.

It is concluded that the disagreement exhibited in the present analysis is due to an incomplete description of the distorted waves in both channels.

v) The reaction $^{28}Si(p,t)^{26}Si$ (ground state)

The primary reason for studying the polarisation analysing powers of this reaction, was to examine, by comparison between observation and theory, the sensitivity of the DWBA analysing power predictions to the signs of the components in the sum over the possible configurations of the transferred nucleons. Since these signs are dependent on the phases of the components of the nuclear wave functions, any sensitivity exhibited by the theory in this respect can be used to test the construction of such wave functions. The proximity of the $2s_{\frac{1}{2}}$ and $1d_{5/2}$ shells suggests that it is unlikely that the configuration of the transferred nucleons in this reaction will be only $(1d_{5/2})^2$. The ground state of ^{28}Si is known to contain a 40% to 50% admixture of 2 particle 2 hole states in the form $(2s_{\frac{1}{2}}^2\ 1d_{5/2}^{-2})$ (eg. Wildenthal and Glaudermans,1967), and it is therefore important to cater for this configuration mixing in the DWBA calculations. Information about the configuration mixing and the signs of the components of the nuclear wave functions can be obtained from a comparison of cross sections of reactions leading to different levels in the residual nucleus (Hardy and Towner,1967a), but when only one reaction is considered, the extraction of this information is dependent on an accurate prediction of the absolute magnitude of the differential cross section. Such a prediction cannot yet be made and it is of interest to discover whether the study of

polarization phenomena can be of some value in this context.

The required spin-dependent triton optical potentials do not exist and once again it is necessary to make use of ^{3}He elastic scattering data. The ^{3}He - ^{27}Al cross section data of Baugh et al., were re-analysed in terms of deeper optical potentials which included a spin-orbit term. The general search procedure was the same as that used for the analysis, described earlier, of the ^{3}He - ^{12}C data. The results of these searches are listed in Table 6 with the labels SN, SN5 etc., together with the published potential of Baugh et al., which is labelled SB. The deeper potential, as in the ^{3}He - ^{12}C case, provides a better fit to the data than the original 99.6 MeV potential. The introduction of a 15 MeV spin-orbit strength appears to have forced the search code to make considerable compensatory adjustments to the real central potential and this result will be discarded.

Table 6.

^{3}He optical potentials.

	Tgt.	En.	V_o	r_o	a_o	W_v	r_v	a_v	V_s*	r_c	A
SB	^{27}Al	29	99.6	1.07	0.85	14.53	1.81	0.69	0	1.07	6.51
SN	^{27}Al	29	164.8	1.03	0.76	29.77	1.52	0.81	0	1.3	4.54
SN5	^{27}Al	29	169.2	0.94	0.81	22.82	1.62	0.79	5	1.3	4.08
SN10	^{27}Al	29	158.9	1.01	0.78	19.31	1.66	0.79	10	1.3	3.83
SN15	^{27}Al	29	138.0	1.05	0.79	24.52	1.57	0.80	15	1.3	4.12

* $r_s = r_o$, $a_s = a_o$. All energies are in MeV and lengths in fermis.

Finite-range local (FRL) calculations with the Saxon-Woods formulation of the effective interaction are shown in Figure 5.21. The proton potential is given in Table 3 and the triton potentials are those of Table 6. The pick-up configuration is taken to be $(1d_{5/2})^2$. The theoretical analysing powers are notable for their insensitivity to the strength of the triton spin-orbit potential. The agreement with the data is fair in that the main peak in the experimental pattern at 50° is approximately reproduced although the subsidiary peak is overemphasized by the calculation. The cross section is also fairly well accounted for by the theory except when the shallow potential SB is used.

The analysis is now extended to include the possibility of pick-up from the $2s_{\frac{1}{2}}$ shell. Extensive modifications to an existing shell model programme are required before the appropriate spectroscopic amplitudes can be extracted and to perform the present calculations some simplifications must be made. The ^{28}Si ground state wave function will be written as:

$$|^{28}\mathrm{Si}\rangle = a|0\rangle + b|2s_{\frac{1}{2}}^{2}\ 1d_{5/2}^{-2}\rangle$$

where $|0\rangle$ represents the closed $1d_{5/2}$ shell configuration. The ^{26}Si ground state wave function will be assumed to be simply $|1d_{5/2}^{-2}\rangle$.

Two finite-range calculations are shown in Figure 5.22 which illustrate the effects of changing the signs of a and b in the

nuclear wave function. The calculation S1 was performed with a = b, while in the calculation S2 a = -b. The two calculations cannot be distinguished with certainty from the differences in the shapes of the two angular distributions. The absolute magnitudes of the cross sections are different, but the inaccuracy of the absolute cross section predictions of the theory implies that this difference cannot be exploited to determine the correct sign of the ratio a/b. The difference between the two polarization analysing powers, however, is considerable and this suggests that a polarization or asymmetry measurement in a single reaction can be used to check the relative signs of components of nuclear wave functions in situations where theoretical predictions of absolute cross sections cannot be made. This calculation will be repeated when the correct spectroscopic amplitudes are available and the wider applicability of an asymmetry measurement to this particular study of nuclear spectroscopy will be examined in greater detail.

vi) The reaction $^{16}O(p,^{3}He)^{14}N$ (ground state)

This reaction is typical of a situation which is not found in studies of single nucleon transfer but is common in two nucleon transfer processes, and that is the simultaneous occurrence in the reaction process of more than one angular momentum transfer. In this case, the selection rules restrict the angular momentum transfers

to S = J = 1 and L = 0 and 2. The usual spin-independent DWBA theory does not permit any interference between reaction amplitudes with different L value, in contrast to the spin-dependent theory where such interference is possible. The analyses that have preceded this section have demonstrated the necessity of using a spin-dependent theory in order to account for the existence of non-zero polarization analysing powers, and now in this section, the effects of this interference will be considered. The proton potential PPO of Table 3 and the ^{3}He potential TC of Table 5 will be used in the calculations which are based on the Saxon-Woods formulation of the effective interaction.

Before the effects of spin-orbit coupling are examined, the predictions of spin-independent theory will be considered. The non-zero polarization analysing powers observed in this reaction do not necessarily require the addition of spin-orbit coupling in the entrance and exit channels. It was shown in Chapter 2 that for these particular angular momentum transfers, the maximum analysing power permitted in the absence of spin-orbit forces is

$$P_o = 0 \quad \text{for } L = 0,$$

$$\text{and } |P_2| \leq 1 \quad \text{for } L = 2,$$

and therefore, provided that these two components appear simultaneously in a spin-independent calculation, the theoretical analysing powers will be non-zero.

A $(1p_{\frac{1}{2}})^2$ pick-up configuration was used in the finite-range spin-independent calculations shown in Figure 5.23 for the separate cases of L = 0 and L = 2 transfer. The squares of the spectroscopic amplitudes for the two cases, weighted by the relevant angular momentum coupling factors, are 0.317 and 2.54 for L = 0 and L = 2 respectively. Consequently, the L = 0 transition amplitude will not have a significant effect on a calculation of the differential cross section in which the L = 0 and L = 2 amplitudes are summed. This is confirmed by the differential cross section, marked IC in Figure 5.23, which was calculated after the two amplitudes had been incoherently summed. The agreement with the experimental differential cross section is fair, but is dependent, as proved by preliminary calculations, on the use of finite-range corrections. The analysing powers are only marginally affected by the presence of the L = 0 component, and the discrepancies between theory and data may be due to the absence of spin-orbit coupling in the optical potentials.

The calculations were repeated with the spin-orbit strengths in the proton and ^{3}He optical model potentials fixed at 5.48 MeV and 4 MeV respectively. The separate L = 0 and L = 2 calculations are shown in Figure 5.24 together with the results of a calculation in which the two amplitudes were incoherently summed. Once again, the 'summed' cross section is comparatively insensitive to the presence of the L = 0 component in contrast to the polarization

analysing power, Marked IC in Figure 5.24, where the L = 0 component does modify the pure L = 2 analysing power predictions. A comparison between the sets of calculations with and without spin-orbit coupling, and the experimental data, shows that the shape of the angular distribution has been modified by the addition of spin-orbit coupling but remains in reasonable agreement with the data. The magnitude of the summed cross section, however, has been increased by about 50%. The magnitude of the L = 2 cross section has been altered while the L = 0 cross section has remained virtually unchanged by the spin-orbit coupling. This result may explain the discrepancies in the comparison of relative cross sections calculated without spin-orbit coupling (Fleming et al., 1968a). This is not an interference effect between reaction amplitudes with different L values, because this possibility has been excluded by the use of an incoherent sum, but is due directly to the sensitivity of the L = 2 amplitude to the presence of spin-orbit coupling.

The interference between amplitudes with different L values depends on the strength of the spin-orbit coupling in the entrance and exit channels and disappears altogether when the spin-orbit forces are removed. The importance of the interference term can be estimated by a comparison of calculations in which the L = 0 and L = 2 amplitudes are summed incoherently (no interference term) and coherently (interference term present). The differences

between the cross sections calculated in these two ways are so small that it is not possible to illustrate them graphically. This result is most likely due to the dominance of the L = 2 component in the reaction process. The analysing powers calculated after a coherent sum are shown in Figure 5.24 with the label C. The basic pattern is only slightly altered by the presence of the interference term in the calculation. The predictions have the correct overall shape although the pattern appears to be 'out of phase' with the data. This disagreement cannot be corrected by alterations to the strength of the ^{3}He spin-orbit coupling.

The $(1p_{3/2})^2$ and $(1p_{\frac{1}{2}}\ 1p_{3/2})$ pick-up configurations have not been considered as preliminary calculations showed that these additional terms in the configuration sum did not have a significant affect on the predictions. It is apparent from this discussion that the importance of the interference between amplitudes with different L value, is negligible for this particular reaction. However, the analysis has revealed from the effects on the magnitude of the differential cross section that the spin-orbit coupling cannot lightly be ignored. This suggests that the use of spin-independent theory in analyses of two nucleon transfer reactions where more than one amplitude can appear, may be incorrect.

vii) Summary and conclusions.

The experimental study of polarization phenomena in two nucleon transfer reactions has been the principal objective of this research. It was undertaken so that an examination of the effects of spin-orbit coupling could be made in terms of two frequently used zero-range DWBA theories of the transfer process. Such an examination was considered to be appropriate in view of the widespread neglect of these effects in reaction analyses. An experimental technique was described whereby asymmetry measurements in double pick-up reactions could be made utilising an incident beam of polarised protons. The subsequent observation of non-zero polarization analysing powers in carefully selected reactions underlined the necessity of incorporating spin-orbit coupling in the formulation of the DWBA theory. An existing zero-range spin-dependent deuteron stripping code was re-written to permit calculations to be made for the case of two nucleon transfer reactions as described by the point 'tri-nucleon' Saxon-Woods approximation or the Gaussian 'tri-nucleon' harmonic oscillator approximation. The theoretical analysis was hampered by the lack of suitable triton and ^{3}He optical model potentials, but, nevertheless, several features emerge from the calculations that have been described.

Theoretical predictions based on either the Saxon-Woods or

harmonic oscillator formulation of the effective interaction, are in substantial disagreement with experimental data if the zero-range approximation is introduced to simplify the numerical calculations. The disadvantages of this simplification can be mitigated by the appropriate choice of a lower radial cut-off, and in all these analyses, if the range of the radial integral is restricted in this way, then the agreement between theory and experiment is considerably improved. Although this procedure is frequently adopted in reported analyses, it is felt that the usefulness of the theory must be limited if the success of its application to experimental data is dependent on the arbitrarily chosen value of a parameter which profoundly affects the theoretical predictions. A method of performing finite-range corrected calculations has been examined and the success of this method has been amply demonstrated in these analyses. It is clear that finite-range corrections are important in two nucleon transfer theory, and, in this work, these corrections have been shown to be essential if the theory is to account for experimental observations of the differential cross section without the unsatisfactory dependence on the range of the radial integral. These corrections, however, cannot be applied in their present form when the infinite harmonic oscillator potential is used to generate the bound state wave functions, and it is not possible, therefore, to make a meaningful comparison between the Saxon-Woods

and harmonic oscillator formulations of the effective interaction.

The predictions of the finite-range theory are in reasonable agreement with the experimental differential cross sections provided that the depth of the real central part of the triton or ^{3}He optical model potential is roughly equivalent to three times the corresponding part of the nucleon optical potential. Two optical model analyses of elastic scattering data have been described which demonstrate that such potentials give a better description of the relevant elastic scattering than shallower potentials. These results are encouraging since the deep potentials are physically more acceptable. The addition of a spin-orbit term to the definition of the optical potential is necessary in order to account for the non-zero polarization analysing powers. The DWBA analyses indicate that the spin-orbit potential of the tri-nucleon should be less than 10 MeV, and also that for reactions in which the spin transfer S = 0, the cross section predictions are only minimally affected by the presence of the spin-orbit terms. The immediate outcome of these results is that spin-independent theories can be used safely when the orbital and spin angular momentum transfers are restricted to unique values. When this condition is not satisfied, the use of spin-independent theories should be carefully justified. The analysis of the $^{16}O(p,^{3}He)^{14}N$ ground state reaction tends to suggest that this justification may not be possible. Although the attempt to

estimate the importance of the interference of different L values in this reaction is inconclusive due to the dominance of one L value, the sensitivity, in this case, of the cross section to the addition of spin-orbit coupling suggests that the use of spin-independent theories in circumstances where such interference can arise, is incorrect.

The theoretical and experimental polarization analysing powers are only in broad agreement, and in the case of the $^{12}C(p,t)^{10}C$ ground state reaction, the agreement is poor. The reasons for this lack of detailed agreement are not known. The absence of detailed agreement observed in analyses of (d,p) and (p,d) reactions may point to deficiencies in the DWBA description of the reaction process. This point cannot be examined in detail for the (p,t) and (p,^{3}He) reactions described here until the triton and ^{3}He optical model potentials are accurately defined.

The problem of this definition is serious. Analyses of elastic scattering data only define the optical model wave function in the asymptotic region whereas the DWBA calculations are very sensitive to the form of the wave function in the nuclear interior. Many workers have found potentials derived from proper optical model analyses to be unsatisfactory when used in DWBA analyses. This fact has, on occasion, led to the artificial construction

of optical potentials, and, in one case, triton parameters have been generated by a DWBA search of (p,t) reaction data after conventional elastic scattering potentials had been entirely discarded. It would appear that some compromise must be reached between the two extremes in order to obtain a comprehensive definition of the potential.

A further important problem in two nucleon transfer theory is the definition of the bound state wave function. The use of Saxon-Woods potentials to generate the wave functions is attractive because finite-range corrections can be made to the calculations. The harmonic oscillator formulation has the opposite characteristics. Other methods of describing the transferred particles are much more complex than the two which have been considered here. Since, in general, the differential cross sections are adequately defined by the simpler formulations, albeit with the use of cut-offs, these methods have not been thoroughly examined. This new asymmetry data will allow the more sophisticated formulations to be studied in detail and it is possible that a better agreement between theory and data will be a result. These methods are to be investigated in the future.

In conclusion, the observation of polarization phenomena in two nucleon transfer reactions has confirmed the presence of spin-orbit forces and the necessity of accounting for this fact in certain circumstances.

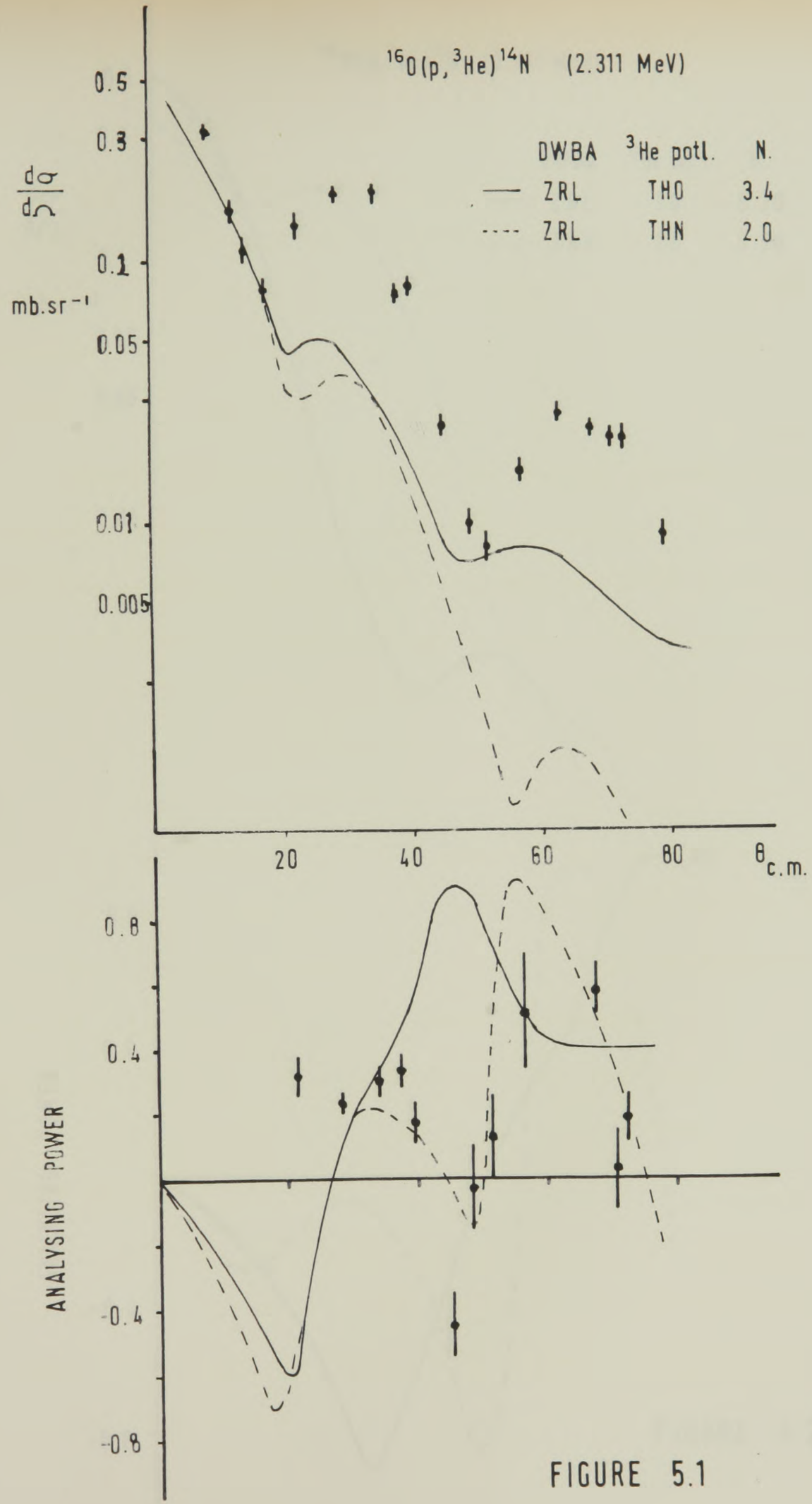

$^{16}O(p,^3He)^{14}N$ (2.311 MeV)
DWBA ³He potl. N.
ZRL THO 3.4
ZRL THN 2.0
$\frac{d}{d\Omega}\sigma$
mb.sr⁻¹
0.5
0.3
0.1
0.05
0.01
0.005
20
40
60
80
θc.m.
0.8
0.4
-0.4
-0.8
ANALYSING POWER

FIGURE 5.1

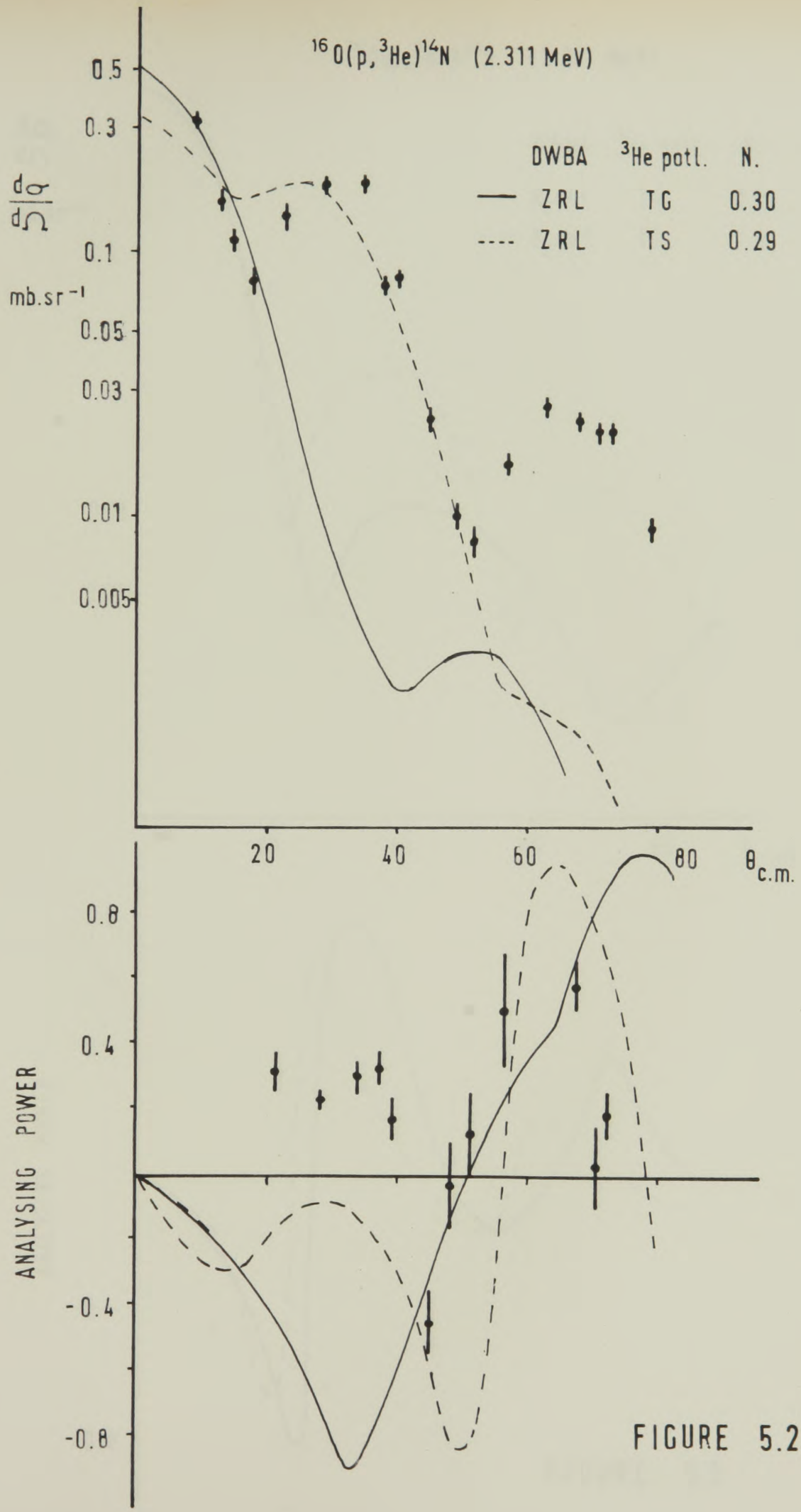

$^{16}O(p,^3He)^{14}N$ (2.311 MeV)
DWBA ³He potl. N.
ZRL TG 0.30
ZRL TS 0.29
$\frac{d\sigma}{d\Omega}$
mb.sr⁻¹
0.5
0.3
0.1
0.05
0.03
0.01
0.005
20
40
60
80
$\theta_{c.m.}$
ANALYSING POWER
0.8
0.4
-0.4
-0.8

FIGURE 5.2

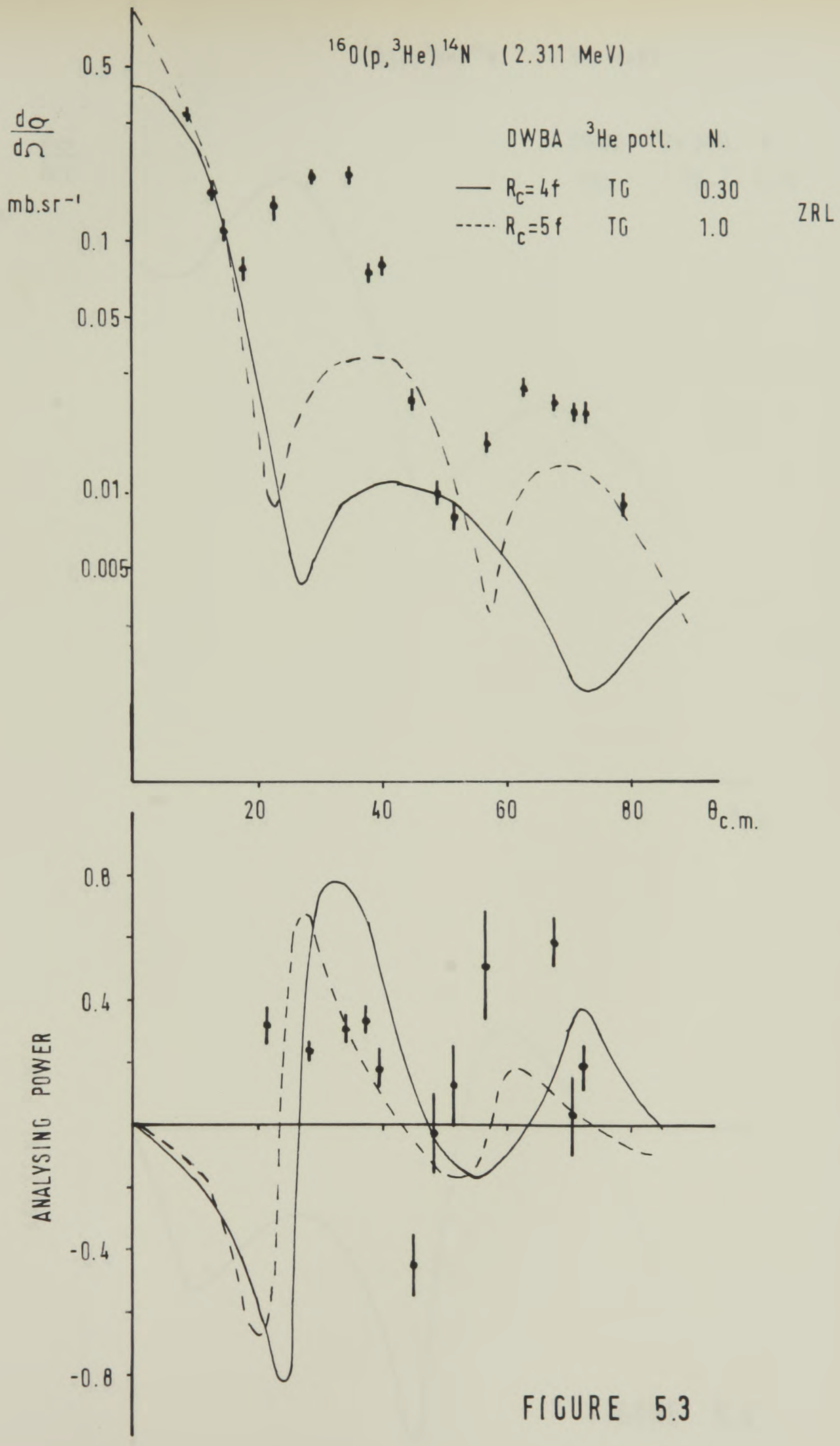

$^{16}O(p,^3He)^{14}N$ (2.311 MeV)
DWBA ³He potl. N.
R_c=4f TG 0.30
R_c=5f TG 1.0
ZRL
$\frac{d\sigma}{d\Omega}$
mb.sr⁻¹
0.5
0.1
0.05
0.01
0.005
20
40
60
80
$\theta_{c.m.}$
ANALYSING POWER
0.8
0.4
-0.4
-0.8

FIGURE 5.3

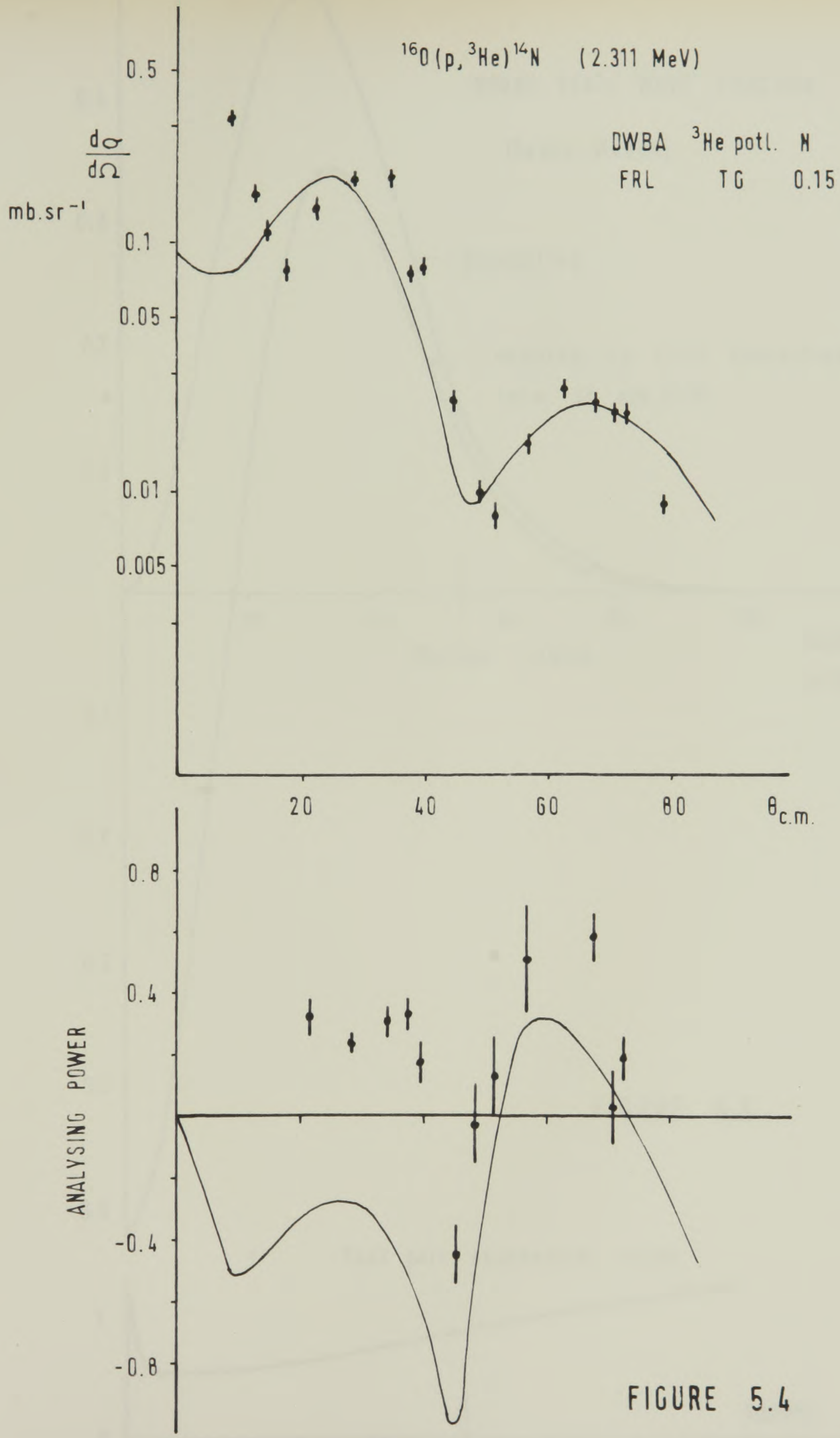

$^{16}O(p,{}^{3}He)^{14}N$ (2.311 MeV)
DWBA ^{3}He potl. N
FRL TG 0.15
$\frac{d\sigma}{d\Omega}$
mb.sr^{-1}
0.5
0.1
0.05
0.01
0.005
20
40
60
80
$\theta_{c.m.}$
ANALYSING POWER
0.8
0.4
-0.4
-0.8

FIGURE 5.4

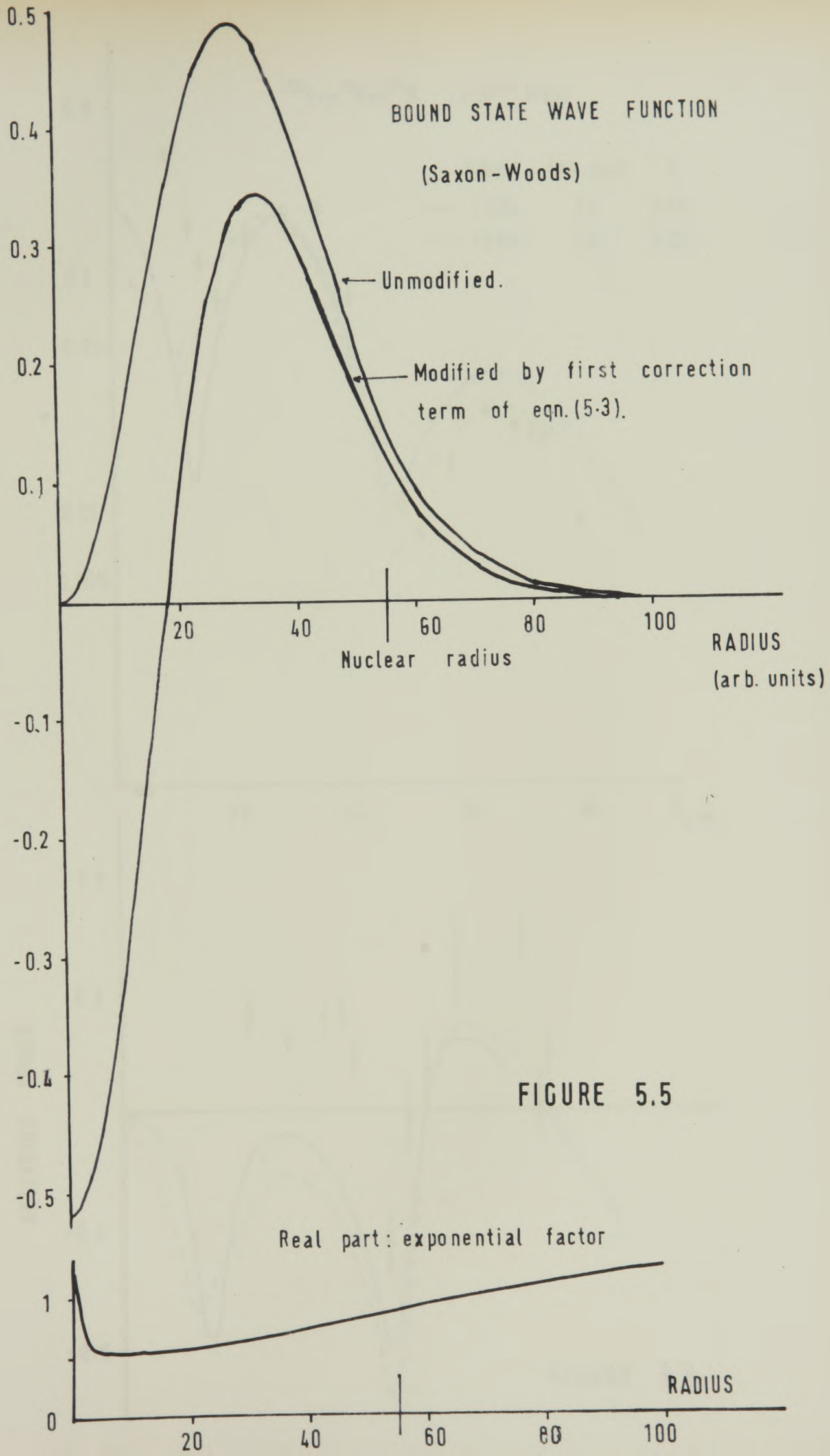

BOUND STATE WAVE FUNCTION
(Saxon-Woods)
Unmodified.
Modified by first correction term of eqn.(5·3).
0.5
0.4
0.3
0.2
0.1
-0.1
-0.2
-0.3
-0.4
-0.5
20
40
60
80
100
Nuclear radius
RADIUS
(arb. units)
Real part: exponential factor
1
0
20
40
60
80
100
RADIUS

FIGURE 5.5

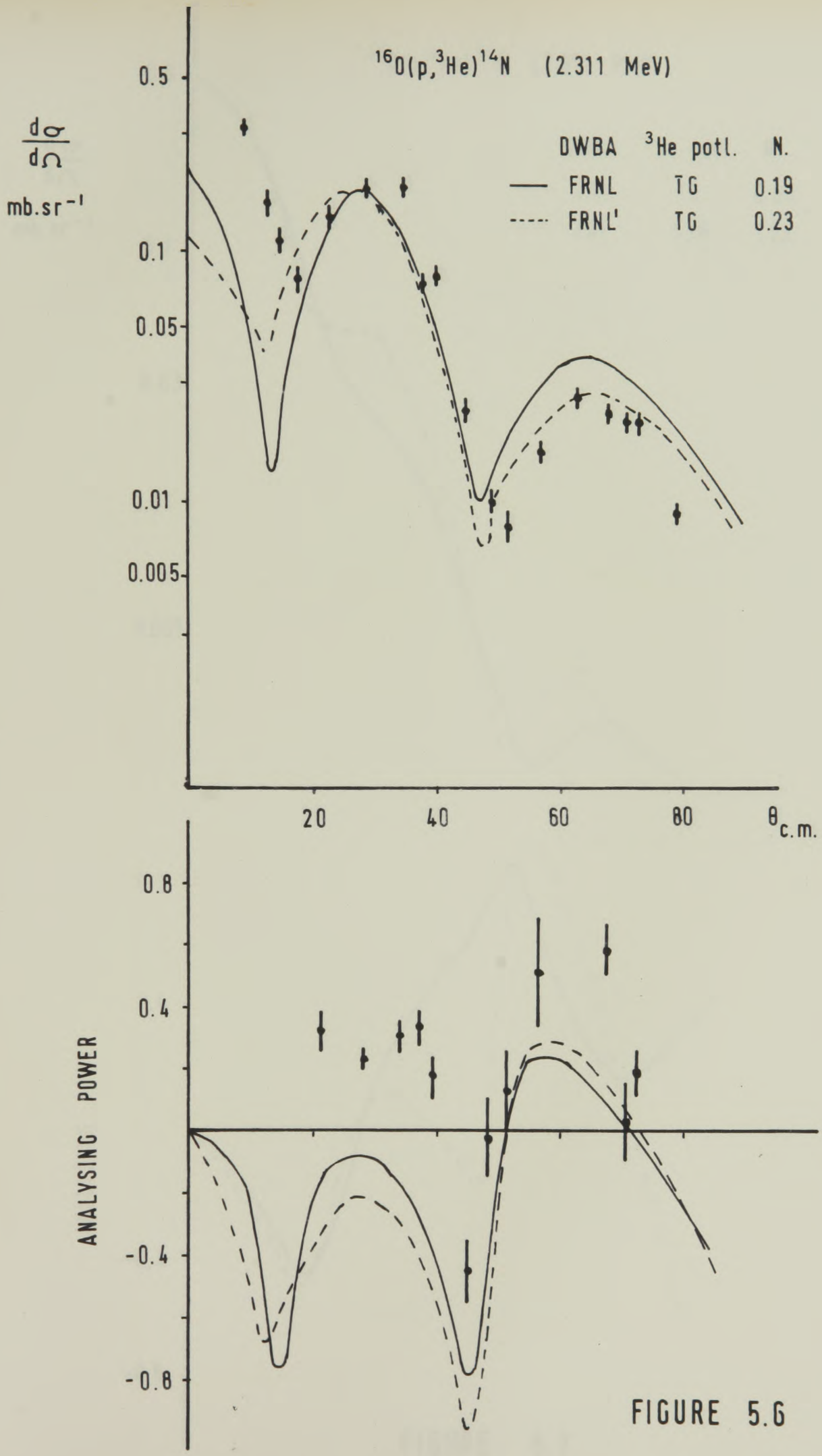

$^{16}O(p,^3He)^{14}N$ (2.311 MeV)
DWBA ³He potl. N.
FRNL TG 0.19
FRNL' TG 0.23
dσ/dΩ
mb.sr⁻¹
0.5
0.1
0.05
0.01
0.005
20
40
60
80
θc.m.
ANALYSING POWER
0.8
0.4
-0.4
-0.8

FIGURE 5.6

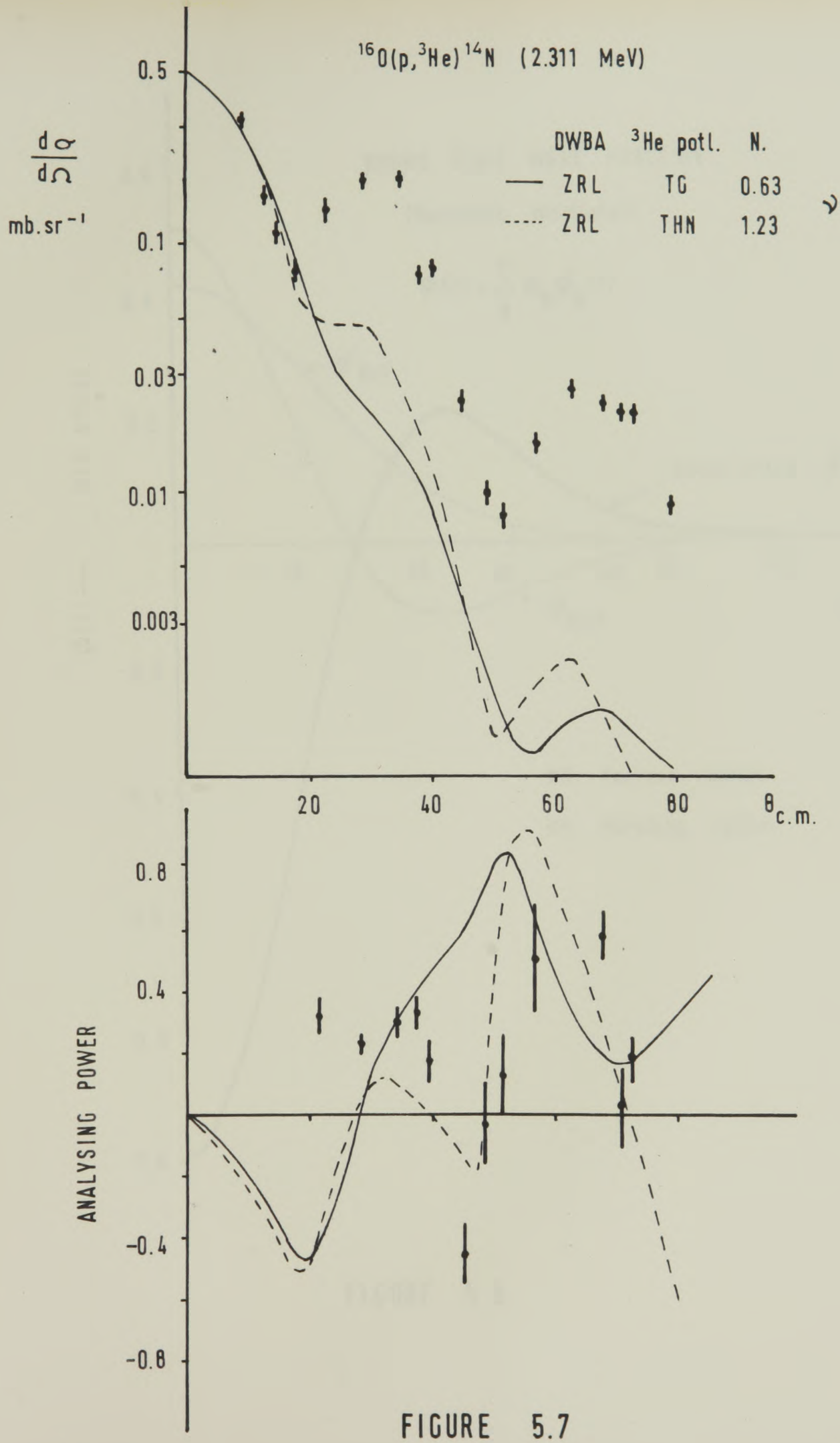

$^{16}O(p,^3He)^{14}N$ (2.311 MeV)
DWBA ³He potl. N.
ZRL TG 0.63
ZRL THN 1.23
ν=0.32 fm^{-2}
$\frac{d\sigma}{d\Omega}$
mb.sr^{-1}
0.5
0.1
0.03
0.01
0.003
20
40
60
80
$\theta_{c.m.}$
ANALYSING POWER
0.8
0.4
-0.4
-0.8

FIGURE 5.7

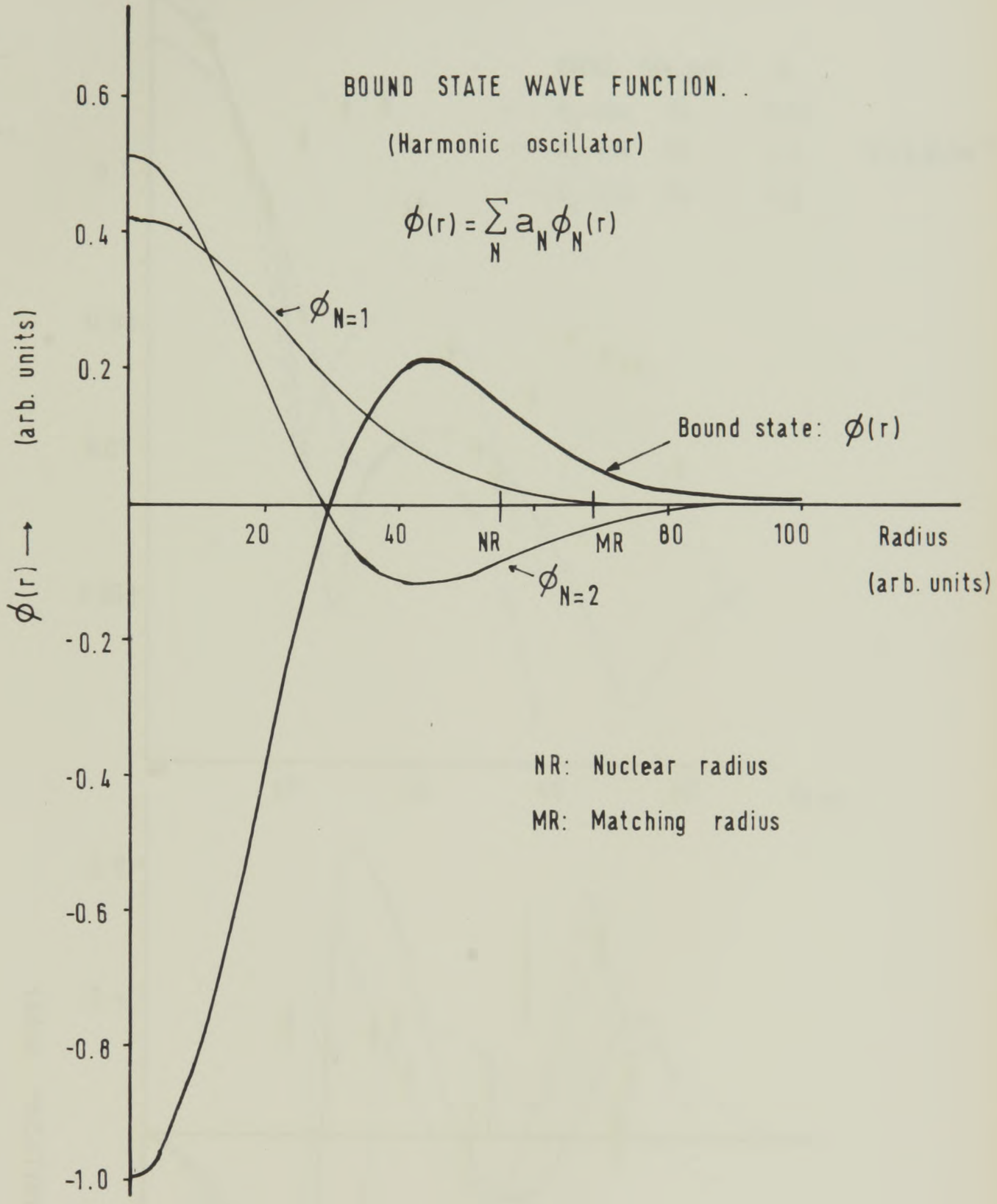

BOUND STATE WAVE FUNCTION. .
(Harmonic oscillator)
$\phi(r) = \sum_N a_N \phi_N(r)$
$\phi_{N=1}$
$\phi_{N=2}$
Bound state: $\phi(r)$
0.6
0.4
0.2
-0.2
-0.4
-0.6
-0.8
-1.0
20
40
NR
MR
80
100
Radius
(arb. units)
$\phi(r)$ → (arb. units)
NR: Nuclear radius
MR: Matching radius

FIGURE 5.8

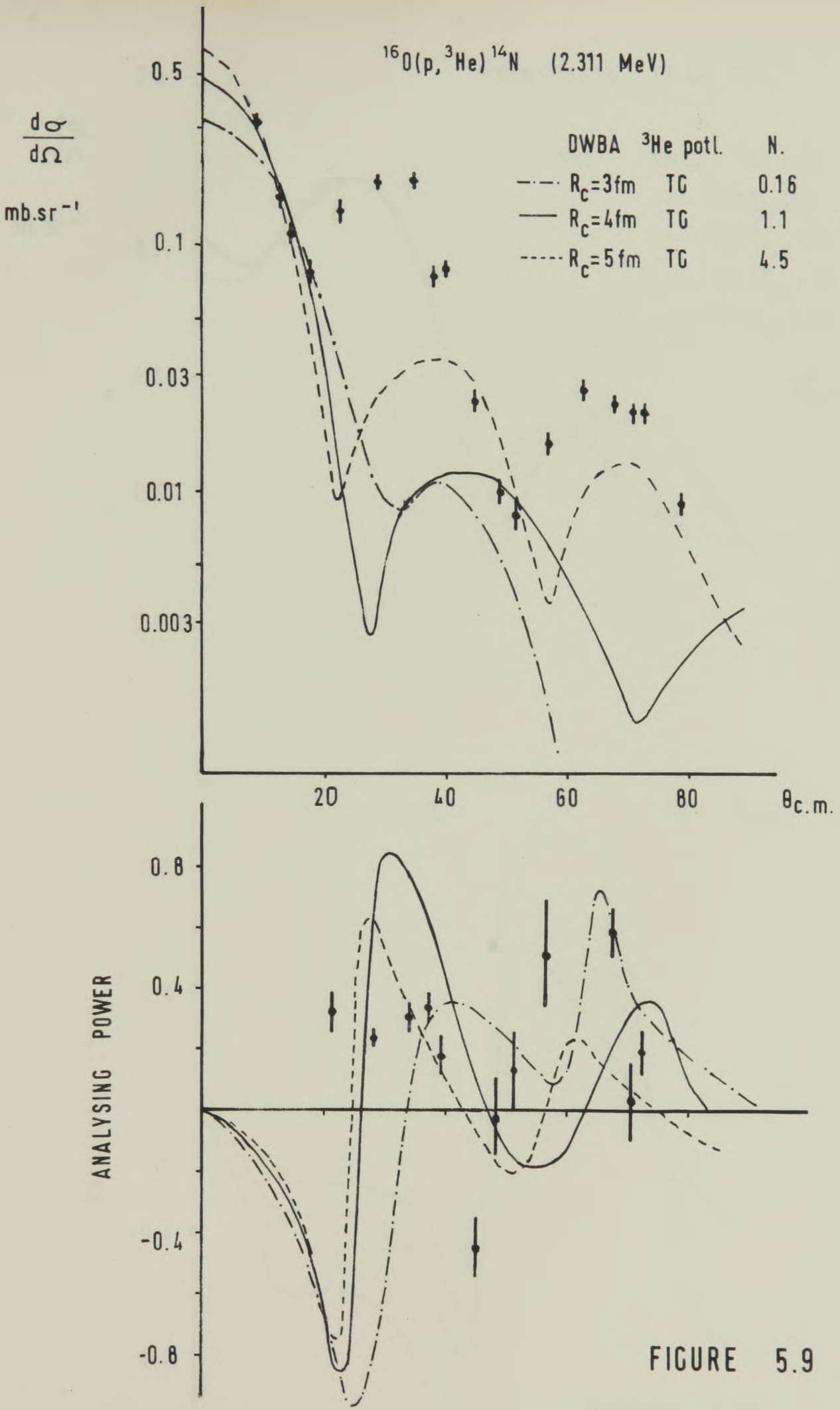

$^{16}O(p,{}^{3}He)^{14}N$ (2.311 MeV)
$\frac{d\sigma}{d\Omega}$
mb.sr^{-1}
DWBA ³He potl. N.
R_c=3fm TG 0.16
R_c=4fm TG 1.1
R_c=5fm TG 4.5
$\nu = 0.32\,fm^{-2}$
0.5
0.1
0.03
0.01
0.003
20
40
60
80
$\theta_{c.m.}$
ANALYSING POWER
0.8
0.4
-0.4
-0.8

FIGURE 5.9

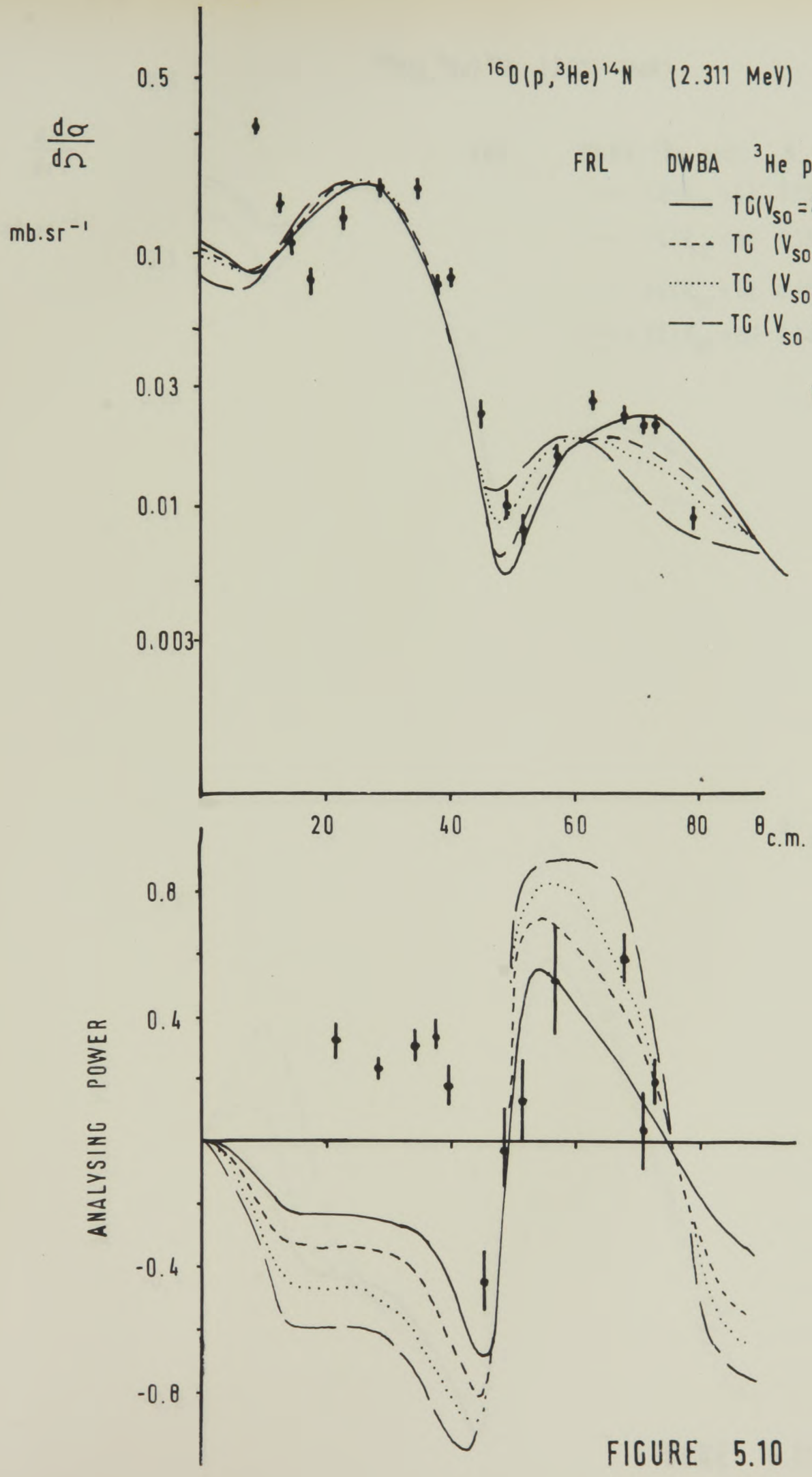

$^{16}O(p,^3He)^{14}N$ (2.311 MeV)
FRL DWBA ^{3}He potl. N.
TG(V_{so}=4) 0.152
TG (V_{so}=6) 0.150
TG (V_{so}=8) 0.148
TG (V_{so}=10) 0.144
V_{so}^{p} = 0
$\frac{d\sigma}{d\Omega}$
mb.sr^{-1}
0.5
0.1
0.03
0.01
0.003
20
40
60
80
$\theta_{c.m.}$
ANALYSING POWER
0.8
0.4
-0.4
-0.8

FIGURE 5.10

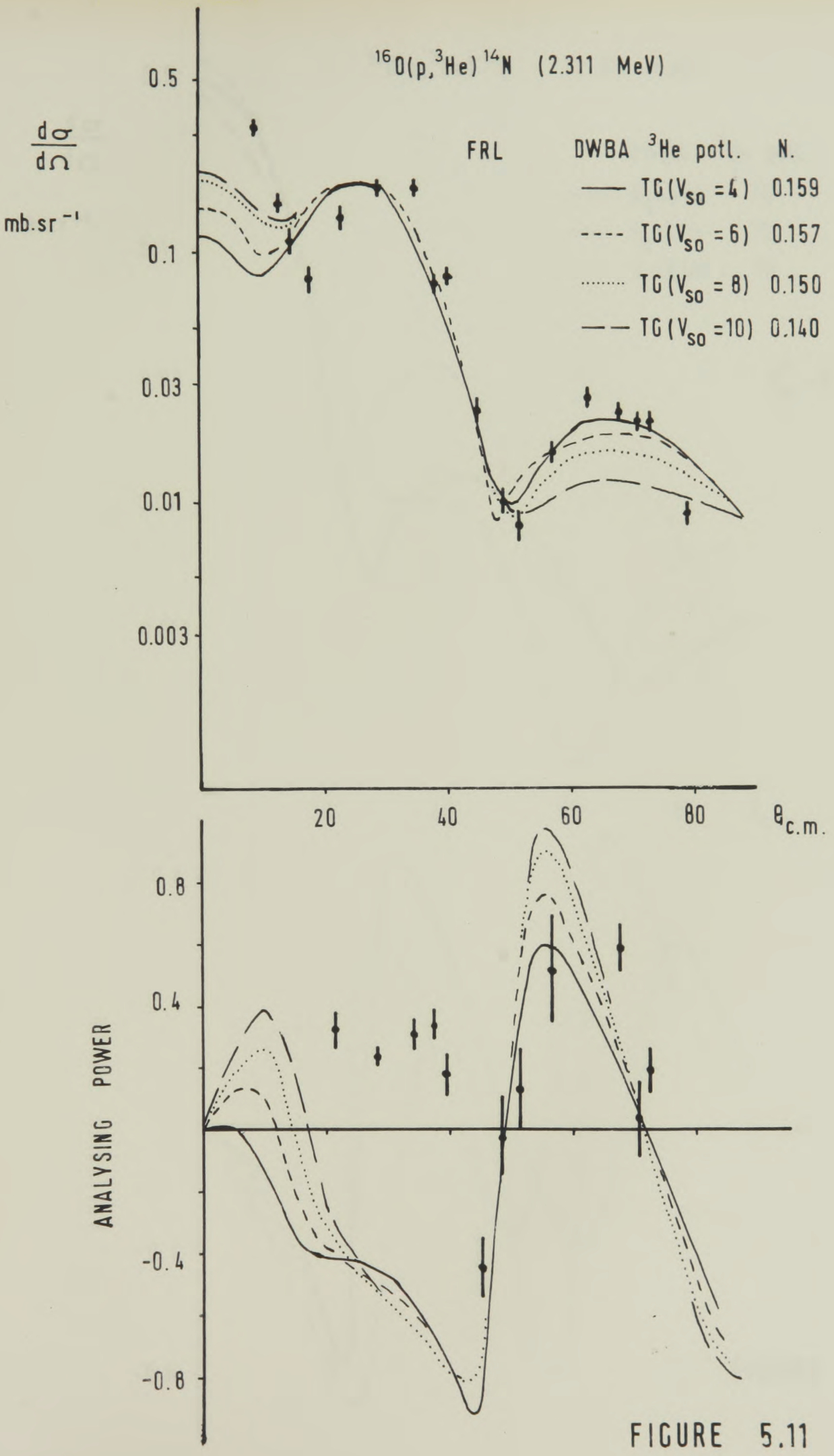

$^{16}O(p,^3He)^{14}N$ (2.311 MeV)
FRL
DWBA ^{3}He potl. N.
TG(V_{so} =4) 0.159
TG(V_{so} =6) 0.157
TG(V_{so} =8) 0.150
TG(V_{so} =10) 0.140
$\frac{d\sigma}{d\Omega}$
mb.sr^{-1}
0.5
0.1
0.03
0.01
0.003
20
40
60
80
$\theta_{c.m.}$
ANALYSING POWER
0.8
0.4
-0.4
-0.8

FIGURE 5.11

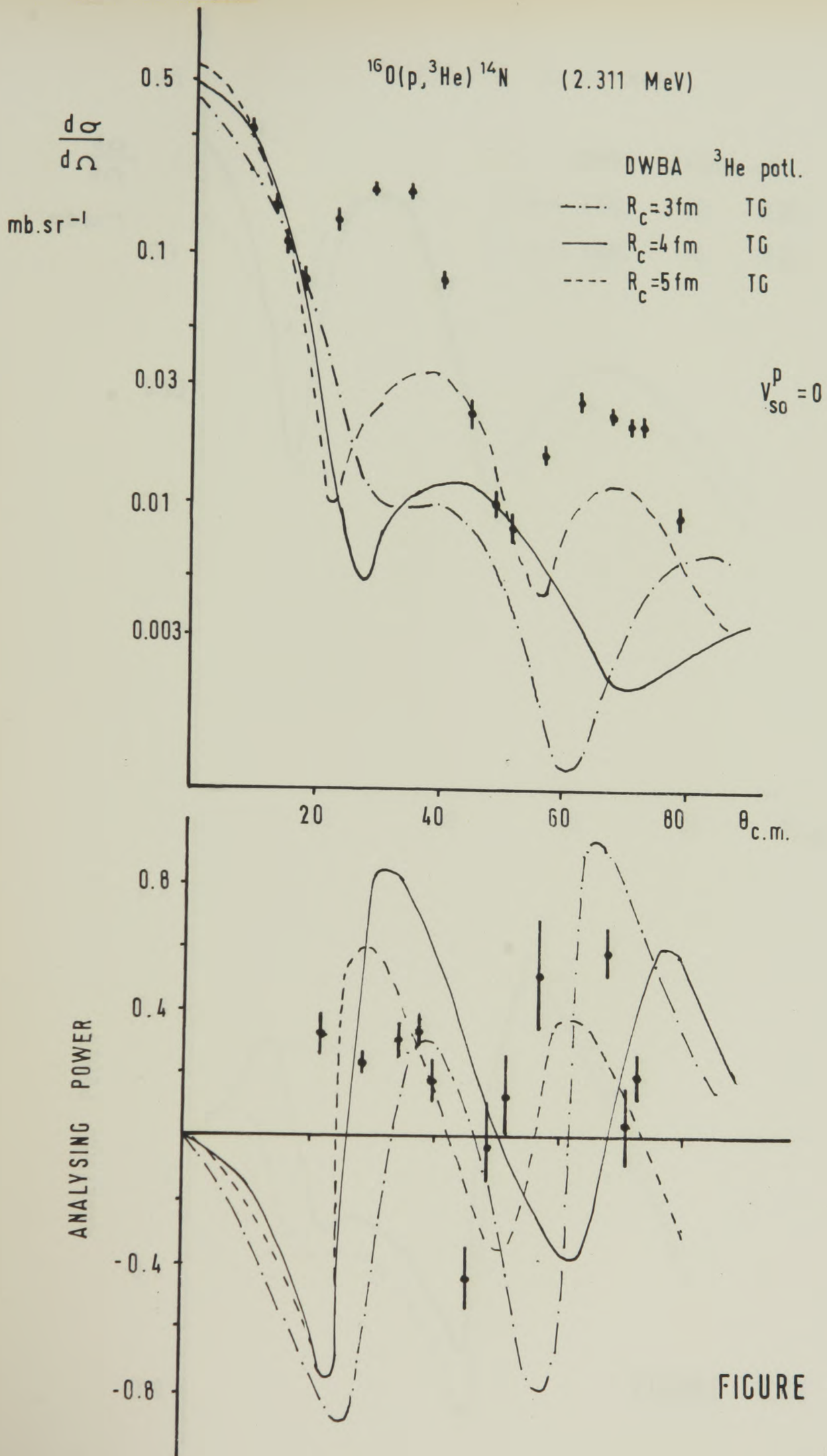

$^{16}O(p,^3He)^{14}N$ (2.311 MeV)
DWBA ^{3}He potl.
R_c=3fm TG
R_c=4fm TG
R_c=5fm TG
V_{so}^p = 0
$\frac{d}{d\Omega}Q$
mb.sr^{-1}
0.5
0.1
0.03
0.01
0.003
20
40
60
80
$\theta_{c.m.}$
ANALYSING POWER
0.8
0.4
-0.4
-0.8

FIGURE 5.12

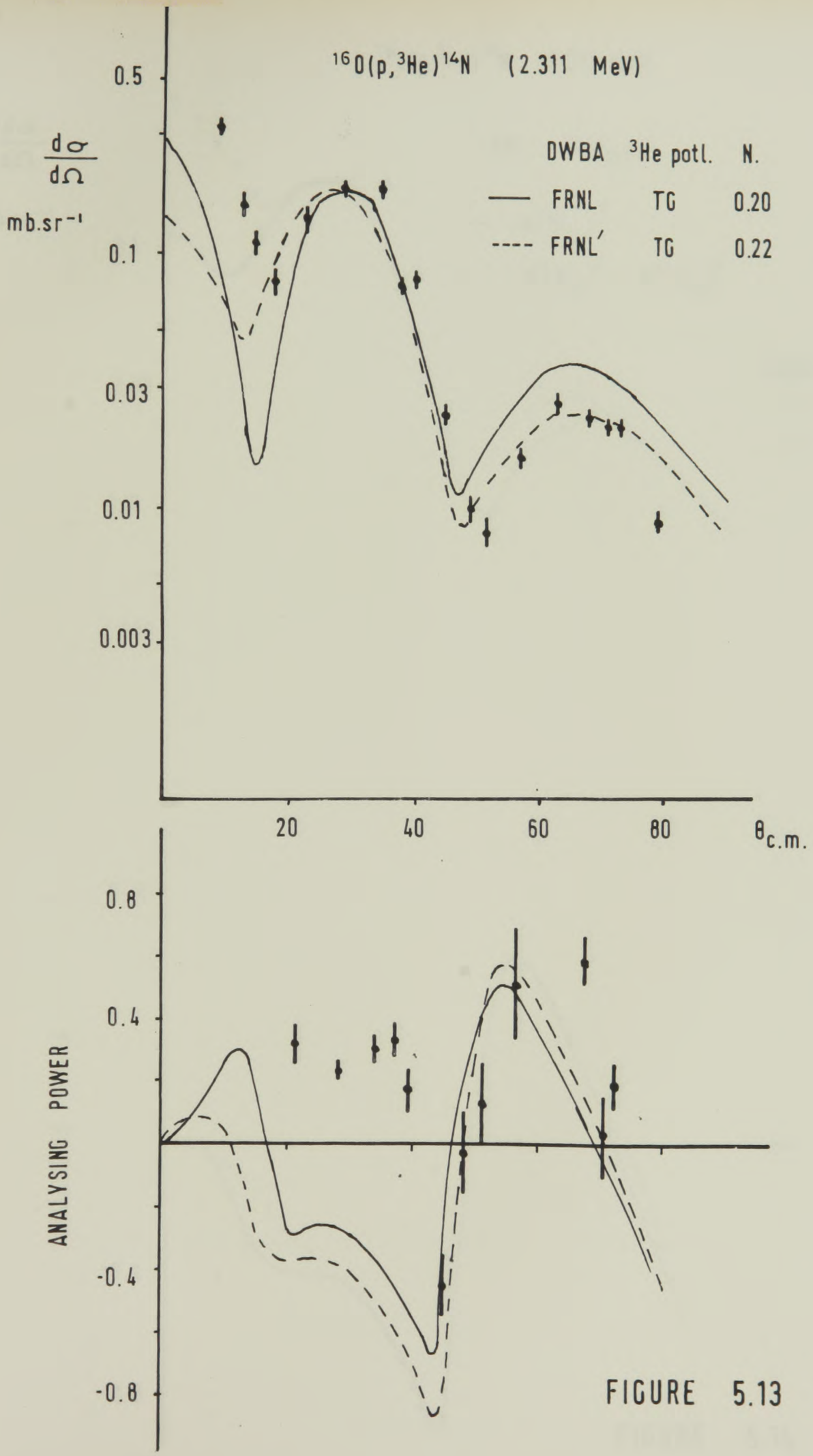

$^{16}O(p,^{3}He)^{14}N$ (2.311 MeV)
DWBA ³He potl. N.
FRNL TG 0.20
FRNL' TG 0.22
$\frac{d\sigma}{d\Omega}$
mb.sr⁻¹
0.5
0.1
0.03
0.01
0.003
20
40
60
80
$\theta_{c.m.}$
ANALYSING POWER
0.8
0.4
-0.4
-0.8

FIGURE 5.13

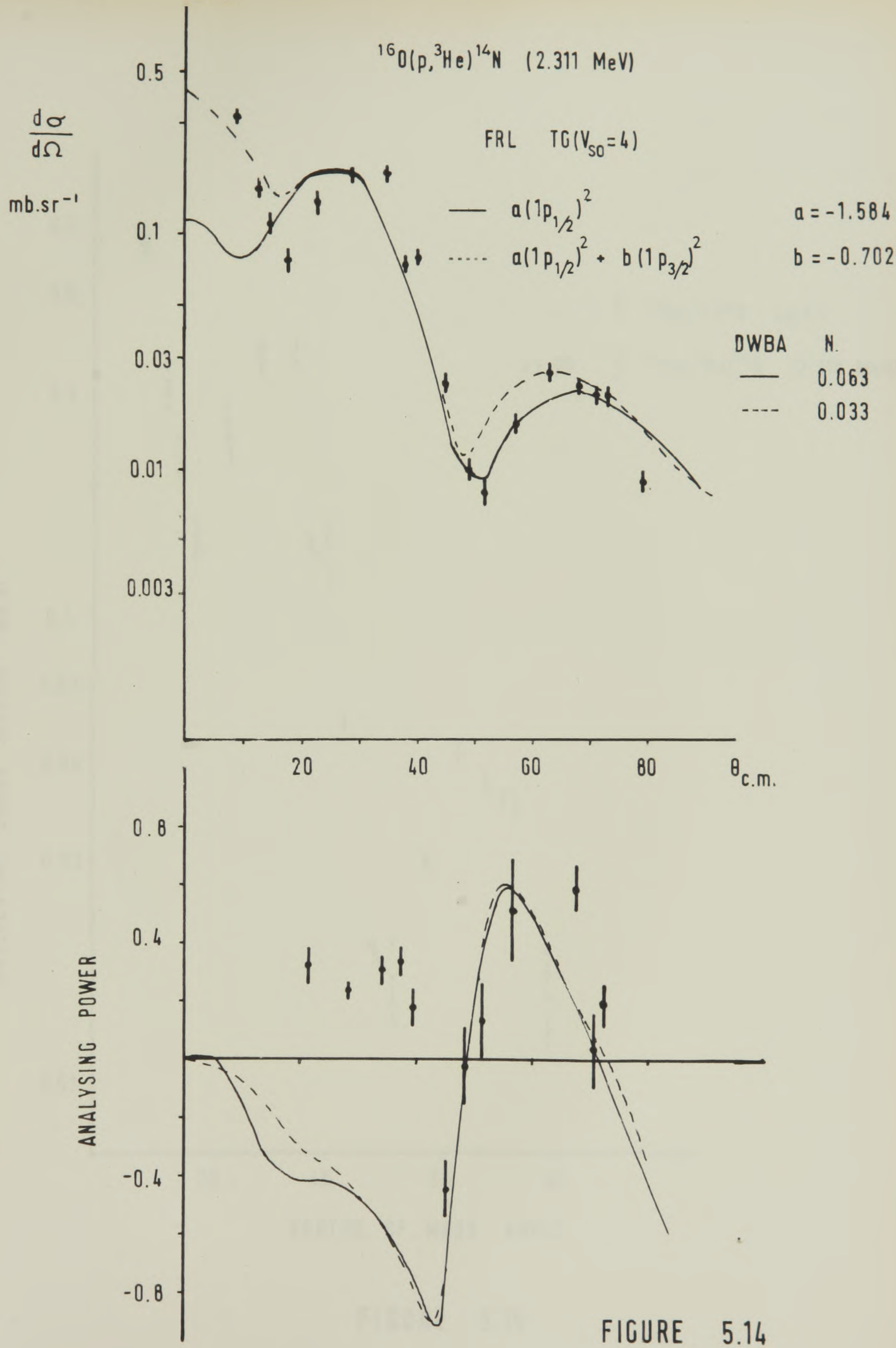

$^{16}O(p,^3He)^{14}N$ (2.311 MeV)
FRL TG(V_{so}=4)
$\frac{d\sigma}{d\Omega}$
mb.sr^{-1}
0.5
0.1
0.03
0.01
0.003
$a(1p_{1/2})^2$
$a(1p_{1/2})^2 + b(1p_{3/2})^2$
a = -1.584
b = -0.702
DWBA N.
0.063
0.033
20
40
60
80
$\theta_{c.m.}$
ANALYSING POWER
0.8
0.4
-0.4
-0.8

FIGURE 5.14

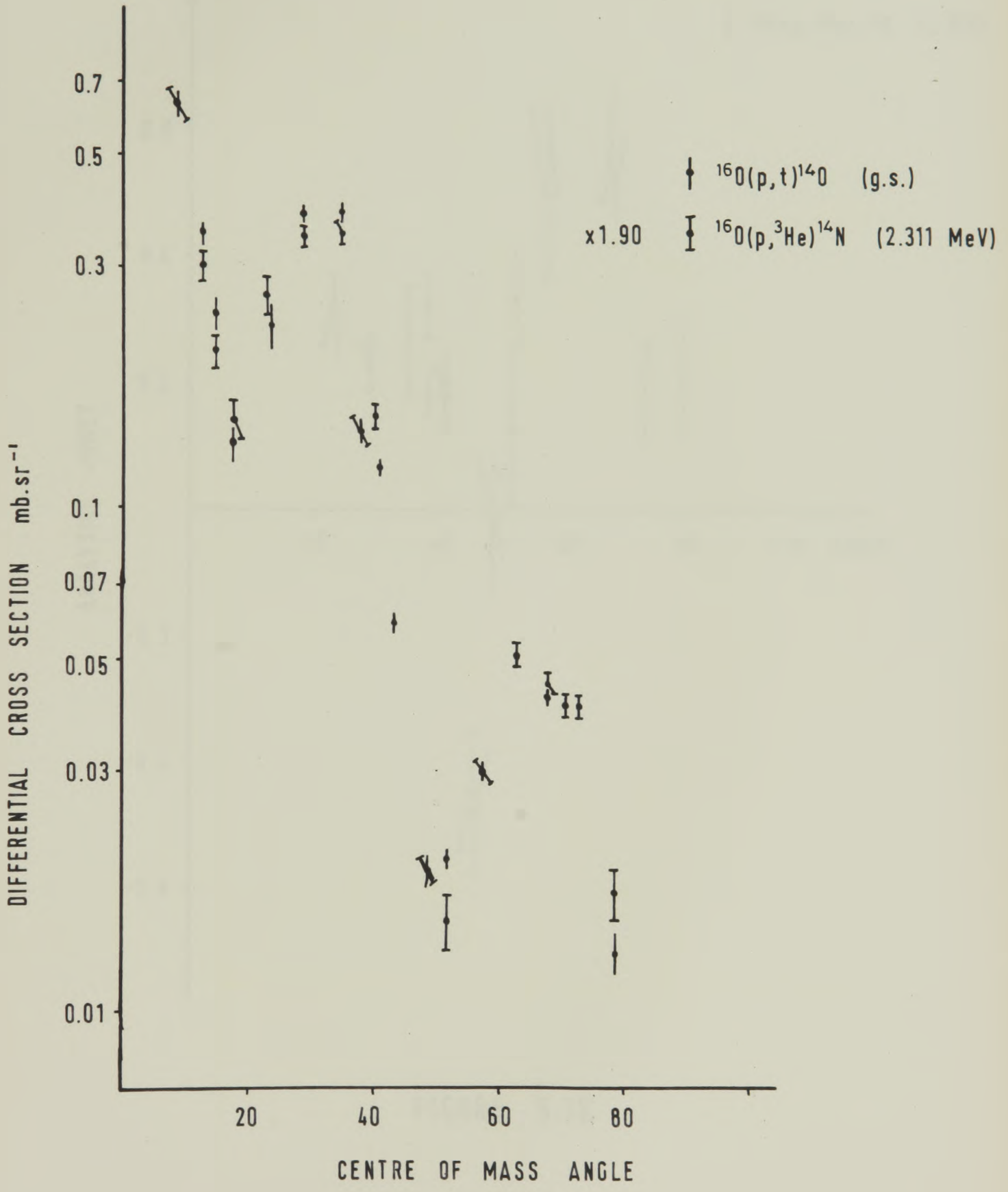

0.7
0.5
0.3
0.1
0.07
0.05
0.03
0.01
DIFFERENTIAL CROSS SECTION mb.sr⁻¹
20
40
60
80
CENTRE OF MASS ANGLE
$^{16}O(p,t)^{14}O$ (g.s.)
x1.90 $^{16}O(p,^{3}He)^{14}N$ (2.311 MeV)

FIGURE 5.15

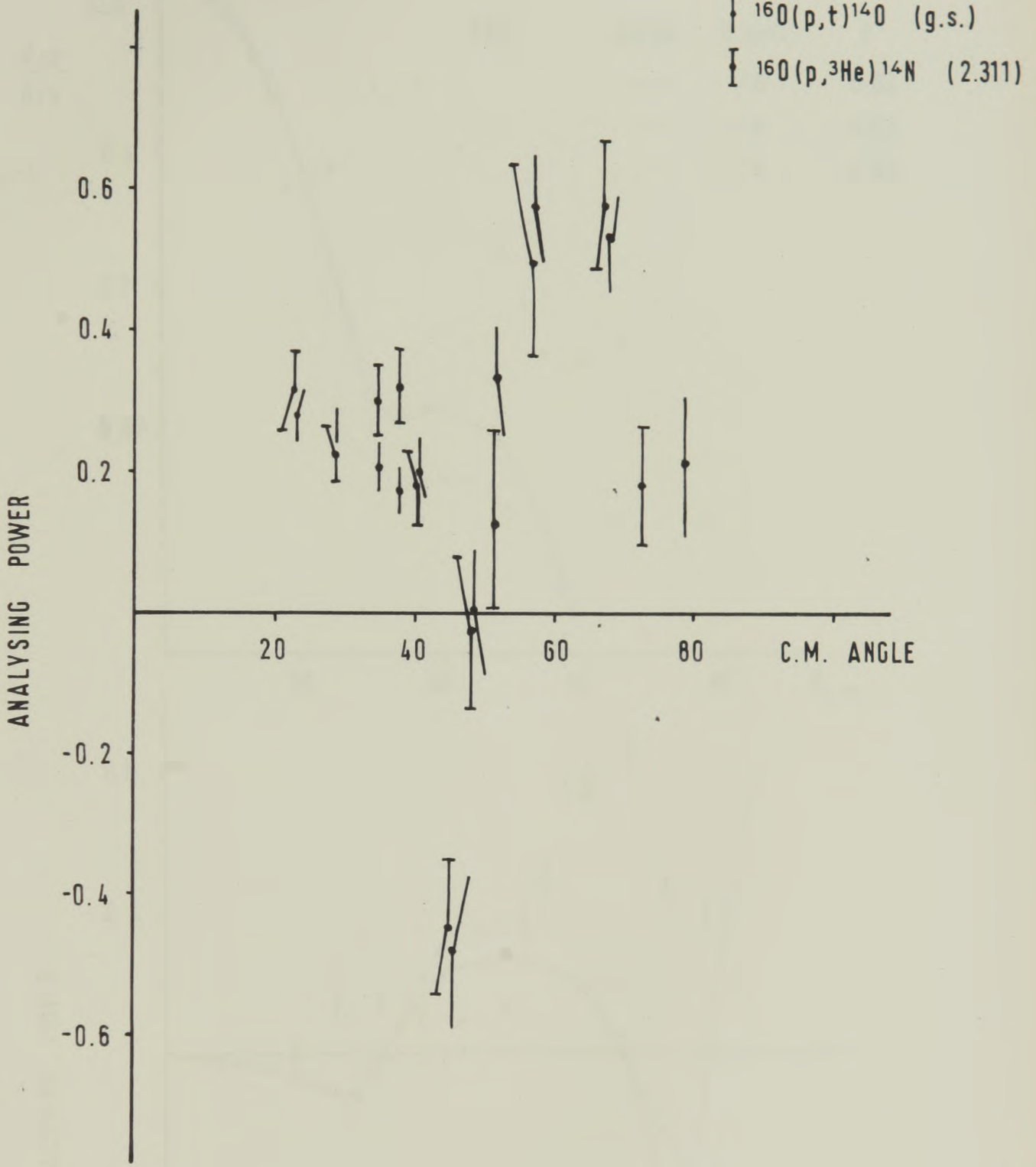

$^{16}O(p,t)^{14}O$ (g.s.)
$^{16}O(p,^3He)^{14}N$ (2.311)
0.6
0.4
0.2
-0.2
-0.4
-0.6
20
40
60
80
C.M. ANGLE
ANALYSING POWER

FIGURE 5.16

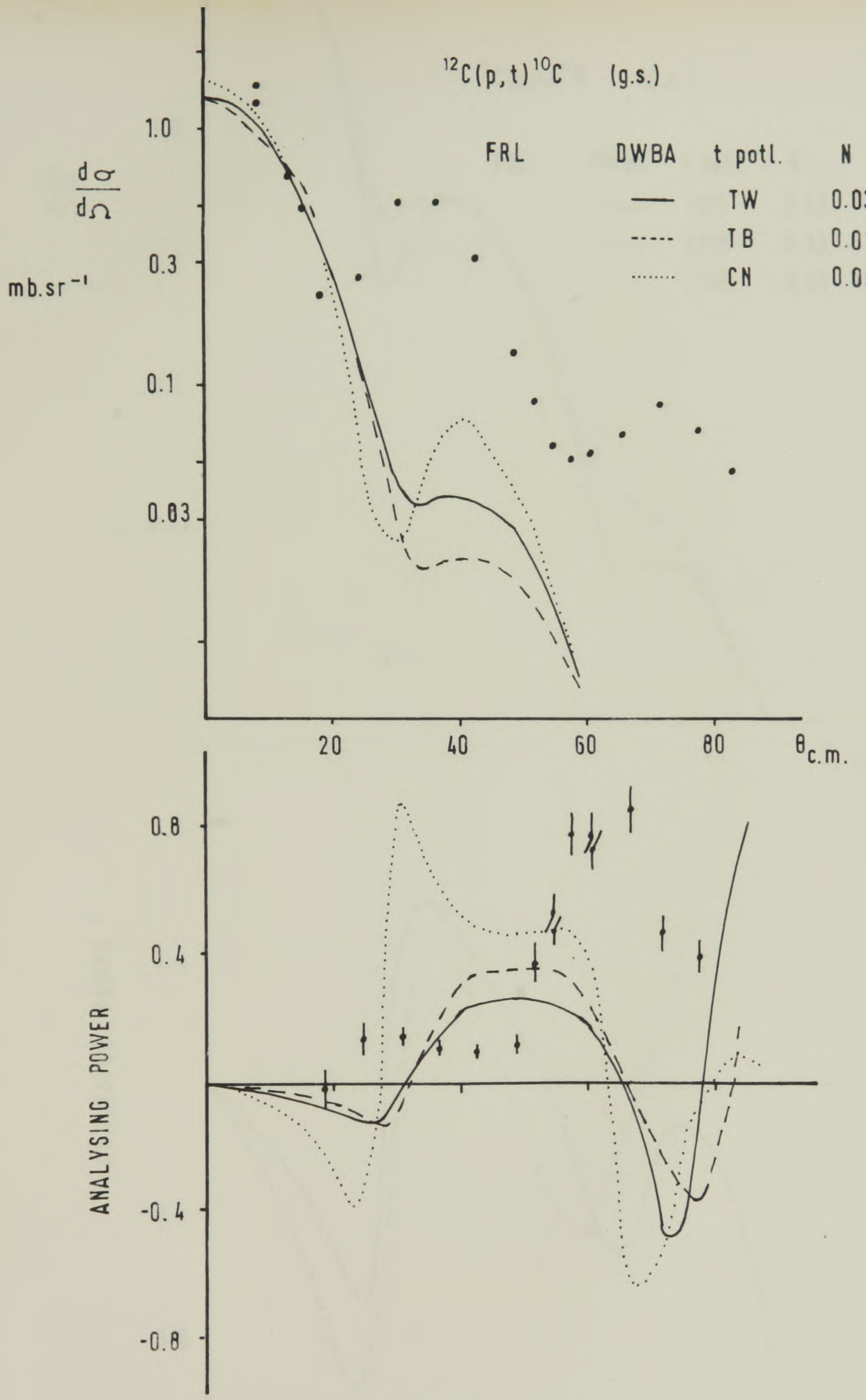

$^{12}C(p,t)^{10}C$ (g.s.)
FRL DWBA t potl. N
TW 0.03
TB 0.02
CN 0.06
$\frac{d}{d\Omega}\Big|_Q$
mb.sr^{-1}
1.0
0.3
0.1
0.03
20
40
60
80
$\theta_{c.m.}$
ANALYSING POWER
0.8
0.4
-0.4
-0.8

FIGURE 5.17

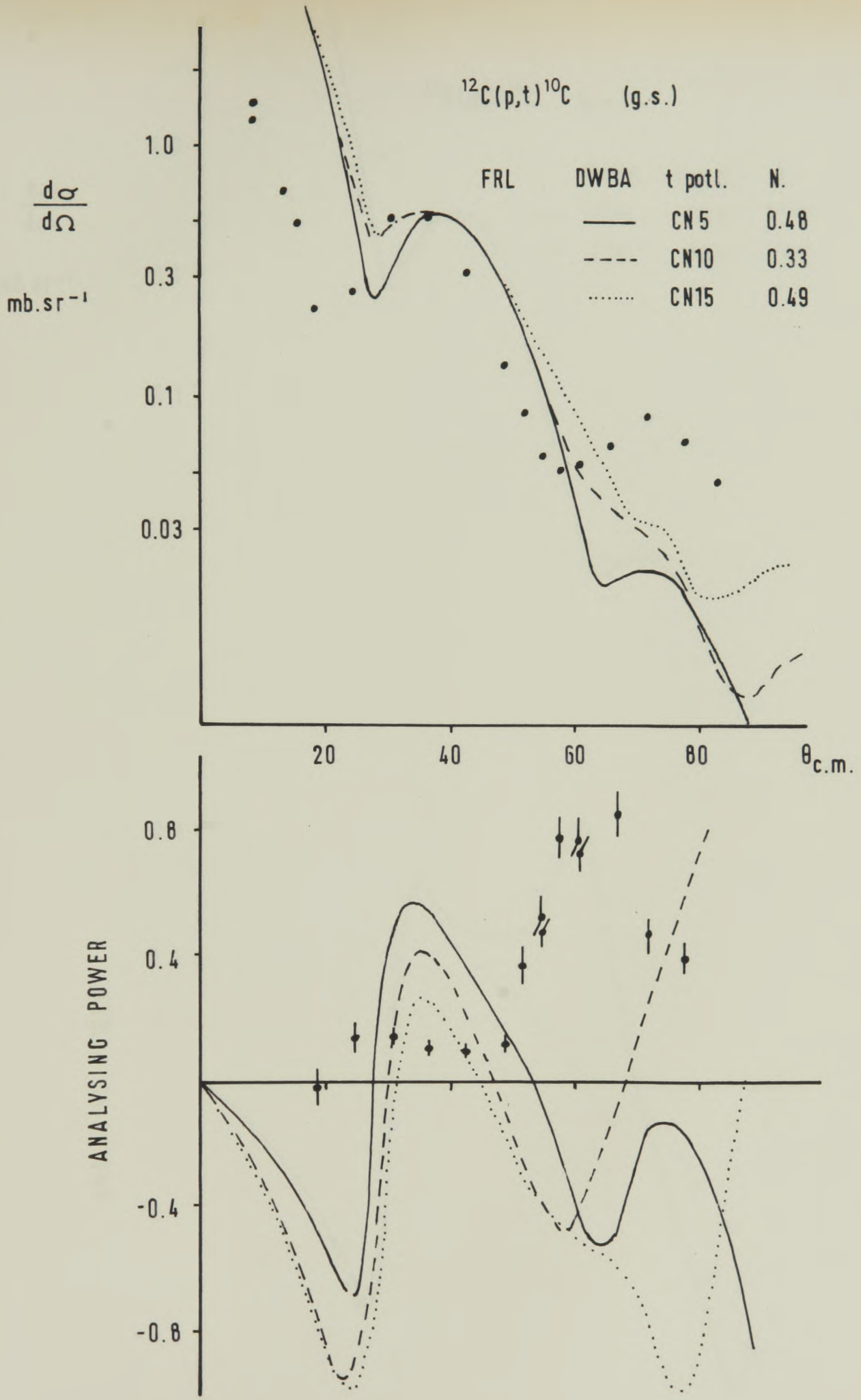

$^{12}C(p,t)^{10}C$ (g.s.)
FRL DWBA t potl. N.
CN5 0.48
CN10 0.33
CN15 0.49
$\frac{d\sigma}{d\Omega}$
mb.sr^{-1}
1.0
0.3
0.1
0.03
20
40
60
80
$\theta_{c.m.}$
ANALYSING POWER
0.8
0.4
-0.4
-0.8

FIGURE 5.18

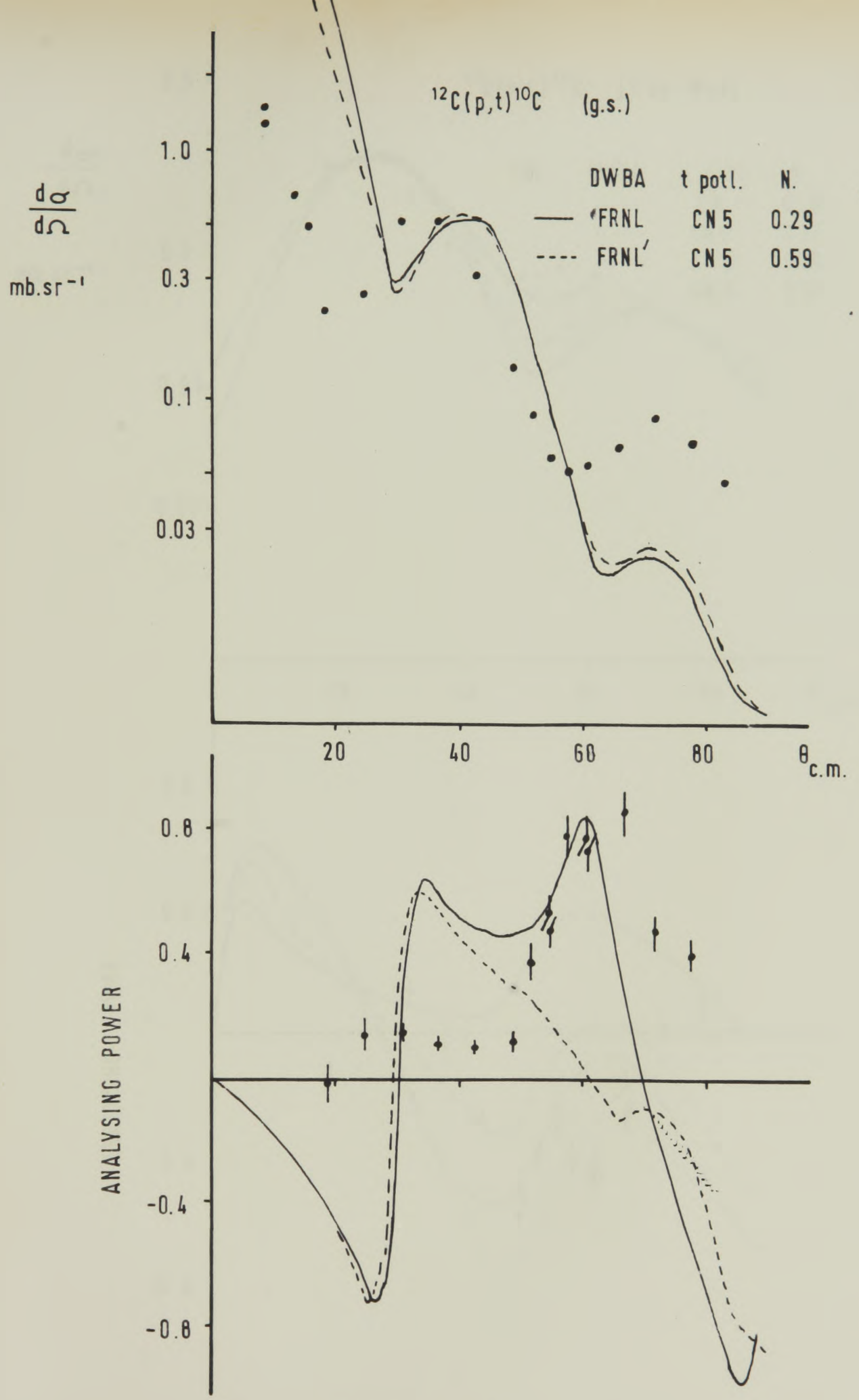

$^{12}C(p,t)^{10}C$ (g.s.)
DWBA t potl. N.
FRNL CN5 0.29
FRNL' CN5 0.59
$\frac{d}{d\Omega}$
mb.sr^{-1}
1.0
0.3
0.1
0.03
20
40
60
80
$\theta_{c.m.}$
0.8
0.4
-0.4
-0.8
ANALYSING POWER

FIGURE 5.19

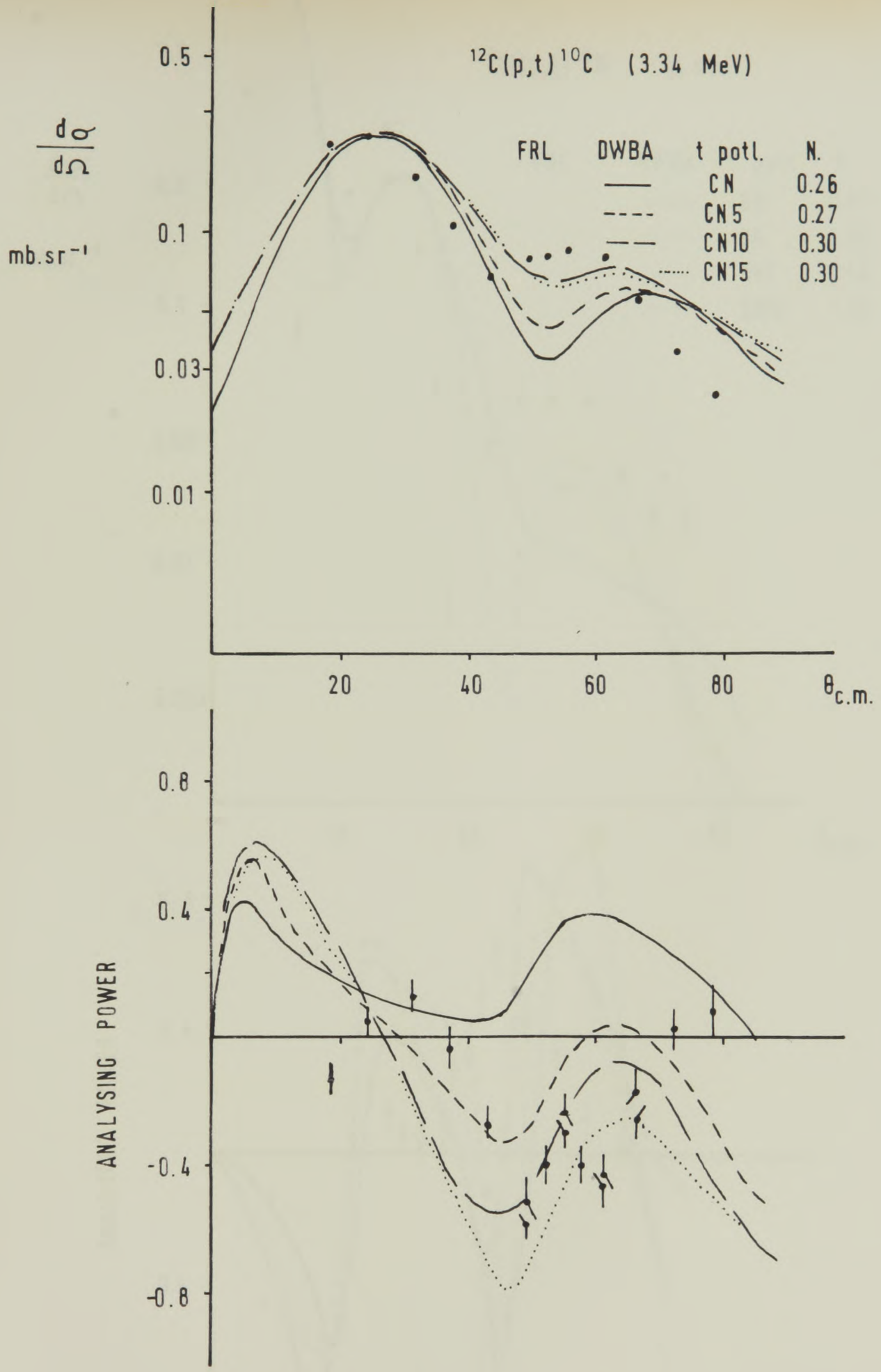

$^{12}C(p,t)^{10}C$ (3.34 MeV)
FRL DWBA t potl. N.
CN 0.26
CN5 0.27
CN10 0.30
CN15 0.30
$\frac{d\sigma}{d\Omega}$
mb.sr^{-1}
0.5
0.1
0.03
0.01
20
40
60
80
$\theta_{c.m.}$
ANALYSING POWER
0.8
0.4
-0.4
-0.8

FIGURE 5.20

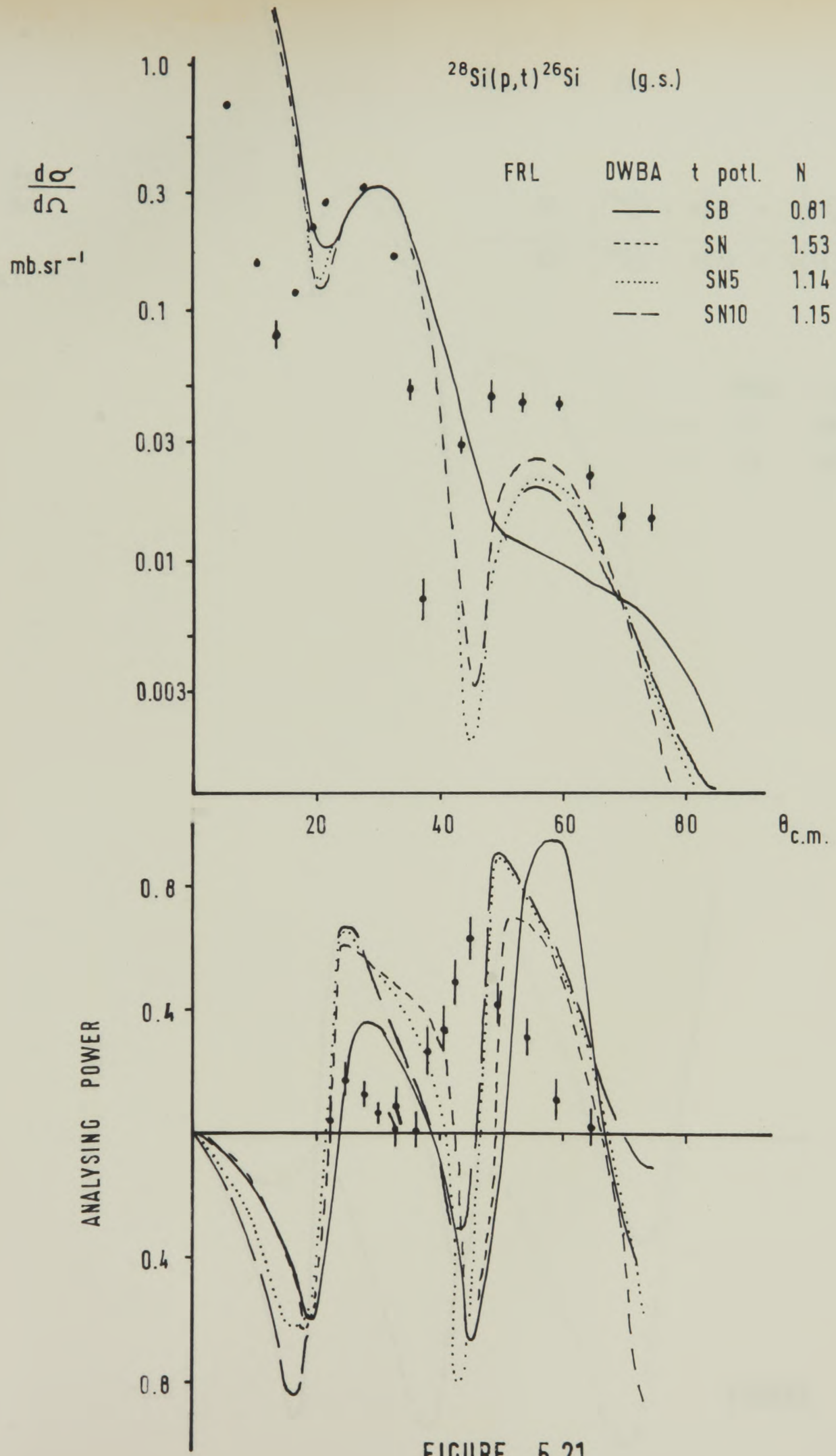

$^{28}Si(p,t)^{26}Si$ (g.s.)
FRL DWBA t potl. N
SB 0.81
SN 1.53
SN5 1.14
SN10 1.15
$\frac{d\sigma}{d\Omega}$
mb.sr^{-1}
1.0
0.3
0.1
0.03
0.01
0.003
20
40
60
80
$\theta_{c.m.}$
ANALYSING POWER
0.8
0.4
0.4
0.8

FIGURE 5.21

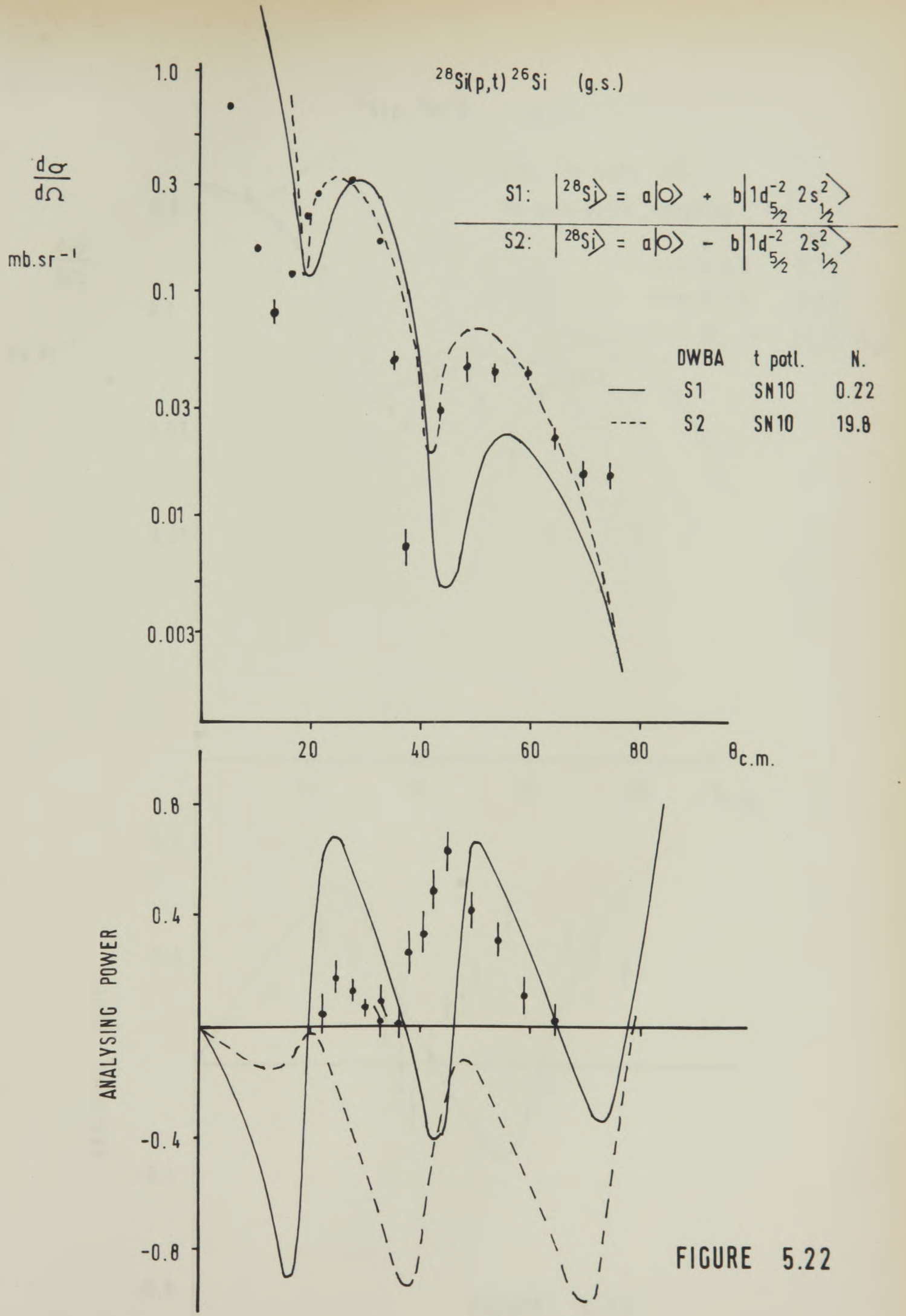

$^{28}Si(p,t)^{26}Si$ (g.s.)
$\frac{d\sigma}{d\Omega}$
mb.sr^{-1}
1.0
0.3
0.1
0.03
0.01
0.003
S1: $|^{28}Si\rangle = a|0\rangle + b|1d_{5/2}^{-2}\ 2s_{1/2}^{2}\rangle$
S2: $|^{28}Si\rangle = a|0\rangle - b|1d_{5/2}^{-2}\ 2s_{1/2}^{2}\rangle$
DWBA t potl. N.
S1 SN10 0.22
S2 SN10 19.8
20
40
60
80
$\theta_{c.m.}$
ANALYSING POWER
0.8
0.4
-0.4
-0.8

FIGURE 5.22

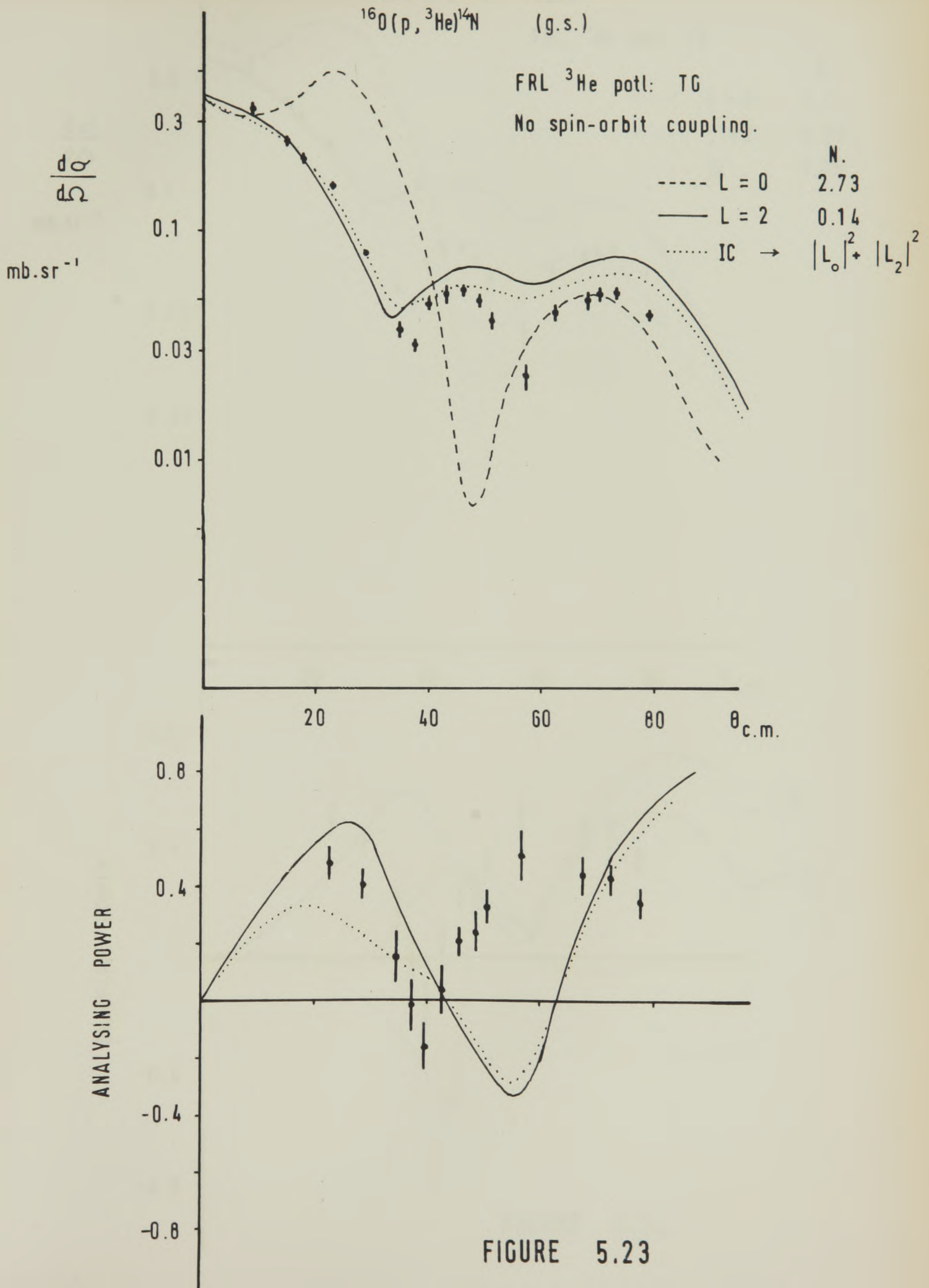

$^{16}O(p, ^3He)^{14}N$ (g.s.)
FRL ^3He potl: TG
No spin-orbit coupling.
N.
----- L = 0 2.73
—— L = 2 0.14
..... IC → $|L_0|^2 + |L_2|^2$
$\frac{d\sigma}{d\Omega}$
mb.sr^{-1}
0.3
0.1
0.03
0.01
20
40
60
80
$\theta_{c.m.}$
ANALYSING POWER
0.8
0.4
-0.4
-0.8

FIGURE 5.23

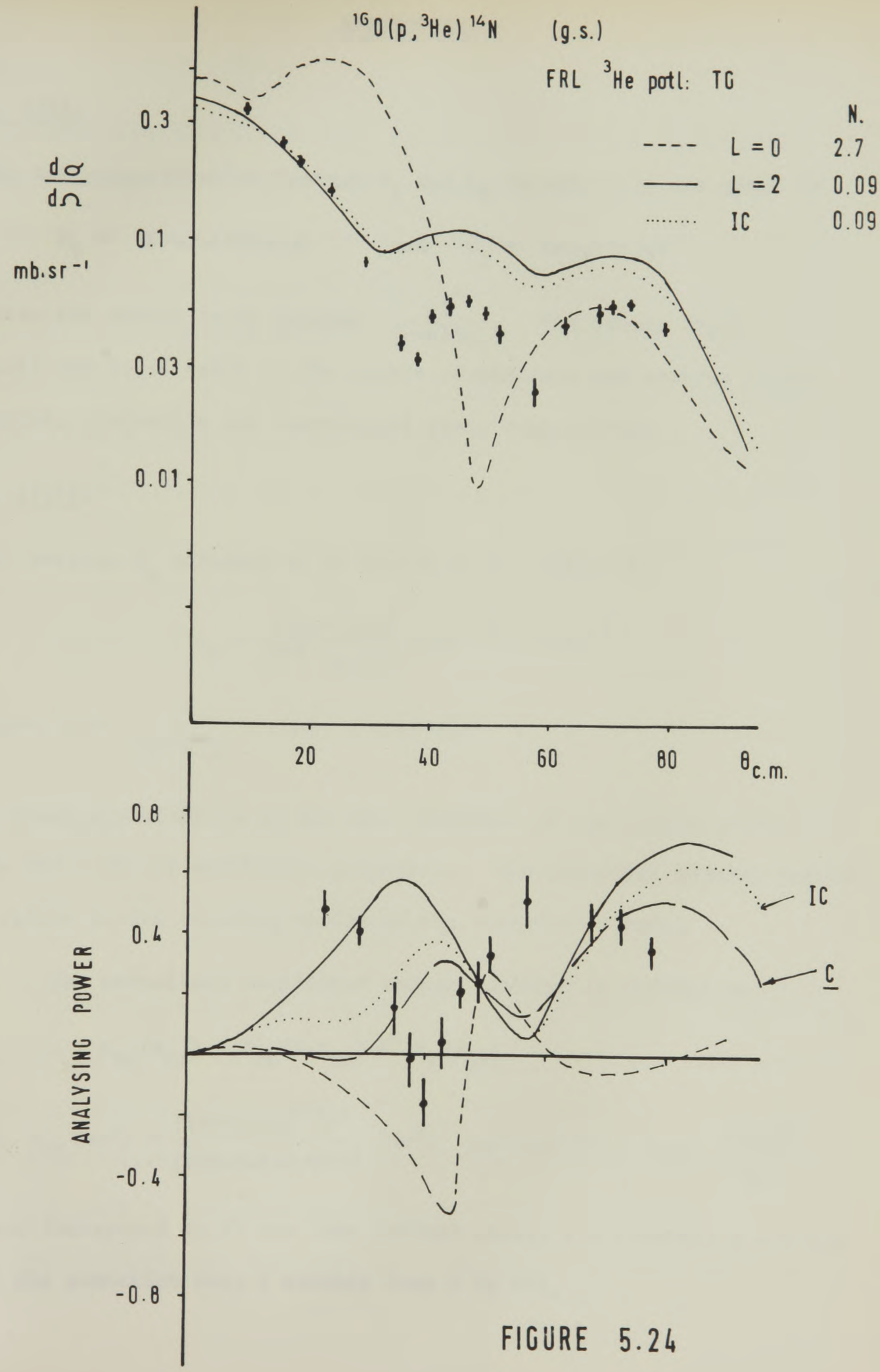

$^{16}O(p,^3He)^{14}N$ (g.s.)
FRL ^{3}He potl: TG
N.
L = 0 2.7
L = 2 0.09
IC 0.09
$\frac{d}{d\Omega}|Q$
mb.sr^{-1}
0.3
0.1
0.03
0.01
20
40
60
80
$\theta_{c.m.}$
ANALYSING POWER
0.8
0.4
-0.4
-0.8
IC
C

FIGURE 5.24

APPENDICES.

A. 1(i):

The antisymmetrisation factors P_1 and P_2 in eqn.(1.2) are given by

$$P_1 = (N+\nu;\nu)(Z+\pi;\pi) \qquad \text{and} \qquad P_2 = (n;\nu)(p;\pi)$$

where the symbol (m;n) denotes $\frac{m!}{(m-n)!n!}$. The labels (N,Z), (n,p) and (ν,π) refer to the number of neutrons and protons in the target, projectile and transferred group respectively.

A. 1(ii):

The overlap Ω_n referred to in eqn.(1.7) is defined by

$$\Omega_n = \frac{\{(2n-1)!\}^{\frac{1}{2}}}{2^{n-1}(n-1)!}(xy)^{3/2}(1-x)^{n-1}$$

where $x = \frac{2\nu}{6\eta^2+\nu}$ and $y = \eta(6/\nu)^{\frac{1}{2}}$

In these equations, η is the size parameter of the triton or ^{3}He ion and ν is the oscillator parameter. The principal quantum number n refers to the relative motion of the transferred pair.

The normalised oscillator radial function is defined as

$$\phi_{NL}(r_{xA}) = R_{NL}(2\nu r_{xA})\, i^L\, Y_L(\hat{r}_{xA})$$

and $$R_{NL}(\nu r^2) = \frac{\{2(N-1)!\nu^{3/2}\}^{\frac{1}{2}}}{\{\Gamma(N-1+L+3/2)\}^{\frac{1}{2}}}(\nu r^2)^L \exp(-\nu r^2/2) \sum_k (s;t)\frac{(-\nu r^2)^k}{k!}$$

where the symbol (s;t) has been defined above; $s = N-1+L+\frac{1}{2}$; $t = N-1-k$; and the summation over k extends from 0 to N-1.

A. 2:

The dead time loss in the electronics system is calculated in the following way. A coincidence-anticoincidence requirement must be satisfied before a pulse reaches the pulse height analyser (PHA), but since the minimum dead time of the analyser is much greater than the dead time of the coincidence circuitry, the total dead time arising from pulse analysis is due solely to the PHA. The analyser dead time is determined from a comparison of the contents of two scalers connected to the ΔE discriminator output, (Figure 3.4). One scaler is inhibited when the analyser is busy and the other is not. If the scaler contents, accumulated in a beam-on time of T seconds, are R and D respectively, then

$$\frac{D}{T} = \frac{R}{T - N\tau_A}$$

where N is the number of pulses analysed by the PHA during the time T, and τ_A is the analyser dead time. The total dead time is therefore

$$N\tau_A = \frac{T(D - R)}{D} .$$

Additional dead time losses are incurred when the discriminators are triggered but the coincidence requirements are not fully satisfied, thus preventing pulse height analysis being performed. Suppose the ΔE and E discriminators triggered simultaneously C times during the beam-on time T, and separately, D and F times respectively. Then if the discriminator dead time is τ_D seconds, the total dead time due

to these losses will be

$$\text{Dead time} = (C-N)\tau_D + (D-C)\tau_D + (F-C)\tau_D$$

$$= (D+F-C-N)\tau_D.$$

The final contribution arises from the anticoincidence circuitry which is designed to have a dead time τ_{AC} seconds in excess of the ΔE and E discriminator dead time of τ_D seconds. Thus, if the anticoincidence discriminator is triggered A times, then the grand total dead time will be

$$\text{G.D.T.} = T(D-R)/D + (D+F-C-N)\tau_D + A\tau_{AC} \qquad \text{A2.1}$$

$$= Z \text{ seconds.}$$

The reaction yield accumulated in a beam-on time T must therefore be corrected for these losses by multiplying the total yield by the factor

$$f = \frac{T}{T - Z}.$$

The standard deviation of this factor cannot be readily determined since the quantities in eqn.(A2.1) are not statistically independent, but in order to obtain some estimate of $\sigma(f)$ this will be ignored. The standard deviation can then be shown to be

$$\frac{\sigma^2(f)}{f^2} = \frac{(D-R)R}{D^3} + \frac{(D+F-C-N)\tau_D^2}{T^2}\left\{1 + (D+F-C-N)\frac{\sigma^2(\tau_D)}{\tau_D^2}\right\}$$

$$+\frac{A\tau_{AC}^2}{T^2}\left\{1 + \frac{A\,\sigma^2(\tau_{AC})}{\tau_{AC}^2}\right\}$$

A. 3:

The differential cross sections of the six reactions considered in this thesis are tabulated below. The cross sections and errors are given in ubarns/steradian in the centre of mass coordinate system.

$^{12}C(p,t)^{10}C$ Ground state.

θ	$\frac{d\sigma}{d\omega}$	Δσ	θ	$\frac{d\sigma}{d\omega}$	Δσ
9.2	1448	35	48.6	138	5
9.2	1227	31	54.4	59	2
13.5	653	21	54.4	61	2
15.4	498	15	51.5	88	3
18.4	225	18	57.3	53	2
18.4	236	11	60.2	50	2
24.5	290	9	60.2	57	2
24.5	258	16	65.9	64	2
30.6	504	9	71.6	84	2
36.7	515	11	77.1	66	2
42.6	319	5	82.6	46	5
48.6	136	3			

$^{12}C(p,t)^{10}C$ 3.34 MeV (first excited state).

θ	$\frac{d\sigma}{d\omega}$	Δσ	θ	$\frac{d\sigma}{d\omega}$	Δσ
18.7	221	18	55.2	87	3
24.9	236	8	50.2	85	3
31.1	167	5	61.1	80	3
37.2	107	4	61.1	79	3
43.3	69	2	66.9	56	2
49.3	80	2	66.9	57	3
52.3	82	3	72.6	35	2
55.2	85	2	78.2	24	2

$^{16}O(p,^{3}He)^{14}N$ Ground state.

θ	$\frac{d\sigma}{d\omega}$	$\Delta\sigma$	θ	$\frac{d\sigma}{d\omega}$	$\Delta\sigma$
8.6	330	23	45.3	55	3
14.3	241	16	48.1	50	3
17.1	203	22	50.9	41	3
22.8	153	16	56.4	23	3
22.8	156	6	61.8	44	3
28.5	79	3	67.2	49	3
34.2	37	2	69.9	54	3
37.0	32	2	72.5	53	3
39.8	48	3	77.8	43	3
42.6	52	3			

$^{16}O(p,^{3}He)^{14}N$ 2.311 MeV (first excited state)

θ	$\frac{d\sigma}{d\omega}$	$\Delta\sigma$	θ	$\frac{d\sigma}{d\omega}$	$\Delta\sigma$
8.6	331	19	39.9	80	5
8.6	320	13	45.5	24	2
12.6	161	12	48.3	10	1
14.4	109	8	51.1	9	1
17.2	81	7	56.6	16	2
17.2	76	11	62.1	27	2
22.9	141	13	67.5	23	2
28.6	181	10	70.2	21	2
34.3	184	9	72.8	21	2
37.1	74	4	78.1	9	1

$^{16}O(p,t)^{14}O$ Ground state.

θ	$\frac{d\sigma}{d\omega}$	Δσ	θ	$\frac{d\sigma}{d\omega}$	Δσ
8.7	671	33	37.4	143	3
8.7	603	30	40.2	120	3
12.7	350	20	43.0	50	2
14.5	243	14	45.8	13	1
17.3	135	12	48.6	19	2
23.1	230	25	51.4	20	2
23.1	223	10	57.0	30	2
28.8	382	7	67.9	42	2
34.5	383	9	78.6	13	1

$^{28}Si(p,t)^{26}Si$ Ground state.

θ	$\frac{d\sigma}{d\omega}$	Δσ	θ	$\frac{d\sigma}{d\omega}$	Δσ
5.4	676	15	35.2	49	5
10.9	155	15	37.9	8	2
13.6	80	11	43.3	29	3
16.3	120	7	48.6	47	5
19.1	213	18	53.9	44	4
21.8	274	15	59.2	44	3
27.2	318	16	64.5	22	3
32.6	182	14	69.7	15	2
32.6	177	10	74.8	15	2

A. 4:

The polarization analysing powers of the six reactions are tabulated below. The angles are given in the centre of mass coordinate system and the analysing powers and errors are given as percentages.

$^{12}C(p,t)^{10}C$ Ground state.

θ	$P_A(\theta)$	δP	θ	$P_A(\theta)$	δP
18.4	-2.96	5.88	54.4	52.48	7.08
24.5	13.51	5.26	54.4	47.54	5.96
30.6	14.04	3.21	57.3	77.16	7.78
36.7	10.42	3.47	60.2	76.96	8.08
42.6	9.91	2.58	60.2	72.39	6.92
48.6	11.20	4.18	65.9	84.79	6.42
48.6	11.87	6.59	71.6	46.24	4.66
51.5	36.25	6.66	77.1	39.61	5.06

$^{12}C(p,t)^{10}C$ 3.34 MeV (first excited state).

θ	$P_A(\theta)$	δP	θ	$P_A(\theta)$	δP
18.7	-23.26	5.68	55.2	-30.39	5.86
24.9	4.99	5.62	58.2	-40.04	5.82
31.1	12.19	5.51	61.1	-47.15	6.01
37.2	-3.31	7.52	61.1	-43.61	6.63
43.3	-26.79	5.43	66.9	-26.41	6.62
49.3	-58.29	5.18	66.9	-16.36	7.40
52.3	-39.03	6.80	72.6	-2.63	7.35
55.2	-22.78	5.08	78.2	7.69	8.46

$^{16}O(p,^{3}He)^{14}N$ Ground state.

θ	$P_A(\theta)$	δP	θ	$P_A(\theta)$	δP
22.8	48.20	5.98	48.1	24.69	6.49
28.5	40.90	5.78	50.9	33.78	7.65
34.2	14.48	9.81	56.4	51.85	11.02
37.0	-2.15	8.90	67.2	44.19	7.14
39.8	-16.95	7.67	72.5	43.29	4.68
42.6	2.18	7.04	77.8	35.96	5.90
45.3	20.09	5.56			

$^{16}O(p,^{3}He)^{14}N$ 2.311 MeV (first excited state).

θ	$P_A(\theta)$	δP	θ	$P_A(\theta)$	δP
22.9	31.67	6.30	48.3	-2.57	12.21
28.6	22.10	3.60	51.1	12.83	15.42
34.3	30.20	4.95	56.6	49.80	16.45
37.1	32.75	5.66	67.5	57.95	8.41
39.9	17.99	5.95	70.2	2.33	14.49
45.5	-45.02	10.75	72.8	17.59	7.58

$^{16}O(p,t)^{14}O$ Ground state.

θ	$P_A(\theta)$	δP	θ	$P_A(\theta)$	δP
23.1	27.26	4.30	45.8	-48.02	12.88
28.8	26.58	2.24	48.6	0.80	9.02
34.5	20.97	3.58	51.4	33.07	8.50
37.4	17.46	3.54	57.0	57.51	8.92
40.2	20.32	5.21	67.9	53.33	6.15
43.0	-6.80	5.64	78.6	21.64	10.56

$^{28}Si(p,t)^{26}Si$ Ground state.

θ	$P_A(\theta)$	δP	θ	$P_A(\theta)$	δP
21.8	3.23	8.61	40.6	31.41	9.64
24.5	16.61	6.42	43.3	48.76	6.89
27.2	11.95	4.12	45.9	62.35	7.19
29.9	6.02	4.21	48.6	41.21	6.01
32.6	0.06	6.10	53.9	30.30	5.58
32.6	6.85	5.40	59.2	10.46	5.86
35.2	-0.12	6.31	64.5	1.59	5.91
37.9	25.22	8.13			

REFERENCES.

A.Y.Abul-Magd and M.El-Nadi,1966; Nucl. Phys. Vol 77 p 182.

L.W.Alvarez,H.Bradner, J.V.Franck, H.Gordon, J.D. Gow, L.C.Marshall, F.Oppenheimer, W.K.H.Panofsky, C.Richman and J.R.Woodyard,1955; Rev. Sci. Instr. Vol 26 p 111

N.Austern, R.M.Drisko, E.C.Halbert and G.R.Satchler,1964; Phys. Rev. Vol 133 p B3.

A.Baldin, V.I.Goldanskii and I.L.Rozenthal',1961; "Kinematics of Nuclear Reactions" (Oxford University Press,1961)

D.J.Baugh,G.J.B.Pyle, P.M.Rolph and S.M. Scarrott,1967; Nucl. Phys. Vol A95 p 115

Gy.Bencze and J.Zimanyi,1966; Nucl. Phys. Vol 81 p 76

L.C.Biedenharn,1959; Nucl. Phys. Vol 10 p 620

R.J.Blin-Stoyle,1951; Proc. Phys. Soc. Vol 165A p 452

E.T.Boschitz, M.Chanbre, ME.Conzett and E.J.Slobodrian,1965; Proc. of the 2nd Internation Symposium on Polarization Phenomena of nucleons (Birkhauser Verlag, Basel 1966)

D.A.G.Broad and K.G.McAiush,1964; PLA Progress Report NIRL/R/81 p 16

T.A.Brody and M.Moshinsky,1960; Tables of Transformation Brackets (Monograficis dal Instituto de Fisica Mexico 1960)

G.E.Brown and A.M.Green,1965; Nucl. Phys. Vol 75 p 401

F.J.A.Buttle and L.J.B.Goldfarb,1964; Proc. Phys. Soc. Vol 83 p 701

J.Carny and R.H.Pehl,1964; Phys. Rev. Letters Vol 12 p 619

N.S.Chant,1966; Private Communication

N.S.Chant, P.S.Fisher and D.K.Scott,1967; Nucl. Phys. Vol A99 p 669

N.S.Chant and J.M.Nelson,1968; Nucl. Phys. Vol A117 p 385

H.Collard, R.Hofstadter, E.B.Hughes, A.Johansson, M.R.Yearian
R.B.Day and R.T.Wagner,1965; Phys. Rev. Vol 138 p B57

S.W.Cosper, H.Brunnader, J.Cerny and K.McGrath,1967;
Phys. Letters Vol 25B p 324

R.M.Craig, J.C.Dore, G.W.Greenless, J.S.Lilley, J.Lowe and
P.C.Rowe,1964; Nucl. Instr. and Methods Vol 30 p 268

R.M.Craig, J.C.Dore, G.W.Greenless, J.Lowe and D.L.Watson,1966;
Nucl. Phys. Vol 83 p 493

A.De-Shalit and I.Talmi,1963; Nuclear Shell Theory (Academic Press,1963)

C.Détraz, J.Cerny and R.H.Pehl,1965; Phys. Rev. Letters Vol 14 p 708

F.Dönau, K.Hehl, C.Riedel, R.A.Broglia and P.Federman,1967;
Nucl. Phys. Vol A101 p 495

J.A.Fannon, E.J.Burge and D.A.Smith,1967; Nucl. Phys. Vol A97 p 263

P.S.Fisher and D.K.Scott,1967; Nucl. Instr. and Methods Vol 49 p301

a) D.G.Fleming, J.Cerny, C.C.Maples and N.K.Glendenning,1968;
Phys. Rev. Vol 166 p 1012

b) D.G.Fleming, J.Cerny and N.K.Glendenning,1968;
Phys. Rev. Vol 165 p 1153

W.E.Frahn and G.Wiechers,1965; Nucl. Phys. Vol 74 p 65

A.Fricke, E.E.Gross and A.Zucker,1968; Phys. Rev. Vol 163 p 1153

N.K.Glendenning,1963; Annual Rev. of Nuclear Science Vol 13 p 191

N.K.Glendenning,1965; Phys. Rev. Vol 137 p B102

R.N.Glover and A.D.W.Jones,1966; Nucl. Phys. Vol 81 p 277

R.N.Glover, A.D.W.Jones and J.R.Rook,1966; Nucl. Phys. Vol 81 p 289

L.J.B.Goldfarb and R.C.Johnson,1960; Nucl. Phys. Vol 18 p 353

R.C.Hanna,1965; Proc. of the 2nd International Symposium on Polarization Phenomena of Nucleons (Birkhauser Verlag Basel 1966) p 280

R.C.Hanna and T.A.Hodges,1965; Nucl. Instr. and Methods Vol 37 p 346

† J.C.Hardy and D.J.Skyrme,1966; Proc. of the Conf. on Isobaric Spin in Nuclear Physics (Academic Press, 1966) p 701

a) J.C.Hardy and I.S.Towner,1967; Phys. Letters Vol 25B p 577

b) J.C.Hardy and I.S.Towner,1967; Phys. Letters Vol 25B p 98

J.C.Hiebert, E.Newman and R.H.Bassel,1967; Phys. Rev. Vol 154 p 896

S.A.Hjorth, J.K.Saladin and G.R.Satchler,1965; Phys. Rev. Vol 138 p. B1425

P.E.Hodgson,1962; Proc. of the Conf. on Direct Interactions and Nuclear Reaction Mechanisms (Gordon and Breach,1963) p 103

P.E.Hodgson,1968; A review of triton and ^{3}He optical potentials. (To be published)

A.D.W.Jones,1965; D.Phil. Thesis, Oxford University. (Unpublished)

K.Kolltveit,1968; Phys. Rev. Vol 166 p 1057

L.L.Lee, J.P.Schiffer, B.Zeidman, GR.Satchler, R.M.Drisko and R.H.Bassel,1964; Phys. Rev. Vol 136 p B971

B.E.F.Macefield,1967; Private Communication.

N.F.Mangelson, B.G.Harvey and N.K.Glendenning,1968; Nucl. Phys. Vol A117 p 161

V.S.Mathur and J.R.Rook,1967; Nucl. Phys. Vol A91 p 305

D.W.Miller,1965; Proc. of the 2nd International Symposium on Polarization Phenomena of Nucleons (Birkhause Verlag Basel 1966) p 410

D.Montague,1967; Private Communication.

W.R.McMurray, P. van der Merwe and I.J. van Heerden,1967; Nucl. Phys. Vol A92 p 401

H.C.Newns,1953; Proc. Phys. Soc. Vol 66A p 477

F.G.J.Perey,1962; Proc. of the Conf. on Direct Interactions and Nuclear Reaction Mechanisms (Gordon and Breach 1963) p 125

F.G.J.Perey and B.Buck,1962; Nucl. Phys. Vol 32 p 353

A.C.Phillips,1966; Phys. Rev. Vol 145 p 733

M.A.Preston,1962; Physics of the Nucleus (Addison and Wesley 1962)

G.H.Rawitscher,1968; Phys. Rev. Vol 163 p 1223

J.R.Rook and D.Mitra,1964; Nucl. Phys. Vol 51 p 96

G.R.Satchler,1958; Nucl. Phys. Vol 8 p 65

G.R.Satchler,1964; Nucl. Phys. Vol 55 p 1

G.R.Satchler,1967; Nucl. Phys. Vol A100 p 497

D.K.Scott,1963; Oxford Nuclear Physics Laboratory Research Report (Unpublished)

N.M.Sen Gupta, J.Rotblat, P.E.Hodgson and J.B.A.England,1962; Nucl. Phys. Vol 38 p 361

N.M.Sen Gupta, J.Rotblat, E.A.King and J.B.A.England,1964; Nucl. Phys. Vol 50 p 549

W.Tobocman,1961; Theory of Direct Nuclear Reactions (Oxford University

Press, 1961)

I.S.Towner,1968; Private Communication.

I.S.Towner and J.C.Hardy,1968; To be published.

H.A.Weidenmüller,1965; Proc. of the 2nd International Symposium on Polarization Phenomena of Nucleons (Birkhauser Verlag Basel 1966) p 219

B.H.Wildenthal and P.D.M.Claudemans,1967; Nucl. Phys. Vol A92 p353

S.Yamabe, M.Kondo, S.Kato, T.Yamazaki and J.Rusn,1960; J. Phys. Soc. of Japan Vol 15 p 2154

S.Yoshida,1962; Nucl. Phys. Vol 33 p 683.

† J.C.Hardy,1968; Private Communication.